UNIVERSITY OF CALIFORNIA,
IRVINE

Using chimeric models to study the interactions between human microglia and Alzheimer's Disease pathology *in vivo*

DISSERTATION

Submitted in partial satisfaction of the requirements
For the degree of

DOCTOR OF PHILOSOPHY

in Biological Sciences

by

Morgan Alexandra Coburn

Dissertation Committee:
Professor Mathew Blurton-Jones, Chair
Professor Brian Cummings
Professor Leslie Thompson
Professor Robert Spitale
Professor Sunil Gandhi

2021

DEDICATION

To all those who are kind and curious,
Let your inquisitive minds be your flashlights
and open hearts be your lightbulbs.

TABLE OF CONTENTS

LIST OF FIGURES

INTRODUCTION

CHAPTER 1

CHAPTER 2

ACKNOWLEDGEMENTS

I would like to thank my PhD advisor, Dr. Mathew Blurton-Jones, for taking me on as a student and helping me become the scientist I am today. I am grateful for the opportunity to learn from you and have always been impressed by the near endless stream of brilliant ideas you synthesize and your amazing writing. Thank you for being supportive of my activities outside of lab as well, where volunteering with the CNLM Ambassador Program, participating in the Pedagogical Fellows Program, and advocating for affordable insulin have all been incredibly enriching. Above all I am deeply grateful for your kindness and patience throughout my time in your lab. Your empathy through the many stressors that often took me away from research for long periods of time was critical in me finding my footing after the storm had passed, thank you for giving me second chance to find ownership and passion for my research. I would also like to thank my thesis committee, Dr. Brian Cummings, Dr. Sunil Gandhi, Dr. Rob Spitale, and Dr. Leslie Thompson for your feedback and support throughout my projects, I'm not sure many students can fondly remember their committee meetings for their laughter alongside the scientific discussions the way that I can. I want to especially thank Dr. Brian Cummings and Dr. Leslie Thompson for your guidance and advice, your support has been integral in gaining confidence as a scientist.

I want to thank the entirety of the Blurton-Jones Lab: Jaclyn Beck, Joia Capocchi, Jean Paul Chadarevian, Dr. Christel Claes, Emma Danhash, Dr. Hayk Davtyan (who serves as the glue that holds our lab together), Dr. Alberto Granzotto, Dr. Jonathan Hasselmann (for collaborating with me to develop the chimeric model and co-chair of the Brain Explorer Academy), Zahara Kreulen, Tau En Lim, Dr. Amanda McQuade (who

has been a tremendous friend, scientific collaborator, and hype-woman), Dr. Samuel Marsh, Jessica Sanchez, Sepideh Kiani Shabestari (who I am tremendously proud of, watching you grow from the time you were my undergraduate assistant to now as a brilliant PhD student has been incredible beyond words), Jorge Silva, Alexandra Sotelo, and Christina Tu. I am grateful to all of you for your scientific advice and for all the fun.

I am extremely grateful for my T32 mentors, Dr. Peter Donovan and Dr. Leslie Thompson. The training the two of them coordinated speaks to their investment and care for students beyond their scientific work, which encouraged self-kindness, mindfulness, and fostered deep and meaningful conversations about mental health that I would never have thought possible in academia. The Gallup Strength-Finders activity especially helped me find my voice and advocate for the feedback I needed. Thank you both for being incredible role models inside and out of the lab.

Furthermore, I would like to thank Manuella Yassa and Center for Learning and Memory for the amazing outreach opportunities. Working with Manuella has been an immense pleasure and she has been as much of a friend as a mentor. She has taught me so much about education and science communication and learning how to teach children about the brain has given me so much confidence in communicating my own science to my field.

I would like to thank my family and friends, who have been endlessly supportive of me throughout this. My best friend since 7th grade, Nicole Serrano; my climbing buddies, Taylor Nakayama, Miranda Chappel-Farley, Dr. Jan Frankowski, Thai Nguyen, and Caden Henningfield; my cohort mates who have gone through this beside me, Natalie DiProspero and Julian Quintanilla; assorted friends Dr. Amanda McQuande,

Hamsi Radhakrishnan, and Rajat Saxana; as well as my family Frances Coburn, Robert Coburn, Gary Coburn, Kerri Coburn, Jackie Coburn, Collin Coburn, Jo Gatlin, and Madeline Scardina. Finally, I would like to thank my partner Dr. Scott Kilianski, who has walked with me through some of the best and worst days of my life, who helped me get through the loss of my mom, who makes me smile, who makes me think. Your kindness, curiosity, and passion inspire me every day and I am so grateful to know and love you.

This work was funded by NINDS-T32-NS082174 (MC), Rose Hills Foundation (MC), NIH-R01-AG048099 AG-055524, 056303 (MBJ), CIRM RT3-07893, AG061895 (HD). It was supported by many core resources at UCI including the Alzheimer's Disease Resource Center (ADRC), Memory Impairments and Neurological Disorders (MIND), Center for the Neurobiology of Learning and Memory (CNLM), Sue and Bill Gross Stem Cell Research Center (SCRC), and the Institute for Immunology (IFI). Finally, this work would not have been possible without generous donations from Alzheimer's disease patients and their families who value and support this research.

CURRICULUM VITAE

Morgan Coburn MSc

Education

University of California, Irvine, CA — Defense: November 2021
PhD, Neurobiology and Behavior GPA: 4.0

Scripps College Claremont, CA — Graduation Date: December 2016
BA, Neuroscience: Cell, Molecular GPA: 3.6

Education

Ph.D.	University of California, Irvine, CA Department of Neurobiology and Behavior; GPA: 3.95 PhD Advisor: Mathew Blurton-Jones	Defense: November 2021
M.Sc.	University of California, Irvine, CA Winter 2020 Received though Ph.D. Program in Department of Neurobiology and Behavior	
B.A.	Mount Holyoke College, South Hadley, MA Major: Neuroscience and Behavior; Minor: Chemistry; GPA: 3.49	Graduation Date: December 2016

Fellowships and Awards

- Brain Camp Pedagogical Award for Excellence in Teaching, *UCI, CNLM* — Summer 2021
  - $1000 award
- DTEI Summer Fellows Program, *UCI DTEI*
  Summer 2021
  - $5,000 award and Pedagogical Training in order to assist UCI Faculty with transitioning classes from virtual to hybrid or in person learning.
- Most Promising Future Faculty Award, *UCI DTEI* — 2021
  - 3 Students awarded out of 600 nominees
- Pedagogical Fellow, UCI DTEI — 12/21–Present
  - $2,000 award and advanced pedagogical training.
- Rose Hills Foundation Science & Engineering Fellowship — 2020—2021
  - $10,000 awarded yearly and *nominated, merit-based fellowship*
- Norman M. Weinberger Memorial Award, *UCI, CNLM Awards* — 2020
  - $1,000 applicant award
- NIH-T32 Training Grant in Stem Cell Translational Medicine for Neurological Disorders — 2019–2021
  - Funding for 75% of stipend for two years
  - Workshops and seminars spanning subjects from Machine Learning, Statistics, Mindfulness, Effective Presentations and Gallup's Strength Finders
- Brain Camp Pedagogical Award for Excellence in Teaching, *UCI, CNLM* — Summer 2019
  - $1000 award
- National Science Foundation Graduate Research Fellowship – *Honorable Mention* — 2019
- Francisco J. Ayala Graduate Fellowship, University of California, Irvine, — 2017
  - *$10,000 Merit based fellowship*
- Mount Holyoke Leadership Award, Mount Holyoke College — 2013 – 2016
  - *Merit based annual tuition award of $10,000 per year*

- Harap Family Fund, Mount Holyoke College, *Travel award to attend SfN 2016* 2016
- Vorwerk Fund, Mount Holyoke College 2016
  - *Travel award to attend SfN 2016*
- LYNK Funding, Mount Holyoke College 2015
  - *$3,000 award for summer research.*

Research

Laboratory of Dr. Mathew Blurton-Jones, UCI 2017–Present

Doctoral Candidate

Development and validation of a chimeric model to study human iPS-microglia in vivo in health and disease. Primary research focus has involved developing a chimeric model to transplant and study human iPSC-derived microglia and how they respond morphologically, transcriptomically, and functionally, to the healthy and diseased brain environment; including Alzheimer's Disease, *in vivo* 2-photon laser induced injury, repeat mild chronic head injury (concussion), and brain-metastasized human breast cancer.

Laboratory of Dr. Jared Schwartzer, Mount Holyoke College 2014 – 2016

Research Assistant and Lab Manager

Maternal immune activation models of Autism Spectrum Disorders. Undergraduate research involved using maternal immune activation (MIA) models of autism in mice to examined how social behavior differs in offspring when pregnant dams were sensitized to develop allergic asthma. Two primary projected involved exposing dams to aerosolized ovalbumin or to concentrated ambient particulate matter, 2.5μm or smaller (CAPs).

Publications

Coburn M, Hasselmann J, England, W., Picard, K., Lau, V., McQuade, A., Silva, J., Beck, J., Kiani Shabestari, S.,Tremblay, M.-È., Spitale, R.C., Davtyan H, and Blurton-Jones M. *Human Microglia Adopt a Rod-like Morphology in a Chimeric Model of Amyloid and Tau Pathology that is Associated with a Type 1 Interferon Response*. (To be submitted Fall 2021, *JEM*)

Kiani Shabestari, S., Morabito, S., Danhash, E.P., McQuade, A., Miyoshi, E.E., Chadarevian, J.P., Claes, C., **Coburn, M.A.,** Hasselmann, J., Silva, J., Martini, A.C., Sanchez, J.R., Head, E., Hume, D.A., Pridans, C., Davtyan, H., Swarup, V., Blurton-Jones, M., Absence of microglia leads to diverse comorbidities and promotes lethality in Alzheimer's disease mice. (Submitted, *Nature Neuroscience).*

Katrina T Evans*; Kerrigan Blake*; Aaron Longworth; **Morgan A Coburn**; Quy H Nguyen; Dennis Ma; Grace A Hernandez; Armani K Oganyan; Davit Orujyan; Robert A Edwards; Clare Pridans; Matthew Blurton-Jones; Devon Lawson. Microglia mount a pro-inflammatory response to suppress breast cancer brain metastasis. (Submitted, *Nature Cell Biology*)

Claes, C., Danhash, E., Hasselmann, J., Chadarevian, J.P., Shabestari, S.K., Lim, T.E., Tu, C., Silva, J., **Coburn, M.A**., Jairaman, A. and Cahalan, M., (2020). Examining the effects of the microglial PLCG2 P522R mutation by transplantation of human stem cell-derived microglia in chimeric AD mice: Molecular and cell biology/stem cells, iPS cells. *Alzheimer's & Dementia*, *16*, p.e041539.

McQuade A., Kang Y., Hasselmann J., Jairaman A., Sotelo,A., **Coburn M.**, Kiani Shabestari S., Chadarevian, J.P., Fote G., Tu C. H., Danhash E., Silva, J., Martinez, E., Cotman C., Prieto, A., Thompson L., Steffan J., Smith, I., Davtyan, H., Cahalan, M., Cho, H., Blurton-Jones, M. (2020) Transcriptomic and functional changes in human TREM2 knockout microglia cause an impaired response to Alzheimer's Disease pathology *in vivo. Nature Communications*, *11(1),* 1-17. PMID: 33097708 PMCID: PMC7584603 DOI: 10.1038/s41467-020-19227-5

Coburn M*, Hasselmann J*, England W, Figueroa DV, Kiani Shabestari S, Tu CH, McQuade A, Kolahdouzan M, Echeverria C, Claes C, Nakayama T, Azecedo R, Coufal N, Han C, Cummings BJ, Davtyan H, Glass C, Healy L, Gandhi S, Spitale R, Blurton-Jones M. (2019) Development of a chimeric model to study and manipulate human microglia *in vivo*. *Neuron, 103, 1–18.* PMID: 31375314; DOI: 10.1016/j.neuron.2019.07.002

- *Awarded the James L. McGaugh Award for Excellence in Graduate Research in Neurobiology and Behavior, UCI, Spring 2020*
- *Listed on "Best of Neuron 2019-2020" – the 10 most widely read papers published in the journal Neuron.*

A. Hovakimyan, T. Antonyan, O. Svystun, S. Kiani Shabestari, G. Chailyan, **M.A. Coburn**, I. Petrushina, D.H. Cribbs, M. Blurton-Jones, M.G. Agadjanyan, A. Ghochikyan, H. Davtyan (2019). A MultiTEP platform-based epitope vaccine targeting the phosphatase activating domain (PAD) of tau: therapeutic efficacy in PS19 mice. *Scientific reports*, *9*(1), 1-12

H. Davtyan, G. Chailyan, A. Hovakimyan, **M.A. Coburn**, I. Petrushina, S. Kiani Shabestari, T. Antonyan, D. Blum, L. Buée, N. Petrovsky, D.H. Cribbs, A. Ghochikyan, M. Blurton-Jones, M.G. Agadjanyan, (2019) Alzheimer's disease AdvaxCpG-adjuvanted MultiTEP-based vaccines reduce Ab and tau pathology in a brain of double transgenic mice. *Alzheimer's research & therapy*, *11*(1), 1-13. PubMed PMID: 31847886; DOI: 10.1186/s13195-019-0556-2

McQuade, A., **Coburn, M.**, Tu, C. H., Hasselmann, J., Davtyan, H., & Blurton-Jones, M. (2018). Development and validation of a simplified method to generate human microglia from pluripotent stem cells. *Molecular Neurodegeneration*, *13*(1), 67. PMID: 30577865 PMCID: PMC6303871 DOI: 10.1186/s13024-018-0297-x

Church JS, Tijerina PB, Emerson FJ, **Coburn MA**, Blum JL, Zelikoff JT, Schwartzer JJ. (2018) Perinatal exposure to concentrated ambient particulates results in autism-like behavioral deficits in adult mice. *Neurotoxicology*. Mar;65:231-240. PubMed PMID: 29104007; PubMed Central PMCID: PMC5857220.

Schwartzer JJ, Careaga M, **Coburn MA**, Rose DR, Hughes HK, Ashwood P. (2017) Behavioral impact of maternal allergic-asthma in two genetically distinct mouse strains. *Brain Behav Immun*. Jul;63:99-107. PubMed PMID: 27622677; PubMed Central PMCID: PMC5346064.

* Denotes First Co-Authorship

Conference Posters

Morgan A. Coburn; Jonathan Hasselmann; Jorge Silva; Jaclyn Beck;, Sepideh Kiani Shabestari; Hayk Davtyan; and Mathew Blurton-Jones. (2021) Using a Chimeric Model to Study the Interactions Between Human Microglia and Alzheimer's Disease Pathology *in vivo.* Presented at the Keystone Symposia on Neuroimmune Interactions in Health and Disease, June 7-9, 2021

Morgan Coburn; Jonathan Hasselmann; Amanda McQuade; Christina Tu, MS; Hayk Davtyan, PhD; Sepideh Kiani Shabestari; and Mathew Blurton-Jones, PhD. (2019) Using human iPS derived microglia *in vivo* to study Alzheimer's Disease*.* Presented at Cell Symposia Neuro-Immune Axis: Reciprocal Regulation in Development, Health, and Disease September 22-24, 2019

Morgan Coburn; Jonathan Hasselmann; Amanda McQuade; Christina Tu, MS; Hayk Davtyan, PhD; Sepideh Kiani Shabestari; and Mathew Blurton-Jones, PhD. (2019) Using human iPS derived microglia *in vivo* to study Alzheimer's Disease*.* Presented at the Keystone Symposia on Neural Environment in Disease: Glial Responses and Neuroinflammation, June 16-20, 2019

Morgan Coburn; Jonathan Hasselmann; Amanda McQuade; Christina Tu, MS; Hayk Davtyan, PhD; Sepideh Kiani Shabestari; and Mathew Blurton-Jones, PhD. (2019) Characterizing human Disease Associated Microglia *in vivo.* Presented at the Alzheimer's Diseases & Parkinson's Disease Conference, Lisbon, Portugal; March 26-31, 2019

Morgan Coburn; Jonathan Hasselmann; Dario Figueroa; Amanda McQuade; Christina H Tu, MS; Jean-Paul Chadarevian; Hayk Davtyan, PhD; Sunil Gandhi, PhD; Mathew Blurton-Jones, PhD. (2018) Development of Murine/Human Microglia Chimeras to Study Neurological Disease. Presented at the Society for Neuroscience Conference, November 3-7, 2018.

Morgan Coburn; Megan E. Johnson; and J.J. Schwartzer, PhD. (2016) ASD-like behavioral deficits in a mouse model of gestational exposure to concentrated ambient particulate matter. Presented at the Society for Neuroscience Conference, San Diego, CA; November 13-16, 2016.

Morgan Coburn; Megan E. Johnson; and J.J. Schwartzer, PhD. (2016) The Behavioral Consequences of Prenatal Exposure to Particulate Matter in Mice. Presented at the Northeast Undergraduate Research Organization for Neuroscience, Quinnipiac University; February 28, 2016.

Talks

Morgan A Coburn. *Development of Murine/Human Microglia Chimeras to Study Neurological Disease*. Irvine, CA. February 25th, 2018. Given as an invited speaker at the 9th Annual REMIND Emerging Scientists Symposium**.**

Morgan A Coburn. *Development Microglia Chimeras to Study Neurological Disease*. Irvine, CA. September 14th, 2018. Given as an invited speaker to Psi Beta, Irvine Valley College Chapter.

Service and Outreach

- Assistant Professor of Teaching Search Committee, *UCI BioSc* Summer 2021
    - Part of a committee responsible for recruiting and hiring a new Assistant Professor of Teaching for the School of Biological Sciences that will be responsible for teaching introductory biology lecturer and lab courses and well as conduct discipline based pedagogical research.
- Co-Chair, Brain Explorer's Academy Committee 2019–Present
    - An 8-week CNLM sponsored educational outreach program held on Saturday mornings geared at introducing children in 2nd-5th and 6th-8th grades (2 sessions a year) about the brain and how it is studied. (Program on hiatus due to COVID).
    - Organizing and running the Spring 2019, and Fall 2019 BEA Session
- Co-Chair, REMIND 2018 – 2020
    - Organizing and running the 10th and 11th Annual REMIND Symposia
    - Participating and leading various outreach events with UCI STEAM K-12 outreach council, a program lead by the Beall Center for Art and Technology
    - Volunteering with UCI MIND conferences and events
- CNLM Ambassador 2017–Present
    - Brain Explorer's Academy Mentor Fall 2018 and Spring 2019
    - Irvine Brain Bee 2019 Mentor
    - Volunteering with CNLM community lectures and outreach events including McGaugh-Gerard Lectures, lab tours, grad student panels,
- Undergraduate Mentorship
    - Sepideh Kiani Shabestari 3/2018–2020
        - 2020: Accepted into UCI's Interdepartmental Neuroscience Ph.D. Program
        - 2019 UROP: Received the Chancellor's Award in Undergraduate Research
        - 2019 Excellence in Research: Finalist in Excellence in Research; Received the Dean's Award for Excellence in Research

Teaching

Experience

- TA Professional Development Program (TAP-DP) Fall 2021
    - Designed and presented 9, 1-hour long, workshops geared towards preparing future TAs to effectively teach; workshops spanned topics on Active Learning, Inclusive Teaching, Course Design, and effective assessment techniques.
- Virtual Brain Camp 2021 Organizer and Instructor Summer 2021
    - Contributed to the curriculum and activity design, coordination, optimization for online learning, and instruction of UCI's Brain Camp for high school and middle school students; a two-week, day-long program geared at first introducing fundamental principles and techniques of neuroscience, then designing and carrying out a student run experiment.
- Pedagogical Liaison *Division of Teaching Excellence & Innovation (DTEI)* April-Sept 2020
    - Assisted with facilitating UCI's 2020 TA Professional Development Program (TAP-DP)
    - Designed and gave a workshop on Diversity and Inclusion for TAP-DP
- Guest Lecturer

    - Bio 47: Stress – Stress and Immunity Feb 20, 2020
- Brain Camp 2019 Organizer and Instructor Summer 2019
    - Contributed to the curriculum and activity design, coordination, and instruction of UCI's First Brain Camp for high school and middle school students; a two-week, day-long program geared at first introducing fundamental principles and techniques of neuroscience, then designing and carrying out a student run experiment.
- Teaching Assistant, University of California, Irvine, CA
    - N113L: Neurobiology Lab Winter 2019
        - Responsible for all student learning and grading for one section.
    - N120B: Infectious Diseases Winter 2020
    - Bio Sci 38: Mind, Memory, and Amnesia Spring 2020
    - Bio Sci 93: DNA to Organisms Summer 2020
        - Part of a team responsible for optimizing this course for remote teaching due to the COVID-19 pandemic.
    - Bio Sci 93: DNA to Organisms Fall 2020

Professional Development

- UCI Division of Teaching Excellence and Innovation Pedagogical Fellow Jan-Dec 2021
    - Over 100 Hours in Advanced Training in Pedagogy
- Transforming Your Research Into Teaching Summer 2020
    - Workshop in Course Design (CIRTL)
- Center for the Integration of Research, Teaching, and Learning (CIRTL): Winter 2020
    - *Associate Level*
    - 12 hours of Evidence-Based Teaching training
    - Participation in one quarter of a learning community that meets weekly
    - 3 hours of training in Learning through Diversity
    - 3 hours of training in Teaching as Research
- UCI DTEI Course Design Certificate Program Winter 2020
- University Studies 390X Winter 2020
    - 10 week course in developing teaching techniques including fundamentals in pedagogical research, course design, diversity, and teaching practices.
- Effective Communication for Scientists Certificate Program Summer 2019
    - 10 week certificate program geared towards teaching effective presentation skills including talk organization and public speaking.

ABSTRACT OF THE DISSERTATION

Using chimeric models to study the interactions between human microglia and Alzheimer's Disease pathology *in vivo*

By

Morgan Coburn

Doctor of Philosophy in Biological Sciences

University of California, Irvine, 2021

Professor Mathew Blurton-Jones, Chair

Alzheimer's Disease (AD) is the leading cause of age-related dementia, effecting an estimated 5.8 million people in the United States alone. Despite considerable progress in our understanding of the two hallmark pathologies that are thought to drive this disease; amyloid plaques and neurofibrillary tangles, no effective disease-modifying therapies have yet been developed. Since the initial reports by Alois Alzheimer in 1907, we have known that, in addition to plaques and tangles, the brains of patients exhibit considerable reactive gliosis[1]. More recently, genetic studies have provided compelling new evidence that microglia in particular play a critical role in the development and progression of AD.

Although the field has known for over a century that microglia migrate to and surround amyloid plaques, the first genetic indication that microglia might play a more prominent role in AD came with the discovering of coding mutations in the microglial-enriched gene TREM2 (triggering receptor expressed on myeloid cells 2). Soon thereafter, Genome Wide Associative Studies (GWAS) begun to identify many additional AD risk genes that were highly or even specifically expressed by microglia.

Yet, despite the identification of these new AD risk genes, much remains to be discovered about the roles of microglia in either the development or progression of this disease.

A major challenge to our understanding of microglia, both in general and in AD, has arisen from the difficulty of studying and manipulating human microglia. As highly plastic cells, microglia are extremely sensitive to their environment and thus examining these cells in disease- and brain-relevant ways has proven to be a challenging and at times misleading process. For example, microglia cultured *in vitro* rapidly change their transcriptional programs from those observed within the brain. Furthermore, studies of microglia in rodent models of AD can suffer from the fact that many AD risk genes lack appropriate homology to their equivalent human genes. Given that microglia are the primary immune cell of the brain and intimately involved in many aspects of both health and disease, it is critical to develop better ways of understanding their response to a changing brain environment. The focus of this dissertation is to develop and characterize a first of its kind chimeric microglia model to better capture the morphology, behavior, and transcriptional patterns of human microglia *in vivo*, and use to apply the model to study how Alzheimer's Pathology effects human microglial genetics.

In this model, human HPCs are directly transplanted into the ventricles and overlaying cortex of postnatal day (P1) immunodeficient mice that are capable of supporting human microglial engraftment (MITRG and hCSF1 mice). These cells display robust long-term engraftment, migrating and populating much of the forebrain and differentiating into mature microglia within 2 months. Transplanted human cells exhibit morphology and markers typical of microglia, including complex ramifications

and establish distinct niches that tile neatly together, making up approximately 80% of the total microglia across several forebrain regions and multiple HPC preparations. Following *in vivo* maturation, human microglia can be isolated from the brain by FACS or MACS sorting and RNA sequencing performed. Bulk RNA-seq demonstrates that xenotransplanted human microglia (xMGs) recover key *in vivo* microglial signature genes and much of the transcriptomic profile which were recently shown by Chris Glass' lab to be lost during *in vitro* culturing of human microglia. Furthermore, when wild type (WT) P1 transplanted animals are compared to those given vehicle (saline) cerebroventricular injections, no deficits in either Morris Water Maze (MWM) or Elevated Plus Maze (EPM) are detected, indicating that this xenotransplantation model could be used to examine how disease-associated mutations in microglial genes might influence memory or anxiety-like behavior. **(Chapter 1)**.

This paradigm can also be used to study the interactions between human microglia and AD-associated amyloid pathology, by using immunodeficient MITRG mice that are backcrossed with 5XFAD mice to produce a colony of xenotransplantation-compatible 5X-MITRG mice which develop amyloid plaque pathology. Following transplantation into this model, iPSC-derived HPCs differentiate into microglia, migrate towards Aβ-plaques, and exhibit several disease-associated microglial (DAM) phenotypes including downregulation of the homeostatic marker P2RY12 and adoption of a more amoeboid morphology**.** Next, wildtype eGFP-expressing iHPCs were transplanted into P1 5x-MITRG and wildtype littermates and allowed to age to 10 months to ensure robust accumulation of plaques. Half-brains were fixed and used for histological analysis, whereas the other half was used isolate human microglia for

single-cell RNA sequencing (scRNA seq). The resulting data was then compared to equivalent existing murine microglial datasets. We found that xMGs display a uniquely human transcriptomic response to amyloidopathy. To further demonstrate the utility of this chimeric AD model, we performed transplantations with isogenic WT and TREM2 R47H HPCs and found that this disease relevant mutation could lead to similar migration deficits as those observed in human *postmortem* samples. **(Chapter 1)**.

Although tau pathology plays a critical role in AD and microglia have been implicated in the propagation of tau, very little research has yet been conducted to understand the responses and interactions of human microglia with neurofibrillary tangles. Given the significant links of microglia with both amyloid plaques and neurofibrillary tangles separately and the co-occurrence of these two hallmark pathologies in human AD, this gap in our understanding becomes even more surprising. In order to address these significant deficits, we have applied our xenotransplantation paradigm to a newly generated mouse in our lab, a cross between the hCSF1-5X mouse and the Tau P301S/PS19 mouse model in order to examine human microglial interactions with both amyloid plaques and neurofibrillary tangles Male mice were genotyped and transplanted on P1, allowed to age, and euthanized at 6 months old to allow for accumulation of both amyloid and tau pathologies. xMGs isolated from animals exhibiting amyloid and tau pathologies demonstrate expanded DAM, INF and IL-1β clusters as well as develop a dramatic Rod phenotype within CA1 that is correlated with a Type 1 Interferon Response. These results provide a wealth of transcriptomic data from mice exhibiting amyloidopathy and/or tauopathy as well as evidence for a

fascinating and little understood interferon-induced microglial Rod phenotype present in AD. **(Chapter 2)**

Taken as a whole, the development of these novel chimeric microglia models has allowed us to ask deep questions about human microglia dynamics in health and disease. We are able to fully recapitulate the transcriptional profiles of *ex vivo* microglia isolated from human patients, transplanted cells respond to both acute and peripheral immunological stimuli, migrate toward amyloid beta plaques, adopt activation profiles reported in AD patient microglia, and morphologically adapt to tau pathology and the changing brain environment. The recapitulated human microglial phenotypes observed in these models coupled with the power of induced pluripotent stem cell modeling allows researchers to alter genes of interest via CRISPR modification and following transplantation gain a greater understanding of how key Alzheimer's risk genes affect human microglial responses to AD pathologies.

INTRODUCTION

Microglia and Alzheimer's Disease

Morgan Coburn, Mathew Blurton-Jones

Models to Study and Manipulate Microglia in Health and AD

Microglia are the primary immune cell of the central nervous system (CNS) and are intimately involved in numerous developmental, homeostatic, and neurodegenerative processes[2-7]. Although much debate has arisen over the precise role of these highly motile cells, as a field we continue to rapidly gain new insight into their roles in both health and disease. Of particular importance, microglial function and genetics have been linked to Alzheimer's Disease (AD) numerous times, where their response—or lack-there-of—to pathology appears to play a major role in the progression of this complex disease[8]. With these revelations it has become critically important that we seek to define and understand the contributions of microglia to brain health and disease.

Unlike the other major cell types of the brain that arise from neuroectodermal lineages, microglia are yolk-sac derived myeloid cells. Stemming from the early stages of hematopoiesis, primitive hematopoietic progenitor cells (HPCs) within the yolk-sac give rise to erythromyeloid progenitors (EMPs) that in turn migrate into the developing central nervous system at embryonic (E) day 9.5 in mice[9, 10]. Upon reaching the brain and spinal cord, EMPs in turn respond to local cues, differentiating into microglia, perivascular macrophages, meningeal macrophages, and choroid plexus macrophages[9, 10].

Once they have colonized the brain, microglia processes remain highly motile, actively surveying their individualized niches for debris or signs of disease and interacting with neurons and other glia. Remarkably, over the course of a few hours microglia are thought to collectively survey the entirety of the brain[11, 12]. When faced

with injury or other inflammatory cues such as bacterial components like lipopolysaccharide (LPS), microglia quickly respond to the stimuli, rapidly extending processes towards acute injuries, migrating to white-matter tracts in cases of chronic traumatic brain injury, and dramatically shifting from their complex branched homeostatic morphology to a more amoeboid activated state[11, 13, 14]. Given these important functions, researchers have for the most part assumed that microglia are both critical and indispensable for neural development, brain homeostasis, and complex behavior. However, recent studies have begun to call some aspects of that assumption into question. For example, many studies have now shown that adult rodents housed within relatively sterile laboratory environments can survive and behave normally following near complete ablation of microglia via CSF1R inhibitors[15]. Likewise, a recently developed knockout model that lacks a microglia-specific enhancer region within the CSF1R locus can develop and survive without ever having microglia within the brain[16]. However, whether this persistent developmental loss of microglia leads to various functional impairments currently remains unknown. Remarkably, microglia have also recently been shown to respond rapidly to an empty niche within the aged or injured brain by dividing and migrating to repopulate as “rejuvenated” or phenotypically-“younger” cells [15]. These new findings suggest that specific pharmacological interventions can likely be developed to modulate not only the number of, but also the phenotype and activation states of microglia.

Microglia have been known to respond to and surround AD plaque pathology for over a hundred years, but it has only been with the advent of more recent genome wide associative studies (GWAS), that the field has come to learn that many of the genes

involved in late-onset AD are greatly enriched in microglia[17, 18]. The highly responsive nature of microglia, their genetic and pathological links to neurological diseases, and more recently, the idea that an entire population of brain cells can be removed and replaced with seemingly few if any short-term consequences, has led many researchers to approach microglia as an attractive new target for therapeutic development and as a result many new methods to study these cells have recently emerged.

Human Primary Microglia

For decades microglial research has employed primary cultures and *in vivo* rodent models. However, with the recent advent of induced pluripotent stem cell (iPSC) techniques, the field has developed promising new approaches and thus the benefits and caveats of each model should to be carefully considered. Primary microglial cultures are most often produced from rodent models, however, a handful of groups have become skilled at isolating microglia directly from human brains and maintaining and using these cells for *in vitro* experiments. Benefits of this approach include the ability to study the potential impacts of a life-time exposure to the human brain environment, where they can participate in the various immunological and peripheral cross-talk that occurs in a living human. For example, the impact of long-term exposure to beta-amyloid plaques can perhaps be examined in human brain-derived microglia.

However, it has recently become clear that microglia are highly dependent on the brain microenvironment to maintain their transcriptional profile, rapidly losing this "*in vivo*" signature within as little as 6 hours of growth in culture conditions (Figure 1A)[19]. (Among the genes rapidly downregulated are CX3CR1 (a fractalkine receptor and

homeostatic microglial marker), P2RY12 (a homeostatic microglia marker and purinergic receptor highly responsive to extracellular ADP), and Sall1 (a transcription factor and master regulator for microglia cell identity) (Figure 1B)[20]. If sequencing or other experimentation is performed directly after isolation instead of being maintained in culture, then primary microglia could in principle remain a valid option for assessing microglial responses to CNS environmental cues.

As a result, several recent studies have examined tissue freshly isolated from *post mortem* AD patients, and provided interesting insights into the role of microglia in AD and how they may differ across species. For example, Mathys and colleagues conducted single-nucleus RNA-seq (a technique similar to scRNA-seq which involved a brief nuclear dissociation process) on 80,660 total cells across 48 individuals to identify distinct populations of cells within the AD brain (2019)[7]. These researchers found some overlap in gene expression patterns of APOE, CD74, and other MHC-II-like genes reported in rodent models, yet found still more genes that had not been detected in studies of murine microglia including C1QB and CD14[6]. Though these insights are useful, still more deep analysis of microglia is necessary, as of all the cells sequenced for AD and control individual, under 2,000 were microglia, and likely less than 100 of those were actively responding to pathology (based on population sizes estimated from Keren-Shaul et al., 2017).

Friedman and colleagues similarly bioinformatically compared bulk RNA-seq data sets from a multitude of rodent disease models and bulk RNA-seq from frozen human patient tissue, assigning “modules” to characteristic sets of genes (2018). Researchers found many overlaps between murine and human gene expression patterns within the

"neurodegeneration" module, with additional elevations in the human gene sets in the modules "neutrophil/monocyte" and "LPS-specific" not observed in mice[21]. Friedman et al. acknowledge though, that the many difficulties associated with obtaining clean RNA from human subjects make it difficult to make deep observations about specific cell types[21].

The technical issues with isolating robust and sufficient microglial RNA from human samples coupled with their sensitivity to the environment, bring up one final caveat to using human primary microglia: the cells must of course be isolated from human patients, which are notoriously difficult to control for. For *post mortem* samples, many factors must be controlled (the process must be performed as soon as possible after death for fresh samples, family must be contacted, brain banks must be ready to receive samples etc.) to ensure the tissue is harvested in a timely enough fashion (which is already 4-24 hours later at best); consequently, fresh human *post mortem* brain tissue is exceedingly difficult to obtain[22]. Also Friedman et al. repeatedly allude to the negative impact of freezing on RNA extraction and quality [21]. Furthermore, *ante mortem* conditions such as agonal state and comorbidities are uncontrolled and vary greatly from case to case; cause of death may be unrelated to the condition of interest, as in the case with AD patients, where up to a third of a patients die from complications due to pneumonia[23]. For tumor or epilepsy resections a similar problem is present, though a "healthy" perimeter region is removed along with the diseased zone, it is difficult to verify that microglia isolated from these samples are truly "healthy/homeostatic" microglia, as there is no good reference point for what a healthy human microglia *is* as of course no one undergoes unprovoked brain surgery and *post*

mortem samples are faced with the issues stated above[24]. Beyond the benefits and consequences of exposure to the brain environment, it should not be overlooked that these human primary cultures are indeed *human* genetically, and therefore this model does not suffer from the considerable evolutionary divergence that impacts rodent studies [22].

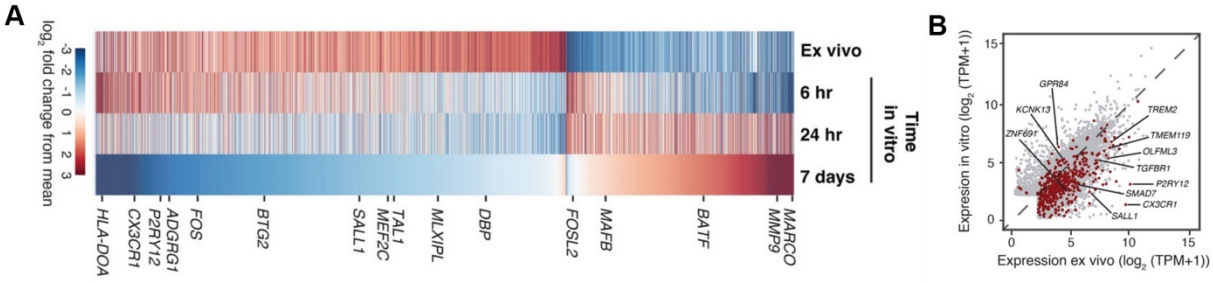

Figure 1. The influence of tissue culture environment and human microglial gene expression. (A) Primary human microglia rapidly change gene expression 6, 24 h and 7 days after transfer to culture environment. (B) After 7 days in vitro, many human microglia genes (red) are downregulated. (Adopted from Gosselin et al. 2017).

Human iPSC-derived Microglia

Despite the caveats with *in vitro* microglia research, such studies still remain an invaluable tool for conducting well-controlled experiments on human microglial genetics, function, metabolism, and disease mechanisms. For these reasons researchers have sought to further improve upon *in vitro* microglial models by methods to differentiate microglia from human induced pluripotent stem cells (iPSCs). Several such protocols have now been established, including an approach developed by our own lab[25-32]. Although these protocols vary in their details, most are similar in that they attempt to mimic microglial ontogeny by first driving iPSCs into a hematopoietic progenitor cell state. In our lab's protocol, these progenitors are then exposed to a combination of different cytokines and growth factors that are necessary for microglial survival,

differentiation, and maturation of homeostatic microglia, namely IL-34, M-CSF(CSF1), TGFβ, CD200, and CX3CL1 as highlighted in McQuade et al., 2018 (Figure 2). The use of iPSC techniques has in turn opened the door to a high degree of manipulability, especially through CRISPR/Cas9 gene modification. Using such approaches, researches can ask highly specific questions about the function of microglia-enriched AD risk genes and the impact of disease-associate genetic variants [33]. Our group and others have already begun to use CRISPR/Cas9 techniques to modify several microglial AD risk genes, assessing the effect of altering TREM2, MS4A6A, PLGC2, and APOE in human microglia[34]. iPSCs can also be derived from patients, allowing for analysis of the impact of risk factors within the greater genetic landscape where many different genes may work together to impact phenotype. Using patient derived lines also lends itself to translation and personalized medicine, where there is less risk for graft rejection. In a field that is ever pushing the evolution of therapies from “bench to bedside”, this should not be overlooked in the context of future therapeutics[35].

Despite the advantages of using *in vitro* iPSC-derived microglia to better understand human disease, the fact remains that these cells are still cultured and are vulnerable to the drastic transcriptional alterations that primary cultures face, highlighted by Gosselin et al., 2017. iPSC-derived microglia additionally suffer from decreased TMEM119 transcripts (a transmembrane, canonical homeostatic microglia protein), a gene that maintains comparable levels in primary cultures, and is likely reliant on some exposure to the brain environment for normal expression levels[19, 36]. 2D and 3D co-culture techniques have also been developed in order to better study the interactions between multiple cell types of the brain. iPSCs can be differentiated into neural

progenitor cells and introduced later to iPSC-derived microglia and maintained in traditional culture, or otherwise coaxed into a spherical 3D brain organoid through scaffolding or self-organizing[37]. These brain organoids can then be co-cultured with iPSC-derived microglia, or in some cases they have also been shown to spontaneously develop microglia, allowing for interactions between multiple cells of the brain[38, 39]. These techniques are a step closer to better representing the brain microenvironment, yet several important issues remain with both 2D and 3D co-cultures. For one, neural cells generated from iPSCs maintain a highly immature fetal-like phenotype, though 3D brain organoids slightly improve upon this deficit, organoid neurons also remain immature presenting a major issue when studying diseases of the aged brain, like AD[40]. Additionally, brain organoids typically possess no vasculature, meaning that there is insufficient nutrient flow throughout the structure, over time leading to a largely dead 'necrotic' core. Researchers attempting to study diseases of the aged brain then must make the trade for slightly more mature neurons for dead internal cells[41]. The lack of vasculature additionally means that there is no blood brain barrier (BBB), another structure implicated in AD and cerebral amyloid angiopathy (CAA), or vascular amyloid accumulations; though methods to model a more complete BBB *in vitro* are being actively developed[42, 43].

Though both beneficial and limiting parallels can be made between primary microglia cultures and iPSC-derived microglia, iPSC techniques appear to outperform primary cultures in practice, simply for the fact that primary microglia are so incredibly difficult to obtain and control for. However, a great deal of important and highly

informative research has been conducted in living rodent models, which do not endure many of the transcriptional consequences observed with *in vitro* studies.

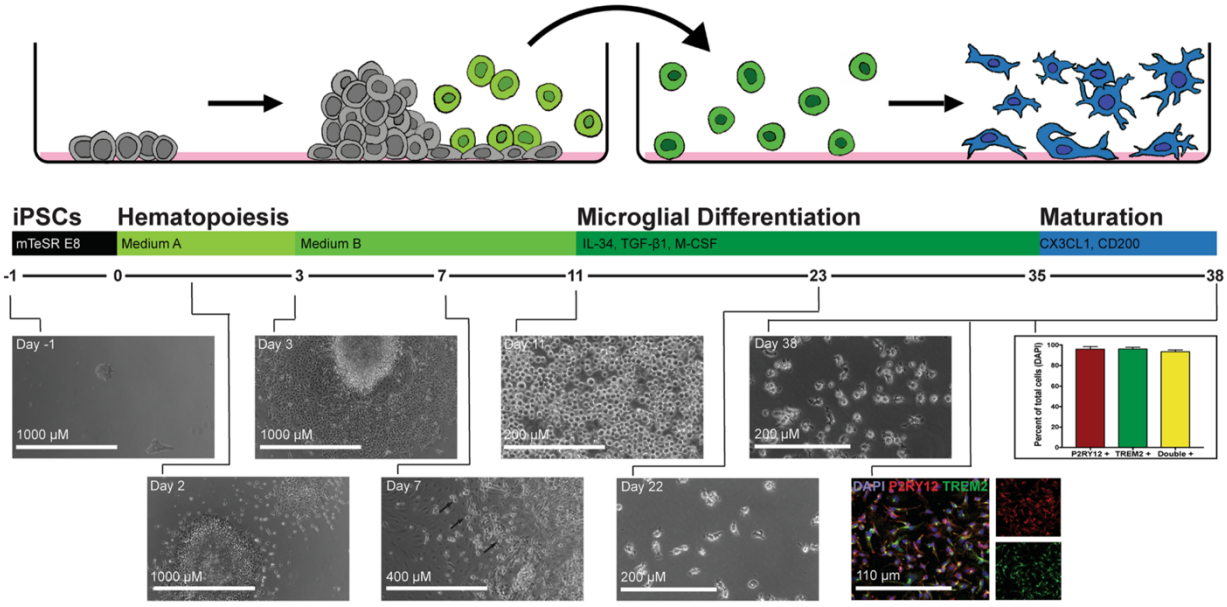

Figure 2. Microglial differentiation protocol from human iPSC. Schematic showing the process of differentiation from iPSCs through the mesoderm lineage (days 0–3) and further promoting hematopoiesis (days 3–11) using the StemDiff Hematopoiesis Kit. Primitive hematopoietic progenitor cells begin to appear on day 7 (black arrows) and by day 11 large numbers of round non-adherent HPCs are observed. Floating HPCs at this point can be harvested and frozen for transplantation or allowed to continue differentiation into microglia over 27 days. The last 3 days of microglial differentiation include additional neuronal and astrocytic ligands to further mimic the brain environment and by day 38 highly pure microglia that stain positively for both P2RY12 and TREM2 (> 94%) have been produced and are ready for *in vitro* experimentation (Adopted from McQuade et al. 2018).

In vivo Rodent Models

It is undeniable that we owe much of our current understanding of microglia dynamics to rodent models, where they have been observed to sculpt neuronal synapses during development, revealing their highly dynamic ability to survey their environment, and have been sequenced deeply to understand their transcriptional response to age, sex, region, health, and disease[3, 11, 12, 44, 45]. Through RNA-sequencing, researchers can glean a snap shot image of what transcriptional programs

a cell has in place for any number of manipulations allowing us to link genes with responses, though it should be noted that the presence of RNA does not always indicate the presence of protein. This is evident especially in the case of secreted proteins like complement protein C3, which exhibit high mRNA transcripts within microglia, yet very little protein is observed due to rapid secretion, with the reverse being observed in astrocytes[46, 47]. Another example of the disconnect between mRNA and protein levels in microglia is with regards to the gene/protein, Axl; a phosphatidylserine receptor that regulates phagocytosis of dead cells [6, 48, 49]. Axl protein is inversely correlated with its own mRNA levels, where Axl promotes upregulation of microRNAs that in turn promote downregulation of Axl mRNA, leading to relatively consistent protein levels and relatively low levels of mRNA[49].

Bulk and RNA sequencing from *in vivo* models have been exponentially used since their development and have vastly expanded upon the data originally collected via more rudimentary approaches such Northern Blots, reverse transcription quantitative PCR (RT-qPCR), and microarray. Briefly, RNA-seq involves isolation of RNA, optional poly(A) selection for mRNA and depletion of ribosomal RNA, and synthesis of cDNA for stability during the amplification process[50]. These procedures can be done at the whole tissue (Bulk) and single-cell level, each presenting their own pros and cons; where Bulk RNA-seq allows for in depth transcriptome analysis and return, and scRNA allows for analysis of multiple specific populations or subpopulations but at the cost of more superficial sequencing (capturing ~10% of the top expressed reads due to smaller amounts of starting material)[51].

In now seminal papers in the field, several groups have used sequencing to better characterize microglial transcriptomic responses to beta-amyloid. Keren-Shaul and colleagues have laid a particular claim to fame by coining the term “Disease Associated Microglia” or DAMs[6]. These researchers preformed scRNA-seq on CD45+ FACS sorted cells from 6 month old 5XfAD transgenic mice, a commonly used model of AD that that expresses five human familial AD gene mutations and develops amyloid beta plaques but not neurofibrillary tangles [52]. Keren-Shaul et al. identified three key sub-clusters of microglia; one large cluster of “homeostatic cells” and smaller AD enriched DAM1 and DAM2 clusters (Figure 3A). Although a larger amount of heterogeneity is likely evident in this work but not presented, sequencing by other groups have identified microglia splitting out into as many as 9 separate clusters) [53]. Interestingly, DAM clusters exhibit a marked downregulation of homeostatic microglia genes including P2ry12/P2ry13, Cx3cr1, and Tmem119 coupled with a pronounced upregulation of known AD-associated genes Apoe, Cstd, Lpl, Tyrobp, and Trem2. (Figure 3B)[54]. Keren-Shaul et al. further proposed that microglia proceed through stages, transitioning from homeostatic, to DAM1, and finally to DAM2 and went on to show that in mice this transition from DAM1 to DAM2 is in part dependent on TREM2 activation. DAM2 microglia present an interesting sub-cluster as they express higher levels of lipid metabolism (Lpl) and phagocytic genes (Cd9), and deeper assessment of these sub-clusters may reveal yet more transcriptional programs that define these cells and further reveal their function. The notion of ‘DAMs’ has become a cornerstone of research surrounding microglia and AD, however, the fact remains this study was performed in rodents, where considerable discrepancies between human and mice

transcription and protein homology exist (Figure 4)[55]. Indeed, Friedman et al. (2018), Mathys et al. (2019), Mancuso et al. (2019), and our own group in Hasselmann and Coburn et al. (2019) have all described key differences in the human and murine transcriptional response to amyloid.

Krasemann, Madore, et al. similarly identified a subset of microglia enriched in neurodegeneration (MGnD) by comparing microglia isolated from mouse models of ALS, AD, and MS (2017)[5]. These researchers found a cluster of homeostatic microglia, represented by canonical homeostatic genes like P2ry12, Cx3cr1, Tmem119, Tgfbr1, Tgfb1 and transcription factors Mef2a, Mafb, and Sall1. Likewise cluster2 or the MGnD cluster was represented by upregulation of inflammatory genes like Spp1, Itgax, Axl, and Apoe (Figure 3C). It was further found that MGnD microglia and the transition to MGnD was regulated heavily by induction of APOE and reduction of TGFβ signaling triggered by TREM2. Furthermore, a similar phenotype was observed in induced neurodegeneration models, where apoptotic neurons are injected directly into the brain of adult mice, indicating that the MGnD transcriptional profile is not restricted to a response to amyloid. Interestingly, Krasemann, Madore, et al. highlight Clec7a as an important surface maker and highly upregulated gene in MGnD microglia, but our own group has found this response to be unique to mouse cells[36]. These scRNA-seq studies have elucidated important alterations in microglia populations in AD conditions, skewing a subset of cells to a more inflammatory/phagocytic class apparently occurring in human AD as well. Taking a closer look at differentially expressed genes (DEG), however, one can easily pick out many genes that unique to either mouse or human

responses, reaffirming the need to study the human microglial response to AD pathology.

Another popular approach for studying the microglia dynamics *in vivo* is the use of endogenous CX3CR1 as a marker for microglia. For instance, the CX3CR1-GFP reporter line, where the coding part of the CX3CR1 gene is replaced by GFP has been incredibly useful for two-photon microscopy where heterozygous offspring display efficient marking of microglia[56]. Expression of CX3CR1-liked GFP remains visible during focal laser ablation, stroke conditions, and excitatory injury making the line ideal for use in imaging both homeostatic and inflammatory states[11, 57, 58]. Additionally, constitutive and inducible CX3CR1-Cre KO mice have been developed[56, 59, 60]. Crossing the constitutive CX3CR1-Cre (JAX Stock No: 025524) with any number of floxed strains can allow researchers to assess the effect of complete deletion or introduce new a new gene in CX3CR1 expressing cells (in the CNS these are primarily microglia). Similarly, these deletions or modifications can be inducible in CX3CR1-Cre/ER mice (JAX Stock No: 020940) when bred to floxed mice and after the delivery of tamoxifen. Unfortunately, many CX3CR1-Cre mouse lines experience a degree of leakiness into neurons, where there is apparent transient expression of CX3CR1 during development[59, 61].

Several groups have also crossed CX3CR1-GFP strains with various models of AD, to visualized microglial response to the accumulation of Aβ plaques in the superficial cortex and hippocampus. Jung et al. assessed if microglial initiation and recruitment to plaques is driven by the presence of plaques alone, or if an external distress signal is necessary as well (i.e. dying neurons) (2015)[62]. Researchers crossed

CX3CR1-GFP mice to APP-PS19(dE9) mice, a model of AD where Aβ plaques (but not tangles) can be seen starting at 6 months, and performed two-photon microscopy using Methoxy-X04 to label plaques (a derivative of congo-red that readily crosses the BBB with high specificity to fibular Aβ)[63, 64]. Jung and colleagues found that microglia take between 7 and 42 days to respond to the formation of plaques after identification, typically inducing a strong response and transition to activated/amoeboid microglial states. Based on these variable latency to response to plaques, these researchers claimed that an external cue is likely necessary to initiate microglial response, though this hypotheses warrants further study as Aβ has been shown to function as a TREM2 ligand and deletion of TREM2 alone can impair microglial migration to plaques[65].

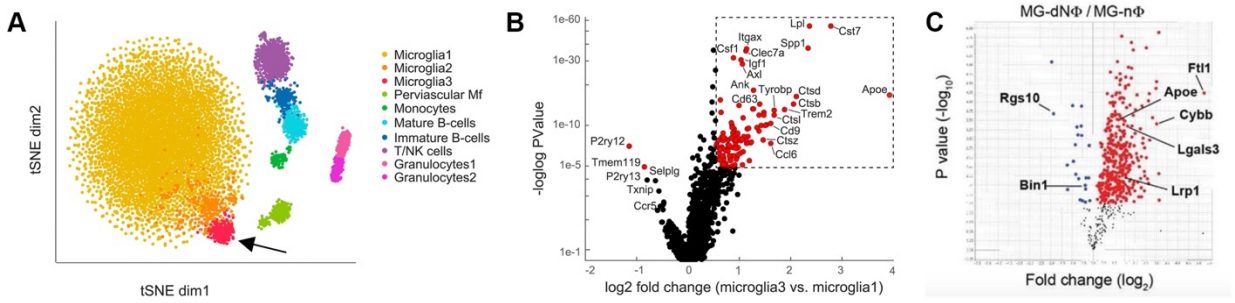

Figure 3. Disease Associated Microglia (DAM) and Microglial Neurodegenerative Phenotype (MGnD). (A) Subpopulations identified by single cell from 5XfAD mice, Microglia 2 and 3 are identified as the plaque responsive cells. (B) Volcano plot depicting log fold changes between the DAM (microglia 3) and homeostatic microglia (Adopted from Keren-Shaul et al. 2017). (C) These findings are similarly reported by Krasemann, et al. 2017 in their MGnD vs homeostatic comparison.

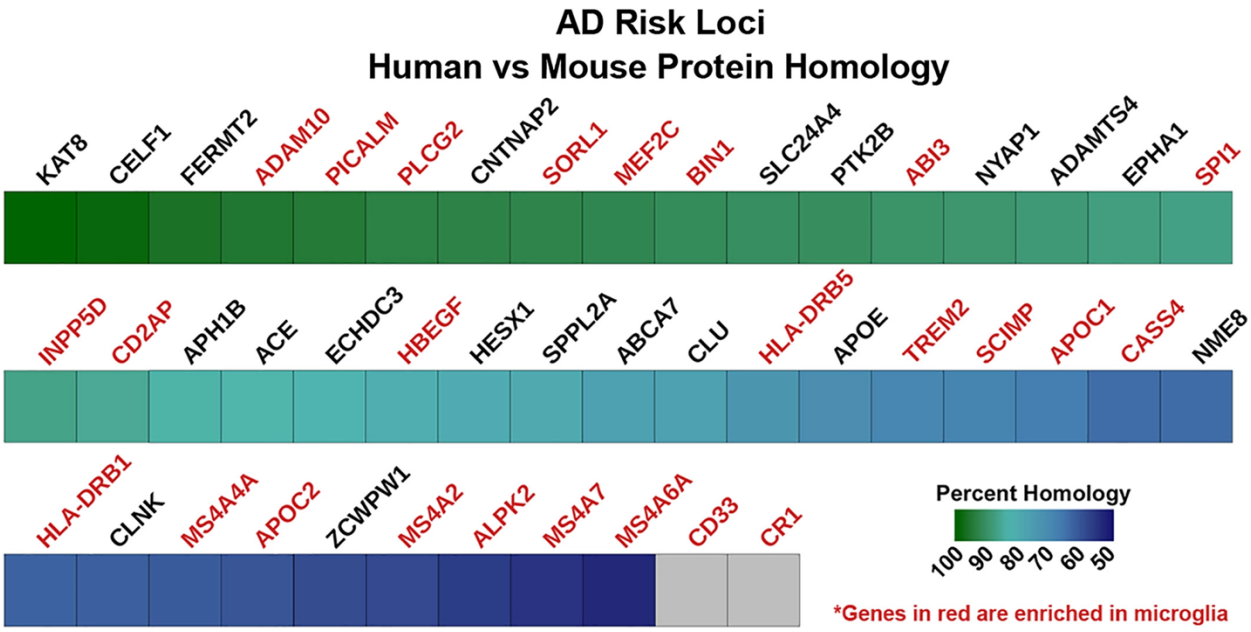

Figure 4. Homology between human and mouse proteins associated with Alzheimer's disease risk. Human amino acid sequences for genes associated with Alzheimer's disease GWAS-identified risk loci were compared to the homologous mouse proteins using NCBI's Homologene database. Genes in red are either highly or specifically expressed in microglia and gray boxes denote genes with no reliable orthologues in the mouse (i.e., <50% homology with any possible murine orthologue) (adopted from Hasselmann and Blurton-Jones, 2020[55])

B. Alzheimer's Disease and Microglia

Alzheimer's Disease (AD) is the leading cause of age-related dementia, effecting an estimated 5.8 million people in the United States alone[66]. Despite being characterized by Alois Alzheimer over 100 years ago, and clinical trials being conducted for decades we are left with only a handful of approved drugs that at best only modestly and temporarily improve cognition. With an estimated financial burden of over $350,000 *per patient* and a significant percentage of patient care placed on families, AD has become a devastating burden for our aging population. AD is a progressive neurodegenerative disease, characterized pathologically by the accumulation of amyloid beta (Aβ) plaques and neurofibrillary tangles caused by hyperphosphorylated Tau. Alzheimer's can generally be subcategorized into two types, familial or fAD—where

dominantly inherited mutations in three key genes: β-amyloid precursor protein (APP), presenilin 1 (PSEN1), and presenilin 2 (PSEN2) lead to early-onset AD, and the less well understood late-onset AD (LOAD) which is a sporadic form of the disease influenced by many genetic and environmental risk factors[18]. These risk factors can occur with varying commonality and risk in the general public, for instance, though fAD mutations are quite rare they are fully penetrant. On the other side of the spectrum LOAD is generally associated with relatively common polymorphisms, many of these being associated with immune and microglial functions, but conferring relatively small individual effects on disease risk ranging from 5-15% (Figure 5). Importantly, however, these common polymorphisms can combine to confer a greater risk of disease and recent genetic studies are beginning to develop polygenic risk scores that calculate the collective effect of these many genetic differences on overall disease risk[67]. The challenge of understanding the functional consequences of these many risk gene is a daunting endeavor. Yet, studying human microglia in which many of these AD risk genes are highly expressed, has therefore become a critical task.

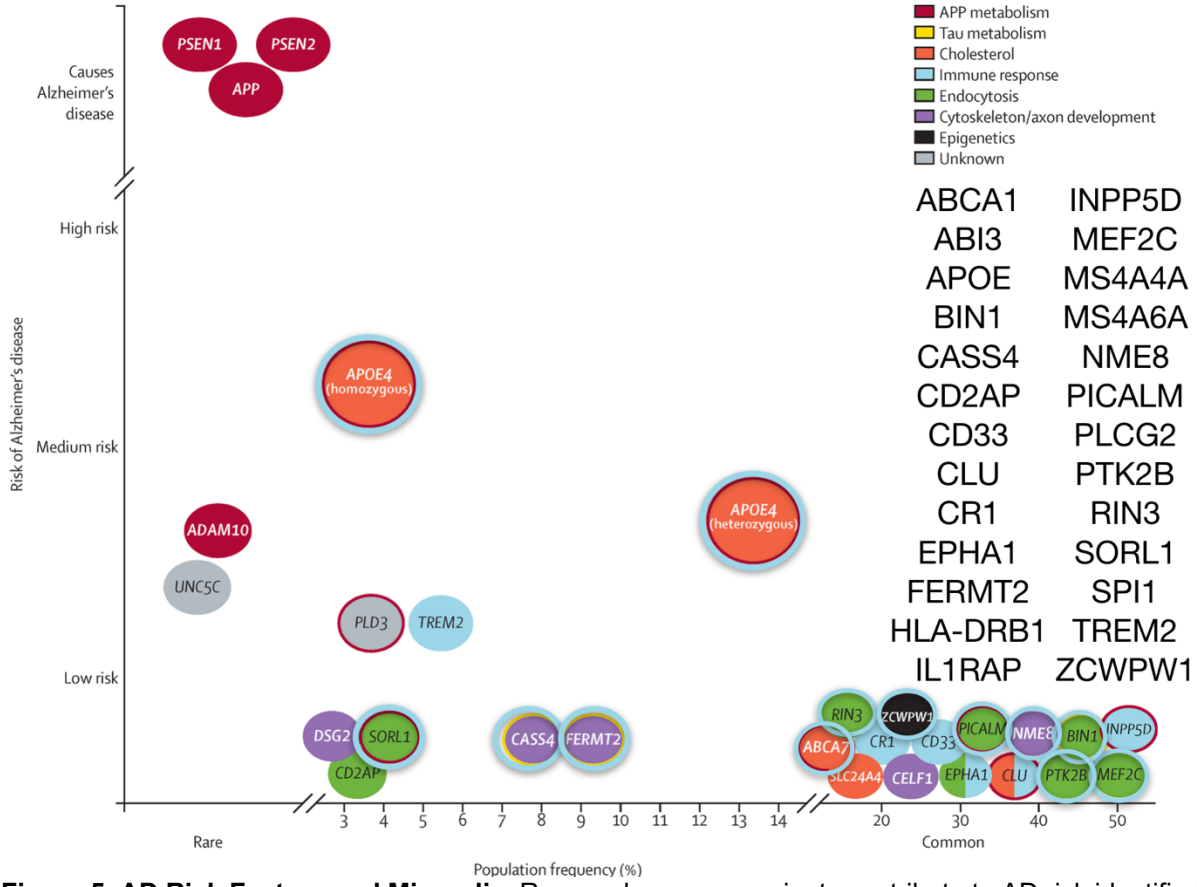

Figure 5. AD Risk Factors and Microglia. Rare and common variants contribute to AD risk identified by GWAS; genes highlighted in light blue relate to immune and microglial processes. Additional microglial enriched genes are listed. (Modified from *The Lancet* adopted from Karch & Goate, 2015.)

Key Microglial AD Risk Genes

Since the start of large-scale genome sequencing projects a growing number of microglia enriched genes and single nucleotide polymorphisms (SNP) have been found to be associated with risk or protection from AD. In turn these genes have begun to be associated with varied functions including lipid metabolism, antigen presentation, chemotaxis, phagocytosis, calcium signaling, and inflammation[8, 68]. I will now briefly discuss some of the key microglia genes that are being carefully examined by our group and many others: TREM2, APOE, MS4A6A, PLGC2, & BIN1.

TREM2

As of now coding mutations in TREM2 (triggering receptor expressed on myeloid cells), though relatively rare in human populations, represent the most well studied and characterized microglia genetic risk factor. TREM2 is a receptor expressed on multiple myeloid cells in the periphery but is enriched within microglia, where it is responsible for modulating immune responses through stimulating phagocytosis, mitigating proinflammatory signaling, and influencing chemotaxis[69, 70]. In humans, TREM2 variants that encode for the p.R47H or p.R62H mutation are associated with a 2-4 fold increase in risk of developing late-onset AD, the former being on par with the risk associated with harboring one *APOE*ε4 allele. Importantly, these variants which occur within the ligand-binding domain are hypothesized to be deleterious towards normal TREM2 function, suggesting that these key functional mutations influence AD through a partial loss-of-function. Precisely how these mutations impair microglia remains unclear, although recent studies by our group and others have shown that R47H mutations impair migration towards plaques in a similar fashion as TREM2 deletion[36, 71]. However, important differences between TREM2 coding mutations and complete loss-of-function mutations clearly exist as the later leads to a different neurodegenerative syndrome; Nasu Hakola disease, which is characterized by the formation of bone cysts and frontotemporal dementia[72].

TREM2 appears to affect migration towards plaques and other stimulants through ligand-receptor binding, where downstream signaling mediated by its adaptor protein, TYROBP/DAP12, stimulates phagocytosis, survival, and mobilization[72, 73]. Absence of TREM2 in microglia impedes their ability to phagocytose and alters their

gene expression signatures. In murine models, TREM2 has been shown to be unregulated in DAMs in a proximity-dependent manner to Aβ plaques, and knocking out TREM2 in the 5xfAD mouse leads to accelerated Aβ plaque formation and neuronal loss[6, 74, 75]. Thus, TREM2 appears to play a critical role in the response of microglia to amyloid plaques and approaches that try to increase TREM2 signaling could potentially provide therapeutic benefit.

APOE

Apolipoprotein E (*APOE*) is the strongest risk factor for LOAD and is one of several AD risk genes, including CLU, ABAC7, and SORL1, involved in cholesterol metabolism[76]. *APOE* encodes three common alleles (ε2, ε3, ε4), with *APOE*ε4 being associated with increased AD risk, where one *APOE*ε4 allele in associated with 3-fold increase in risk, harboring two *APOE*ε4 alleles increases AD risk by 12-fold[77, 78]. Conversely, *APOE*ε2 is associated with decreased risk for AD and later age at onset[77, 78]. This significant increase in risk coupled with the relatively high frequency in the population of the *APOE*ε4 allele, has led many researchers to examine the role of this protein in AD. Many important disease-associated changes have been attributed to APOE. However, in regards to microglia, our understanding of APOE biology is nascent with only a few simple observations such as the finding that APOE binding to Aβ can influence the clearance and aggregation of Aβ by microglia, and that APOE is upregulated in DAM microglia [6, 79, 80]. The effectiveness with which APOE is able to perform these critical functions is influenced by isoform and lipidation status of APOE, where *APOE*ε3 has greater affinity for Aβ and is more easily lipidated than *APOE*ε4,

and delipidated APOE significantly decreases affinity for Aβ[81]. These lipid associations are critical in understanding microglial interactions with APOE and Aβ as APOE mediates cholesterol efflux into microglia, facilitating delivery of Aβ to lysosomes and increasing the efficiency of degradation[82].

MS4A6A

Though Membrane-Spanning 4-Domains Subfamily A Member 6A (MS4A6A) Is one of the most significantly associated microglia-AD risk genes, the function of this protein is still largely unknown. Interestingly, one identified SNP, rs983392, is associated with lower transcript levels in the brain and with a reduced risk for AD[8]. Conversely, high levels of MS4A6A is associated with increased Braak tangle and plaque scores, indicating advanced disease pathology; these findings suggest that less MS4A6A may be protective in AD[83]. Our group has also found significantly increased MS4A6A expression in the 5X-MITRG “MHC-II” cluster, as MS4A6A has no mouse homologue this finding provides further support for the utility of this chimeric model. Some estimated functions of MS4A family proteins include mediating calcium influx, regulating endocytosis, trafficking, and signaling[84, 85]. Additionally, unpublished work from our lab has suggested MS4A6A is involved in microglial metabolism as RNA sequencing of MS4A6A knockdown lines revealed 10% of differentially expressed genes (DEG) categorized as mitochondria. Additionally, it was found that DEGs closely resemble those induced by inhibiting SYK kinase, which is involved in calcium release from the ER, and further supports a role for MS4A6A in calcium homeostasis published by others. As dysfunction in calcium homeostasis has been implicated in AD, better

understanding the role of this protein in microglial calcium signaling will likely provide important new information.

PLGC2

Another gene that exhibits protective SNPs against LOAD is PLCG2, that encodes the enzyme phospholipase C-gamma-2 (PLCγ2). PLCγ2 cleaves the membrane phospholipid PIP2 to secondary messengers IP3 and DAG which further propagate a wide range of downstream signals, including calcium release from internal endoplasmic reticulum stores[86]. PLCγ2 is additionally part of the cascade of signaling proteins that can be activated by TREM2 signaling, where receptor activation leads to SYK signaling and downstream PI3K activation which in can in turn influence PLCγ2 activity[87]. Though it is unclear the extent to which PLCG2 is involved in AD, functional characterization of the AD protective variant PLCγ2 p.P522R revealed a small increase in activity compared to the wild type enzyme[86]. Our group is currently using CRISPR-edited iPSC lines coupled with *in vitro* and *in vivo* approaches to better understand how PLCG2 influences microglial function in the context of AD pathology.

BIN1

Bridging integrator 1 (*BIN1*) is the second most statistically-significant gene associated with LOAD by GWAS studies, and as is the story with many other microglial-enriched risk factors, the exact function of this gene in AD is still largely unknown. However, it is known that BIN1 can regulate aspects of endocytosis and trafficking, immune response, calcium homeostasis, and apoptosis[18]. The SNPs in BIN1 are

associated with increased risk of LOAD, and one SNP, rs59335482, is associated with higher mRNA levels of BIN1 and elevated tau loads[88, 89]. Furthermore, BIN1 is linked to tauopathy, where BIN1 knockdown suppresses tau-induced toxicity in Drosophila[89]. BIN1 is also implicated in spreading tau pathologies as well, where over-expression promotes the release of tau filled extracellular vesicles *in vitro* and contributes to worsened of Tau pathology in PS19 mice[90]. Our group is currently collaborating with Dr. Nicole Coufal and the Gage Lab at UCSD, to transplant their iPSC and ES-derived isogenic BIN1 KO and WT HPCs into the 5X-MITRG, to better understand how BIN1 deletion influences human microglial interactions and responses to amyloid.

Interactions with Amyloid and Tau

Because we know the exact genetic mutations that cause degeneration in fAD, and that these mutations are highly penetrant, many mouse models of AD have been developed that utilize these rare fAD mutations, as is the case with the 5XFAD mouse. These models and the genetic risk conferred by mutations in APP, PSEN1, and PSEN2 (which increase the production of Aβ or more toxic Aβ42), strongly support the "Amyloid Cascade Hypothesis" which posits that accumulation of amyloid provides the initiating factor that leads to a cascade of pathological processes including neurofibrillary tangle formation, neuroinflammation, and degeneration"[91 92]. Although the Amyloid Cascade Hypothesis remains one of the most popular in explaining AD pathogenesis, therapies aimed at diminishing Aβ production or clearing Aβ plaques have thus far failed in late-stage clinical trials [93 94-96]. Therefore, there is an urgent need to examine alternative approaches that target other aspects of the disease.

The formation of Aβ plaques of course does not occur in a bubble, and though the process by which amyloid precursor protein is processed into amyloidogenic or non-amyloidogenic forms is well known, the initiation of new plaques is not well understood, though microglia have been implicated in the process several times. For example, Venegas et al. claim that deposition of amyloid-β involves NLRP-3 inflammasome-dependent formation of ASC-specks (apoptosis-associated speck-like protein containing a CARD (ASC)) in microglia (2017)[97]. Wherein initial Aβ plaques or other activation lead to a cycle of microglial activation of the NLRP-3 inflammasome and subsequent release of IL-1β and ASC fibrillar specks. These specks in turn bind to Aβ in the parenchyma causing aggregation and spreading of Aβ into plaques. Further evidence to support the idea that microglia are "seeding" plaques was recently presented by Spangenberg and colleagues (2019). In this study, the group performed early and long-term microglia ablation in 5XfAD mice using a CSF1R inhibitor and find that mice treated with the inhibitor exhibit almost no parenchymal plaques. Remarkably, these mice instead form CAA throughout the cortex strongly suggesting that microglia play an important role in the initial formation of plaques [16].

Though processes involving microglia and initial formation of plaques are unclear, the field has known for 3 decades that microglia migrate to, and express activation markers like HLA-DRB1 around existing plaques (their transcriptomic DAMs/MGnD response is also described under '*in vivo Rodent Models'*)[17]. Microglia also undergo a dramatic change in morphology, retracting their many processes and adopting an amoeboid shape. Examples of microglia that have internalized Aβ have also been shown in both mouse models and AD patient samples. and large plaques

recruit more microglia and decrease in size over time, all providing evidence of microglial Aβ phagocytosis or some other form of maintenance[98]. This maintenance has further been hypothesized to provide a mechanism of “plaque compaction,” wherein microglia surround and wall off large diffuse plaques into tight dense insoluble cores. In both mice and humans it has been found that loss of or mutations in TREM2 leads to less migration towards, and compaction of Aβ plaques, coupled with increased axonal dystrophy[99]. Though it should be noted that this increased dystrophy was seen alongside both diffuse and dense plaques of the TREM2 mutants compared to non-mutant AD cases, indicating a potential tangential protective role through TREM2 signaling, beyond the migration deficit alone.

In addition to Aβ pathology, neurofibrillary tangle (NFTs) represent the other major pathological hallmark of AD. In healthy neurons, tau protein is essential in assembly and stabilization of microtubules and tau phosphorylation is a key step in the regulation of this process[100]. In AD, tau becomes hyperphosphorylated and polymerizes into paired helical filaments (PHF) forming NFTs[101]. This phenomenon has proved difficult to study in rodent models as mice express only 3 isoforms of tau in contrast to the 6 human isoforms and mouse tau has important structural differences and resists conversion into a pathological state[102]. One approach to studying human tau dynamics in the murine brain is humanization so that only the human versions of tau isotypes are expressed, leading to tangle formation by 9 months[103]. Another widely used model, the Tau P301S PS19 mouse, was created by overexpressing human tau carrying a mutation that is associated with frontotemporal dementia. While this approach uses a

mutation that doesn't occur in AD patients, it leads to an age-dependent accumulation of tau into NFTs that closely resembles that of human AD tangles [104].

Although microglial response and interaction with amyloid beta plaques has been relatively well characterized (in partial due to the popularity of the Amyloid Hypothesis and to the prevalence of rodent amyloid models), the interactions of microglia with phosphorylated tau and neurofibrillary tangles are less well understood. It has been shown that murine microglia can internalize hyperphosphorylated pathological tau isolated from human AD tissue in vitro and eliminate NFTs on P301S slices, and furthermore this process is improved with anti-tau antibodies[105]. Microglia are also implicated in spreading tau pathologies as they are capable of phagocytizing seed-competent tau particles, however they do so inefficiently and will release these tau particles *in vitro*[106]. Interestingly, recent work from David Holtzman's group has shown that TREM2 deletion and mutations increase microglial tau seeding *in vivo*, suggesting that TREM2 may play an important role in the progression of both amyloid and tau pathologies[107].

Surprisingly, as RNA sequencing has become more and more popular in understanding microglia dynamics in AD, very few studies have been conducted to better understand microglial transcriptional responses to tau[46, 108, 109]. Matarin et al. lead one such study, presenting microarray data comparing microglial responses from whole brain lysates in rodent amyloid models (mutant human *APP*, *PSEN1*, or *APP/PSEN1*) and tau models (mutant human MAPT) at 4 timepoints (2, 4, 8, & 18 months) (2015). This study demonstrated that by 18 months of age, genes that overlap between amyloid and tau mice generally fall in the immune response category, those unique to amyloid

seemed to also fall within the immune response category, whereas those unique to tau mice aligned more closely with genes involved in DNA packaging (histone core, nucleosome) and in later stages, the zinc finger/BTB domain protein, ZBTB8A, stands out as unique. Notably several genes identified by GWAS as microglia enriched risk factors were uniquely downregulated in the tau group (Ms4a6d, Ptk2b/Pyk2B, and RIN3-Slc24a4). By performing network analysis, Matarin and colleagues also identified a similarity in hubs between the amyloid and tau group, mainly identifying complement genes as major hubs in both groups. Differences in hubs identified Trem2 as being unique to amyloid accumulation and Dectin-1 (Clecsf12), ccl4, ms4a6d, and lysozyme 2 gene (Lyz2) to name a few are enriched hubs in Tau pathologies (Figure 6). These findings indicate that both amyloid and tau drive strong murine immune responses, though important differences between the two are evident.

Complement activation in AD and tauopathy models was similarly reported by Liddelow et al. 2017 and Litvinchuck et al. 2018. The former finding that complement crosstalk between microglia and astrocytes in P301S mice, where C3 and C3aR1 mRNA and protein increase with age. Interestingly, deleting the microglial C3aR1 receptor abolished the C3 expression seen in neurotoxic astrocytes and improved tau pathology[46]. Litvinchuck et al. likewise found that PS19-C3aR1 KO mice exhibited an improvement in tauopathy and cognitive deficits and further report that C3aR1 is a regulator for immune pathway genes, with correlates seen in several human AD microglia-risk factors (*Abi3*, *Sall1*, *Spi1*, *Trem2*), immune response genes (*Bcl3*, *Gal3st4*, *Hla-Dqa1*, *Inpp5d*, *Lrrc25*, *Pycard*, *Sbno2*), and the complement pathway (*Clu*, *Ms4a6a*)[108]. Taken together, the findings from these two groups indicate

that microglial response to tau is likely to be skewed towards complement activation, although it is clear that further investigation of the human microglial response to tau is needed.

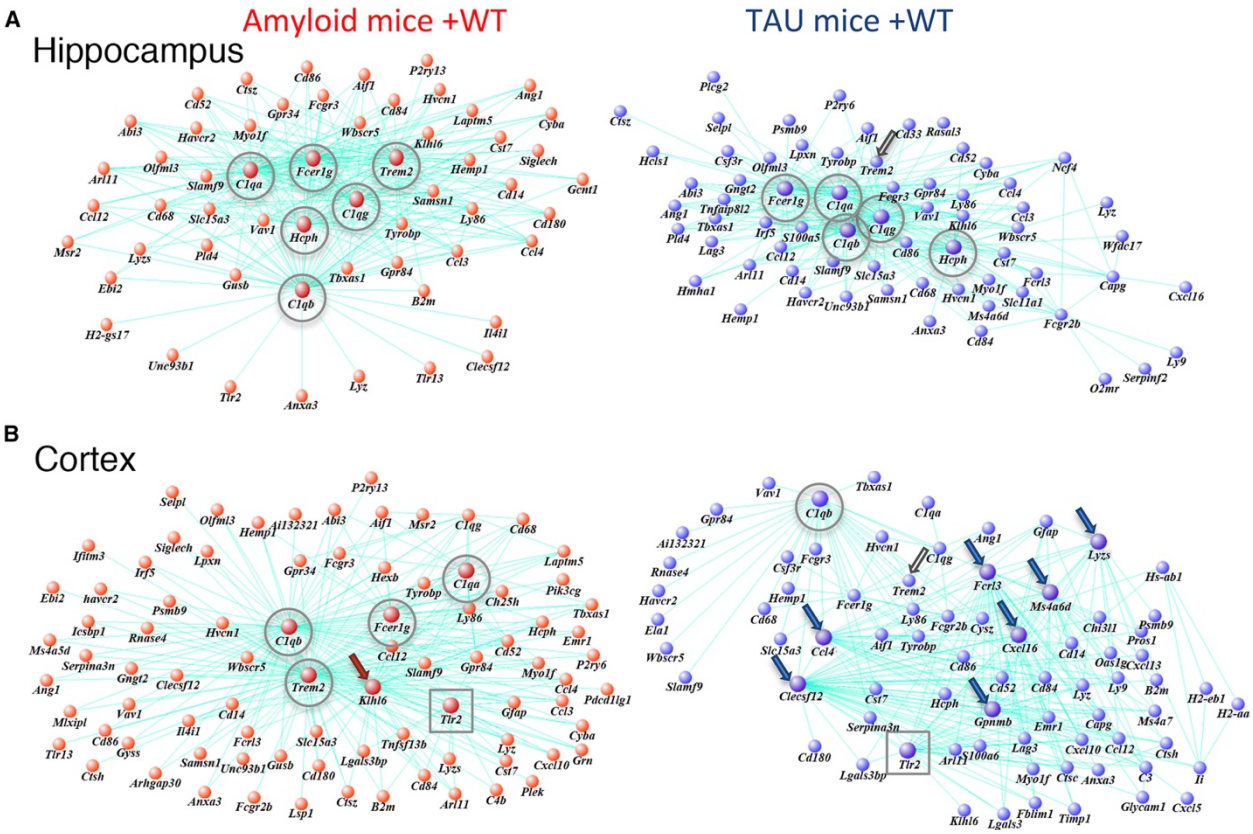

Figure 6. Network analysis of immune genes in amyloid and tau mice. Key drivers of the "immune" module (M1) described in Matarin et al. 2015 in amyloid and WT mice (left) and tau and WT mice (right). Lines between genes denote significate correlation in gene expression and larger circles indicate "hubs". Circles and squares represent hub genes preserved between brain regions and/or genotypes. Red and blue arrows indicate unique genes that have not achieved hub status in any other network plot. Open black arrow in right panels highlights nonhub *Trem2* evident in the tau group.

Differential Activation States

Microglia adopt and shift through different activation states as both a part of normal homeostatic function and as part of response to pathogen or disease[53, 110]. It is thus important to understand how these differential activation states influence microglial activity, one another, and the surrounding brain environment; knowing this can allow us

to better contextualize the cascading effects when gene expression is altered in one way or another. Here, I will discuss several of the microglial states relevant to health and especially AD:

Purinergic Signaling

Purinergic signaling has been implicated in neurodevelopment, neuronal-glial crosstalk, inflammation and more[111, 112]. The purinergic receptor family is divided into two subgroups: P1 are metabotropic receptors sensitive to adenosine and P2 receptors that are activated by ADP, ATP, UDP and UTP. P2 receptors are then further classified into P2X and P2Y, the former are ATP-gated ion channels, the latter are metabotropic G-protein coupled receptors that respond to purines and pyrimidines[113]. The ADP receptor P2RY12 is expressed almost exclusively by microglia in the brain and is often regarded as a homeostasis marker, regulating ramification and surveillance and is especially important for microglial-neuronal crosstalk[114].

Cserép and colleagues showed that P2RY12 receptors form dense clusters on microglial processes directly facing the neuronal potassium channel, Kv2.1, which are also characterized by increased mitochondria numbers and altered activity. In experimental stroke, microglia dramatically increase their neuronal coverage which is associated with delustering of neuronal Kv2.1 proteins and reductions in mitochondria numbers in a P2RY12-mediated fashion. Inhibition of P2RY12 lead to an increase in the area of functional disconnection after stroke as well as an increase in the infract volume. Authors propose here that healthy neurons release ATP and other signaling molecules at P2RY12/Kv2.1 junctions to communicate “well-being.” When proinflammatory stimuli

disrupt this connection, microglia are rapidly transitioned into a neuroprotective state wherein they restore neuronal function or isolate and phagocytose dying neurons[112]. Microglia have also been shown to effect neuronal electrical signaling where neurons will release ATP, which is then converted to ADP by microglial CD39 (and then AMP), which will bind to P2RY12, AMP is the converted into adenosine which is known to be a powerful anti-convulsant, sleep regulator, and inhibits neuronal excitability[115, 116].

In Alzheimer's disease, P2RY12 expression has been shown to be downregulated in proximity to amyloid beta plaques in both mice and huma AD patients, and our group further showed this to be the case for our chimeric microglial model [36, 117]. Interestingly, P2RY12 may work in conjunction with TREM2, where reports currently in review from our group show that *in vitro* TREM2 knock-out microglia show less acuity to changing extracellular ADP levels, suggesting that AD patients with TREM2 mutations may have downstream alterations to purinergic signaling. P2RY12 has additionally been reported to be downregulated in other inflammatory and neurodegenerative brain states including Multiple Sclerosis and Amylotrophic Lateral Sclerosis[113]. Interestingly, mice with genetically deleted P2RY12 show increased seizure sensitivity when exposed to kainic acid as well as reduced seizure-induced process extension, suggesting a potentially neuroprotective role[118]. Data later addressed in Chapter 2 suggests there may be a role for pathology-induced P2RY12+ microglia in Alzheimer's disease as well, where we show a unique Rod-like microglial phenotype expresses high levels P2RY12 and can be induced by Type 1 Interferons. Rod-like microglia are relatively understudied and the connection between this phenotype and P2RY12 expression has only been described once before in experimental TBI[119].

Purinergic signaling also clearly has a proinflammatory role with one example being through ATP activation of P2X7. The effect of local release of purines has been described above, where immunologically junctions make small adjustments as needed, on the other hand large quantities of extracellular purines may be a result from widespread trauma or disease[120]. Prolonged exposure to extracellular ATP induced P2X7-mediated pore formation which leads to a dramatic increase in intracellular Ca^{2+} and ultimately microglial cell death[121]. Furthermore, P2X7 induces inflammasome activation and IL1 family cytokine release, which hence leads to the following important discussion[121].

NLRP3 Inflammasome and IL-1β

The NLRP3 Inflammasome is a critical component of innate immune responses that mediated caspase-1 activation and IL-1β/IL-18 secretion in response to pathogen-associated molecular patterns (PAMPs) or damage-associated molecular patterns (DAMPs)[122]. The priming and activation of the inflammasome are summarized in Figure 7. In brief, Priming (Signal 1) involves NF-κB activation by IL-1β, TNF, or PAMPs induces expression of NLRP3 and pro-IL-1β. Then in Activation (Signal 2), NLRP3 is activated through a barrage of different stimuli which leads to Caspase-1 activation via proximity-induced autocatalytic processing upon recruitment to an inflammasome. Active caspase-1 then cleaves pro-IL-1β and pro-IL-18 into their mature and biologically active forms.

In AD, inflammasome activity has been linked to worsening pathological outcomes, where in NLRP3 KO or Caspase-1 KO APP/PS1 mice were largely protected

from reductions in spatial memory loss and show enhanced beta-amyloid plaque clearance[123]. ASC specks released by microglia have been implicated in seeding new plaques, where once secreted, ASC rapidly binds to extracellular amyloid beta and increase the formation of oligomers and aggregates[97]. Likewise ASC has been implicated in the seeding and spreading of Tau pathology in PS19 mice[124]. CX3CR1 deficiency has also been shown to reduce amyloid load in APP/PS1 mice, which is correlated with reduced expression of TNFα and CCL2 but curiously elevated IL-1β mRNA[125]. Though this form of inflammation may not always be villainized, building upon the previous section, excessive glutamate release in epilepsy triggers CX3CL1 release from neurons, in turn binds to microglial CX3CR1, inducing IL-1β release which then stimulates neuronal dendrites to release ATP, in turn activating purinergic signaling and microglial process convergence[126]. Additionally, more neuronal death was induced in microglial ablated mice in response to excitotoxin-induced retinal damage, and IL-1β stimulated the proliferation and reactivity of microglia in response to excitotoxin[127]. These studies suggest that IL-1β may have a neuroprotective role in models of excitotoxicity but a potentially damaging role in AD pathologies.

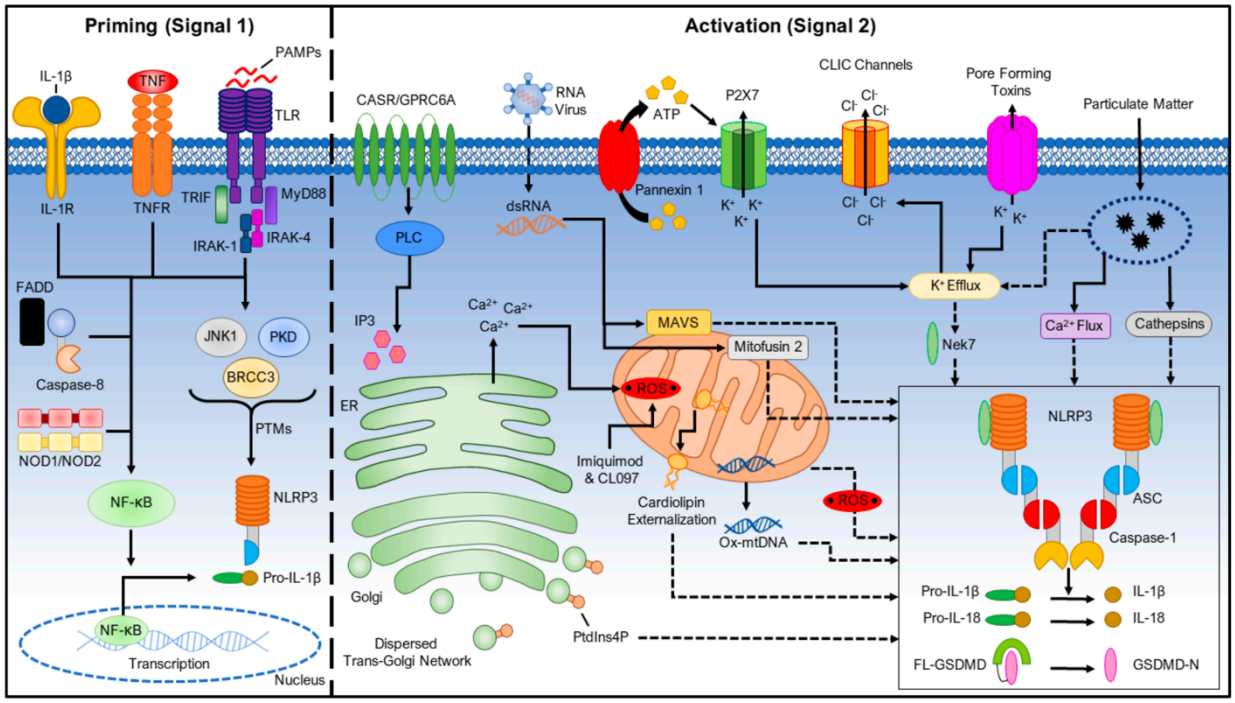

Figure 7. A Two-Signal Model for NLRP3 Inflammasome Activation. In brief, Priming (Signal 1) involves NF-κB activation by IL-1β, TNF, or PAMPs induces expression of NLRP3 and pro-IL-1β. Then in Activation (Signal 2), NLRP3 must be activated through barrage of different stimuli and Caspase-1 is activated via proximity-induced autocatalytic activation upon recruitment to an inflammasome. Active caspase-1 then cleaves pro-IL-1β and pro-IL-18 into their mature and biologically active forms. (Schematic adopted from Kelley et al., 2019.)

Interferon Responses

Type 1 (IFNα and IFNβ family) and Type 2 (IFNγ) Interferons (INFs) play a key role in activating early innate immune responses to viral and bacterial infections[128]. Peripherally, Type 1 IFNs are produced by inflammatory monocytes, and activate a variety of innate immune cells such as natural killer (NK) cells, macrophages and dendritic cells[129]. IFNγ on the other hand serves to bridge the innate and adaptive immune systems, and is produced by primarily by T cells and natural killer cells[129, 130]. Here, I will delve into Type 1 Interferon responses for its relevance to Chapter 2 and AD microglial responses in general.

In the brain, Type 1 Interferon signaling has been associated with neuroprotective functions. For instance, neurons will produce Type 1 IFNs during viral infections and launching a sufficient Type 1 Interferon response early on in viral infection improves neuronal survival[131-133] Additionally, exogenous IFNβ induces upregulation of CCL4 which may confer neuroprotection in HIV infection[132]. Type 1 IFNs have likewise been found to have neuroprotective effects in experimental prion models and pretreatment with recombinant IFNs inhibits prion propagation in infectious cells and animals[134]. This pretreatment may be necessary in some parts to confer protective effects however, as Type 1 IFNs can suppress the functions it enables, in *listeria monocytogenes* infection early treatment with IFNβ initiates NK response and clearance of infection, where the natural IFNβ release 24 hours later suppresses NK cells[128]. Type 1 IFNs can be suppressive of macrophages, where their presence downregulates IFNGR1 making them less responsive to IFNγ, in *L. monocytogenes* this effective exacerbates systemic infection[135]. This suppressive phenotype has been described in human Tauopathy patients where microglia shift from a “pro-inflammatory” TLR response to an “immune-suppressive” Type I IFN response, as signatures of the disease shift from peptides to nucleotides[110]. It appears that Type 1 Interferons can also suppress inflammasome activity, IFNβ can reduce the amount of IL-1β secreted by cultured iPSC derived microglia in the presents of fibrillar Aβ[110]. Likewise in models of bacterial infection, IL-1 family cytokines can inhibit the production of IFNα/β[130].

On the other hand, Type 1 Interferons have been associated with synapse loss and neuropsychiatric symptoms. In systemic lupus erythematosus, an elevated IFNα profile has been associated with mild cognitive impairment, fatigue, depression, and

psychosis; systemic recombinant IFNα lead to microglial phenotypic changes and upregulation of C4b which authors hypothesize may play a role in aberrant synaptic pruning[136]. Likewise, Type 1 Interferon responses have been reported in AD patients and in models, and treatment with recombinant IFNβ leads to synapse loss[110, 137, 138]. One proposed initiator of Type 1 IFN signaling is extracellular nucleotides, seen in middle-stage FTD patients as degeneration occurs[110]. DNA in the extracellular space sends off alarm signals to the immune system, resembling viral double stranded DNA, cyclic GM-AMP cyclase can bind to extracellular DNA and trigger downstream antiviral/Type 1 IFN responses[139]. Similarly, cytosolic damaged DNA is sensed through the stimulator of interferon genes (STING) pathway and leads to a Type 1 Interferon Response[140]. Despite these findings, the role of Type 1 IFN responsive microglia in AD is still unclear, data discussed in Chapter 2 may provide new microglial subtypes to be further explored.

In typical aging, Type 1 IFNs are upregulated and overexpression of IFNβ leads to cognitive decline and increases a microglia “ageing” phenotype characterized by upregulated B2M (MHCI protein) and C4b (complement protein)[141]. Furthermore, Type 1 signaling is negatively correlated with Mef2C expression, and lose of Mef2C in mice increases levels of inflammatory cytokines and produces social behavioral deficits in immune challenged mice, but not in Mef2C KO alone[141]. These studies suggest increases in Type 1 IFNs in normal aging may contribute to a brain state that is more vulnerable to inflammatory stimuli. Interestingly, microglial Type 1 Interferon mediated synaptic alteration might be an aspect of repairing connectivity, a fascinating manuscript uploaded on Biorxiv describes the role of IFITM3+ phagocytic microglia in barrel cortex

remapping after whisker lesioning, these data open the door for more research into the role of Type 1 IFN responsive microglia in cortical remapping during learning[142]. Type I interferon Responses may be a classic story of antagonistic pleiotropy, where activity in the young brain promotes remapping and protects the brain from viral infection but as the brain ages these processes bleed into chronic Type 1 IFN signaling with negative behavioral outcomes.

Antigen Presentation and Interactions with T cells

Regulation of the genes encoding major histocompatibility complex (MHC) class I and II proteins (known as human leucocyte antigen-HLA in humans), and their accessory molecules is critical for effective adaptive immune responses[143]. For brevity and relevancy, MHCII processes will be described here for their relevance in AD and as microglia, MHCI proteins are more involved with autoimmunity and will thus be left for other to delve into. Antigen presentation is the process by which antigenic epitopes are processed and presented on antigen presenting cells (APCs). In the case of exogenous antigen and MHCII, antigen captured via pathogen recognition receptors (PRRs), phagocytosed and then encompassed vesicles which eventually fuse with the lysosome. The increasingly acidic environment allows proteases to activate and degrade antigen into peptide fragments, these peptides then bind to MHCII complexes and are trafficked to the cell membrane[143, 144]. In the brain parenchyma, microglia are the main antigen presenting cells and thus play an important role in adaptive immune activation. Microglia have been known for decades to increase expression of MHCII molecules such as HLA-DR around amyloid beta plaques[145]. More recently, numerous GWAS have identified single-nucleotide polymorphisms within several MHCII genes,

including *HLA-DRB1 and HLA-DRB5*, to be risk factors for Alzheimer's disease, outlining their importance in AD [146, 147].

On the other side of antigen presentation, T cells have been implicated in many neurodegenerative and neuroinflammatory states, out group has shown that immunodeficient 5XFAD mice show expanded amyloid pathology compared to immune competent controls[148]. Genetic predisposition coupled with T cell infiltration after injury has been shown to have protective effects against progressive neurodegeneration after optic nerve injury or toxic glutamate excitotoxicity, more degeneration is seen in strains previously shown to be "resistant" to experimental autoimmune encephalomyelitis (EAE) after neonatal thymectomies than WT counterparts, though this effect is not seen in "susceptible" strains[149]. This neuroprotection after injury is conferred through myelin reactive T helper type 1 (Th1) cells interacting with CD4+ T cells[150]. In actual EAE, IFNγ-secreting Th1 cells and CD4+ IL-17-secreting cells termed Th17 cells have been shown to have a pathogenic role in EAE[151]. Both Th17 and or Th1 cells enhance proinflammatory cytokine production (IL-1β, TNFα, and IL-6), MHCII expression, and costimulatory surface receptors in microglia (CD40 and CD80)[151].

Microglia can also suppress T cell action as well as mirror some inhibitory actions exhibited by T cells. Engagement of PD-1 on microglia, typically recognized as potent co-inhibitory receptor on T cells where stimulations reduce cytotoxic behaviors, has been found to reduce infract volume, recruitment of peripheral inflammatory cells, activation of MHCII+ and TNFα+ microglia, and neurological deficits in models of experimental stroke[152]. These studies suggest there is a delicate balance between T cell mediated repair or progressive damage in the CNS, and regulation of microglial

MHCII expression can mitigate damage. Type 1 IFN responses suppress Th17 cell action in a microglia mediated fashion by inhibiting intracellular Osteopontin expression, a gene upregulated in AD, and thus increasing secretion of the Th17-inhibiting IL-27[153, 154]. Interestingly, both Type 1 and Type 2 Interferon signaling can increase expression of MHCII molecules, in data discussed in Chapter 2, we show that Type 1 Interferon responsive microglia also show an interesting perinuclear expression pattern of HLA-DR[128]. More research into microglial and T cell interactions is an active area of research in our group and others, where more and more studies have shown alterations in MHCII proteins in AD and much more is yet to be discovered in the interplay between the innate and adaptive immune systems in the CNS.

CHAPTER 1

Development of a Chimeric Model to Study and Manipulate Human Microglia In Vivo

Morgan A. Coburn, Jonathan Hasselmann, Whitney England, Dario X. Figueroa Velez, Sepideh Kiani Shabestari, Christina H. Tu, Amanda McQuade, Mahshad Kolahdouzan, Karla Echeverria, Christel Claes, Taylor Nakayama, Ricardo Azevedo, Nicole G. Coufal, Claudia Z. Han, Brian J. Cummings, Hayk Davtyan, Christopher K. Glass, Luke M. Healy, Sunil P. Gandhi, Robert C. Spitale,
and Mathew Blurton-Jones

Introduction

Microglia play critical roles in sculpting brain development, modulating neural plasticity, and maintaining homeostasis[155-157]. As the primary immune cell of the CNS, microglia are highly responsive, reacting rapidly to local injury, neuroinflammation, and a multiplicity of brain pathologies[12, 158]. Recent genetic studies have further highlighted the importance of these cells in disease, with the discovery of many polymorphisms in microglial-eniched genes that are associated with a variety of neurological disorders including Alzheimer's disease (AD), frontotemporal dementia, amyotrophic lateral sclerosis, autism, and schizophrenia[155, 159]. However, despite these important findings, experimental platforms that enable systematic analyses of human microglia *in vivo* and the effects of genetic variability on microglia function within the brain have yet to be realized.

While transgenic mouse models have provided invaluable tools for examining the role of microglia in these disorders, rodents cannot fully recapitulate the growing complement of hu- man genetic variability implicated in these polygenic diseases[21, 29, 160]. Fortunately, the ability to generate induced pluripotent stem cells (iPSCs) from patients and then differentiate iPSCs into defined cell subtypes has generated exciting opportunities to examine the relationships between complex genetic backgrounds and disease-associated phenotypes. The recent development of methods to differentiate iPSCs into microglia has further allowed researchers to begin unraveling the contribution of microglial risk genes to human disease[26]. Yet, while these protocols have provided researchers with the ability to generate an abundance of human microglia *in vitro*, a recent study has highlighted that microglia, as highly plastic cells undergo

dramatic alterations when maintained outside of the brain environment, exhibiting numerous changes in gene expression within hours to days of transfer to culture conditions[19]. Unfortunately, many of these *in vitro*-related transcriptional programs are mirrored in iPSC-derived microglia (iMGLs), demonstrating an important limitation to the modeling of microglial biology in a cell-culture environment. Overall, this suggests that experiments utilizing *in vitro* microglia to model disease states may present an incomplete picture of their genetic state or how they respond to stimuli, presenting a major roadblock to a deeper and more complete understanding of *in vivo* microglial biology.

To begin to address this challenge, we and others performed initial experiments to determine the feasibility of transplanting human microglia or hematopoietic stem cells (HSCs) into the brains of immunodeficient mice[25, 27, 161, 162]. Yet, to date no studies have thoroughly examined and validated the phenotype, transcriptional profile, and functional responses of engrafted human microglia to injury or disease-associated pathology, steps that are critical for determining the suitability of this approach for studying *in vivo* microglia biology. Toward this goal, we present the development and validation of a chimeric model system that allows researchers to examine iPSC-derived human microglia in the context of the living mammalian brain.

Materials and Methods

Animals

All animal procedures were conducted in accordance with the guidelines set forth by the National Institutes of Health and the University of California, Irvine Institutional Animal Care and Use Committee. The MITRG mouse was purchased from Jackson Laboratories (stock #017711); this BALB/c/129 model includes two knockouts alleles, Rag2 (Rag2 tm1.1Flv), γc (Il2rg tm1.1Flv), and three humanized knockin alleles, M-CSFh (Csf1 tm1(CSF1)Flv), IL-3/GM-CSFh (Csf2/Il3 tm1.1(CSF2,IL3)Flv), TPOh (Thpo tm1.1(TPO)Flv). The related and parental M-CSFh mouse line was also purchased form Jackson Laboratories (stock # 017708) and contains Rag2 and Il2rg deletions and humanized M-CSFh. The 5xFAD-MITRG model was created by backcrossing the MITRG mouse with 5xFAD mice which overexpress co-integrated transgenes for Familial Alzheimer's Disease (FAD) mutant APP (Swedish, Florida, and London) and mutant FAD PS1 (M146L and L286V). Progeny of these pairings were then genotyped and backcrossed with MITRG mice to return the 5 MITRG genes to homozygosity and maintain the APP/PS1 transgenic loci in the hemizygous state, resulting in the MITRG5x ($Rag2^{-/-}$; $\gamma c^{-/-}$; M-CSF h ; IL-3/GM-CSF h ; TPO h ; Tg(APPSwFlLon,PSEN1*M146L*L286V)6799Vas). To generate mice that lacked M-CSFh but included GM-CSFh and TPOh, MITRG mice were crossed with M-CSFh mice and then F1 progeny were crossed and genotyped to select mice that lacked either both or one copy of M-CSFh. For 2 photon living-imaging of mouse microglia, the CX3CR1-GFP (B6.129P2(Cg)-Cx3cr1 tm1Litt /J; stock # 005582) mouse was used. All mice were age and sex matched and group housed on a 12h/12h light/dark cycle with food and water ad libitum.

Acquisition and maintenance of iPSC lines

iPSC lines were purchased from Coriell and the European Bank for induced pluripotent Stem Cells. The GFP cell line (Coriell, AICS-0036) was generated by CRISPR modification of the line WTC11 to insert a monoallelic mEGFP into the AAVS1 safe harbor locus (chromosomal location 19q13.4-qter) under the control of a CAGG promoter. The WT iPSC line (EBisc #BIONi010-C) was modified by CRISPR gene editing to generate the TREM2 R47H isogenic iPSC line (EBiSC #BIONi010-C-7). Maintenance of all iPSC lines involved culturing in feeder-free conditions in complete mTeSR E8 medium (StemCell Technologies, Inc.), in a humidified incubator (5% CO_2, 37°C), with medium changed daily. Passaging was performed every 7-8 days using ReLeaSR (StemCell Technologies, Inc.) and cells were plated onto 6-well plates (Corning), coated with growth factor-reduced Matrigel (1mg/mL; BD Biosciences), in mTeSR E8 medium, supplemented with 0.5uM Thiazovivin (StemCell Technologies, Inc.) for the first 24 h post-passage. All cell lines were tested for mycoplasma on a monthly basis, and confirmed to be negative, and cell line karyotyping was performed every ten passages.

Differentiation of Hematopoietic Progenitor Cells and in vitro Microglia from iPSCs

iHPCs and iPS-microglia were differentiated according to the protocol published by McQuade et al. (2018). To begin iHPC differentiation, iPSCs were passaged in mTeSR-E8 to achieve a density of 80 colonies of 100 cells each per 35mm well. On day 0, cells were transferred to Medium A from the STEMdiff Hematopoietic Kit (Stem Cell

Technologies). On day 3, flattened endothelial cell colonies were exposed to Medium B and cells remained in medium B for 7 additional days while iHPCs began to lift off the colonies. On day 10, non-adherent CD43+ iHPCs were collected by removing medium and cells w`ith a serological pipette. At this point, d10-d11 iHPCs can be frozen in Bambanker (Wako). Cells used for early-postnatal iHPC transplantation were thawed in iPS-Microglia medium (DMEM/F12, 2X insulin-transferrin-selenite, 2X B27, 0.5X N2, 1X glutamax, 1X non-essential amino acids, 400 mM monothioglycerol, and 5 mg/mL human insulin freshly supplemented with 100ng/mL IL-34, 50ng/mL TGFb1, and 25 ng/mL M-CSF (Peprotech)) and allowed to recover for 24 h, then resuspended at 62,500 cells/uL in 1X DPBS (low Ca 2+ , low Mg 2+). Cells utilized for in vitro experiments continued microglial differentiation for 28 days. During the last 3 days in culture, 100ng/mL CD200 (Novoprotein) and 100 ng/mL CX3CL1 (Peprotech) were added to mature microglia in a brain-like environment.

Early Postnatal Intracerebroventricular Transplantation of iHPCs

P0 to P1 MITRG mice were placed in a clean cage over a heating pad with a nestlet from the home cage to maintain the mother's scent. Pups were then placed on ice for 2-3 min to induce hypothermic anesthesia. Free-hand transplantation was performed using a 30-gauge needle affixed to a 10 mL Hamilton syringe, mice received 1 mL of iHPCs suspended in sterile 1X DPBS at 62.5K cells/mL at each injection site (8 sites) totaling 500K cells/pup. Bilateral injections were performed at 2/5 th of the distance from the lambda suture to each eye, injecting into the lateral ventricles at 3mm and into the overlying anterior cortex at 1 mm, and into the posterior cortex in line with the forebrain

injection sites, and perpendicular to lambda at a 45° angle (Figure 1.1B). Transplanted pups were then returned to their home cages and weaned at P21.

Adult intracranial transplants

All mouse surgeries and use were performed in strict accordance with approved NIH and AALAC-certified institutional guidelines. Direct bilateral intracranial injections of WT iMGL into the cortex and hippocampus were performed on adult MITRG mice. Briefly, adult mice (3 months old) were anesthetized under continuous isoflurane and secured to a stereotaxic frame (Kopf), and local anesthetic (Lidocaine 2%) was applied to the head before exposing the skull. Using a 30-guage needle affixed to a 10 mL Hamilton syringe, mice received 2 mL of mature iMGL suspended in sterile 1X DPBS at 50,000 cells/mL at each injection site. Transplantation was conducted bilaterally in the cortex and hippocampus at the following coordinates relative to bregma: anteroposterior, -2.06 mm; dorsoventral, -1.75 mm (hippocampus), -0.95 mm; mediolateral, ± 1.75 mm. Cells were injected at a rate of 50,000/ 30 s with 4min in between injections. The needle was cleaned with consecutive washes of PBS, 70% (vol/vol) ethanol, and PBS in between hemispheres and animals. Animals were allowed to recover on heating pads before being placed in their home cages and received 2 mg/mL Acetaminophen (Mapap) diluted in water for five days. Animals were perfused 2 months following surgery with 1X PBS followed by 4% paraformaldehyde, entire brains were removed for immunohistochemistry.

Immunohistochemistry and Confocal Microscopy

Animals were administered Euthasol and monitored for loss of consciousness. Once animals no longer responded to toe pinch, mice were intracardially perfused with ice cold 1X DPBS. If xMGs were being isolated from ½ brains, the remaining half brain was drop fixed in 4% (w/v) PFA for 48 h, otherwise, the mice were intracardially perfused with 4% PFA and post-fixed for 24 h. Samples were then cryoprotected in 30% (w/v) sucrose until the tissue sank in the solution. Brains were then cut either coronally or sagittally at a section thickness of 40um on a sliding microtome cooled to -79°C. Tissue sections were collected as free-floating sections in PBS with and 0.05% sodium azide. For staining, tissue was blocked for 1 h in 1X PBS, 0.2% Triton X-100, and 10% goat or donkey serum. Immediately following blocking, sections were placed in primary antibodies diluted in 1X PBS and 1% goat or donkey serum and incubated overnight on a shaker at 4°C. Sections were then incubated in conjugated secondary antibodies for 1 h, before washing and mounting on microscope slides. Immunofluorescent sections were then visualized and captured using an Olympus FX 1200 confocal microscope. In some cases, brightness and contrast settings of confocal images were slightly adjusted to reveal fine structures and morphology. Importantly, no such changes were made to any images used for quantification.

Quantification Percent xMG Engraftment

For analysis of xMG engraftment and its reproducibility, two separate preparations of iHPCs (HPCs #1; n = 4 & HPC #2; n = 4) were transplanted as described above, on separate days, and perfused at 2 months. Brains were section sagittally and stained

with Ku80 (human nuclear marker) and PU.1 (myeloid nuclear marker). The Allen Brain Atlas was used to identify regions where, 4, 40x images per region were captured (Somatosensory Cortex: CTX; Hippocampus: HIP; and Striatum: STR), all images were acquired using identical settings with an Olympus FV1200 scanning laser confocal microscope. Using the ‘‘Spots’’ function in IMARIS software (Bitplane) total Ku80+ and PU.1+ spots were quantified separately. Then total human cells (all Ku80+ spots) and total mouse cells (all PU.1 positive spots minus total number of Ku80+ spots) were determined. Total percentage of human cells was then found by dividing total human cells by mouse cells and multiplying by 100. To determine any significant interactions between transplantation preparation and brain region a 2-way ANOVA was run using Prism 7 (Figure 5).

Antibody Immunoreactivity after systemic LPS Treatment

For analysis of antibody immunoreactivity all images for a given antibody were acquired using identical settings with an Olympus FV1200 scanning laser confocal microscope, then analyzed using the image processing package FIJI, a distribution of NIH ImageJ software. Images were first split into single channels (GFP and P2RY12) and thresholded to create a mask around cells. The resulting mask was then overlaid onto the original images and mean intensity values were measured within the ROI. For normalization, human cells were hand counted in the GFP channel and mean intensity was divided by total cell counts, then divided by the saline mean values. For analysis of CD45 immunoreactivity, IMARIS ‘‘Surfaces’’ function was used to detect CD45 immunoreactivity, then mean intensity values within CD45+ surfaces were measured.

For normalization, intensity values for each animal were divided by the saline mean values. Normalized intensity values for all antibodies were tested for statistical significance ($p < 0.05$) though unpaired t test using Prism 7 (n = 5 LPS; 4 Saline).

Plaque Proximity and Total Plaque Area

To examine the impact of the TREM2 R47H mutation on plaque migration, iHPCs derived from isogenic wild-type and R47H mutant iPSCs (EBiSC # BIONi010-C and #BIONi010-C-7) were transplanted into P1 5X-MITRG mice. 9-months later, immunohistochemistry was performed, and confocal Z stacks collected within the Piriform Cortex at 40x magnification using identical confocal settings (n = 3 mice per TREM2 genotype). Human microglia numbers and locations were detected and quantified through Ku80 immunofluorescence using the ‘‘Spots’’ function in IMARIS software. IMARIS based quantification of human microglial proximity to plaques was done by first identifying Ab plaques using the ‘‘Surfaces’’ function, then using the ‘‘Spots close to Surfaces’’ MATLAB extension (threshold set to 10 mm). Total plaque area was measured from sum of surfaces for each image. Proximity to plaque and total plaque area were tested for statistical significance ($p < 0.05$) though Welch’s t test using Prism 7.

Tissue dissociation for bulk RNA-seq

Following perfusion with ice cold PBS, whole or half brains were dissected, and the cerebellum was removed. Tissue was stored briefly in 1X HBSS until subsequent perfusions were completed. Tissue dissociation was then performed utilizing the Adult

Brain Dissociation Kit (Miltenyi) and the gentleMACS Octo Dissociator with Heaters (Miltenyi) according to manufacturer guidelines with modifications. Briefly, tissue was cut into ~1mm 3 pieces and placed into the C-tubes with the kit's enzymes and samples were dissociated using the preprogrammed protocol. Following enzymatic digestion, samples were strained through a 70um filter and pelleted by centrifugation. Myelin and debris were removed by resuspending the pellet in 6mL 23% Percoll, overlaid with 2mL of 1X DPBS, and spinning at 400xg for 25 min at 4°C, with acceleration and brake set to 0. The supernatant was discarded, and the cell pellet was processed for flow cytometry.

Fluorescence activated cell sorting of xMGs

For sorting of xMGs expressing endogenous GFP, dissociated cell pellets were resuspended in 400uL of FACS buffer (2% BSA in 1X DPBS) containing either Zombie Violet (Biolegend, 1:100) or Propidium Iodide (PI) (Biolegend, 1:400) as a viability marker. For animals transplanted with non-fluorescent cell lines, cell pellets were resuspended in 100uL of FACS buffer containing 5ug of mouse and human Fc block (BD) and incubated for 5 min on ice. 100uL of FACS buffer including the following antibodies was then added to the sample for a final staining volume of 200uL: Rat anti-HLA-ABC-PE clone YTH862.2 (Novus, 1:100) and mouse anti-human CD11b clone ICRF44 (Biolegend, 1:200). Samples were then spun down and resuspended in 400uL of FACS buffer containing either Zombie Violet (Biolegend, 1:100) or PI (Biolegend, 1:400) as a viability marker. Samples were then sorted on a FACSARIA Fusion II (BD Biosciences) directly into 900uL of Trizol (Thermo Fisher), immediately vortexed to ensure rapid lysis, and placed on dry ice.

Bulk RNA Isolation from xMGs

FACS or bean sorted xMGs, ranging from 40,000-172,000 cells, were stored at -80°C until RNA isolation. Samples were then thawed on ice and RNA was isolated by adding 140uL of TET (10mM Tris 8.0/0.01mM EDTA/0.05% Tween20) followed by 140uL Chloroform:Isolamyl alcohol 24:1 (Sigma). Samples were centrifuged at 15,000xg for 10 min. at 4°C and the aqueous phase was collected and added to 1.5uL of GlycolBlue (Thermo Fisher). 55uL (~1/10 supernatant volume) of 3M sodium acetate and 550uL (~1 supernatant volume) of isopropanol (Sigma) were added and the samples were mixed by inverting then stored at -20°C overnight. Samples were then spun at 15,000xg for 30 min. at 4°C, supernatants were removed from pellets, and 500uL of 75% ethanol was added to the pellet. Samples were then spun at 15,000xg for 30 min. at 4°C, and supernatants were removed from pellets. RNA pellets were dried at RT to remove any residual ethanol, resuspended in 14uL of RNase-free H_2O, and used immediately or aliquoted and stored at -80°C for downstream analysis.

Isolation of microglia from human tissue

Human microglia were isolated from adult, normal appearing cortical tissue resected from non-malignant cases of temporal lobe epilepsy. Tissue was mechanically dissociated followed by gentle enzymatic digestion, using DNase and trypsin, to generate a single cell suspension. Cells were then passed through a nylon mesh filter and separated from debris via ultracentrifugation. Pelleted cells were resuspended in PBS (0.4% BSA), counted, stained with cell surface markers, and purified by flow

cytometry (BD Biosciences FACs ARIA Fusion). Microglia were defined as live (Zombie Aqua Fixable Viability stain, Biolegend), CD11b + (Anti-human PE, Biolegend) CD45 low (Anti-human APC/Cy7, Biolegend), CX3CR1 high (Anti-human FITC, Biolegend) single cells. ExVivo samples were immediately pelleted, resuspended in Trizol LS (Thermo Fisher Scientific), and stored at -80°C until subsequent RNA isolation. InVitro samples were pelleted, resuspended, counted, and plated at 2x10 6 cells/mL in MEM supplemented with heat-inactivated FBS (5%), P/S (0.1% v/v) and glutamine (0.1% v/v.). Microglia were grown for 3 days, collected and plated at 1x10 5 cells/mL, and maintained in culture for 6 days during which time cells received two treatments of TGFb (20 ng/mL) on days 3 and 5. Human fetal brain tissue was obtained from the Fetal Tissue Repository (Albert Einstein College of Medicine, Bronx, NY). Total RNA was isolated using standard Trizol LS (Thermo Fisher Scientific) protocols and stored at -80°C.

RNA analysis, Library Construction and Bulk RNA-seq

RNA integrity (RIN) values were determined using an Agilent Bioanalyzer 2100 series and RNA concentrations were assayed by Qubit and the average RIN value for RNA samples used in sequencing was 9.4. 10ng of RNA was used for library construction using ClonTech SMART-seq V4 Ultra Low Input kit (Takara Bio) which utilized poly-A selection to enrich for mRNAs. The quality of the DNA libraries was assayed using the Agilent 2100 bioanalyzer high sensitivity DNA assay and the DNA high sensitivity Qubit. The libraries were quantified by Kapa qPCR, normalized to 2nM and then multiplexed

for sequencing on the Illumina HiSeq 4000 platform with single read 100 base chemistry.

Tissue dissociation for scRNA-seq

Following perfusion with ice cold PBS containing 5ug/ml actinomycin D (act D), half brains were dissected, and the cerebellum was removed. Tissue was stored briefly in RPMI 1640 containing 5ug/mL act D, 10uM triptolide, and 27.1ug/mL anisomycin until subsequent perfusions were completed. Tissue dissociation was then performed utilizing the Tumor Dissociation kit, human (Miltenyi) and the gentleMACS OctoDissociator with Heaters (Miltenyi) according to manufacturer guidelines with modifications. Briefly, tissue was cut into ~1mm 3 pieces and placed into the C-tubes with the kit's enzymes, 5ug/mL act D, 10uM triptolide, and 27.1ug/mL anisomycin and samples were dissociated using the preprogrammed protocol. Following enzymatic digestion, samples were strained through a 70um filter and pelleted by centrifugation. Myelin and debris were removed by resuspending the pellet in 8mL 23% Percoll, overlaid with 2mL of 1X DPBS, spinning at 400xg for 25 min at 4°C, with acceleration and brake set to 0, and discarding the myelin band and supernatant.

Magnetic Isolation of xMGs for scRNA-seq

Dissociated cell pellets were resuspended in 160uL FACS buffer (0.5% BSA in 1X DPBS) + 40uL Mouse cell removal beads (Miltenyi) and incubated at 4°C for 15 min. Samples were then separated using LS columns and the MidiMACs separator (Miltenyi) and the human cells were collected in the flow through. Cells were pelleted via

centrifugation (10 min, 400xg) and resuspended to ~1,000 cells per microliter in FACS buffer, according to counts performed on a hemocytometer.

Magnetic Isolation of xMGs subpopulations for Bulk RNA-seq

After centrifugation step after mouse cell depletion cells are resuspended in 1mL of FACs and placed in FACs tubes. 1:100 Mouse Fc Block and 1:100 Human Fc block is added along with 10uL of biotylated antibody (1:100) and incubated at RT for 10 min. Then 50uL of EasySep Mouse Streptavidin RapidSheres are added (StemCell Tech cat#19860), mixed, and incubateed 2.5 min. This is then topped off to 2.5mL by adding 1.5mL FACS and incubated on the magnet 2.5min. After incubation the supernatant is removed, placed in new tube and spin for 5min at 4 degrees C, for the next antibody incubation. Wash the walls and cells conjugated to beads several times with 500uL of Trizol, freeze at -80 degrees C until RNA isolation. For serial isolation, the supernatant removed from conjugated beads is then incubated with biotynlated antibody and the steps are repeated.

Single-cell sequencing via 10X

Following magnetic isolation, the scRNA-seq library preparation was performed according to the Chromium Single Cell 3 0 Reagents kit v2 user guide. Briefly, a volume of single cells to target a capture of 10,000 cells was used in the generation of GEMS (gel bead in emulsions). The workflow was followed according to the 10X protocol and sequenced on an Illumina HiSeq 4000. All samples were multiplexed and sequenced to a depth of 60-100K reads per cell.

Intraperitoneal LPS injections

A neuroinflammatory state was induced via systemic LPS treatment. Animals received i.p. injections of either 2mg/kg LPS (eBioscience) (n = 5 mice) or PBS (n = 4 mice) once every 24 h over a 72-h period (3 injections total). 12-h after the final LPS treatment, animals were euthanized, perfused with PBS, and half brains were collected for either IHC or transcriptomic analyses, as described above.

In vitro iMGL LPS Stimulation

Day 38 iMGLs were plated at 200,000 cells/well on a Matrigel-coated (1mg/well) 24-well-plate containing 2mL of microglia medium (McQuade et al., 2018). Cells were treated with either LPS (100ng/mL; eBioscience) or DPBS (Ca 2+ and Mg 2+ free) and allowed to incubate for 24 h at 37°C before immediate lysis for RNA isolation (n = 3 wells per treatment group).

Cranial Window Implantation

Mice were anesthetized with isoflurane (Patterson Veterinary) in O 2 (2% for induction, 1%–1.5% for maintenance). To provide perioperative analgesia, minimize inflammation, and prevent cerebral edema, Carprofen (10 mg/kg, s.c., Zoetis) and Dexamethasone (4.8mg/kg, s.c. Phoenix) were administered immediately following induction. Ringer's lactate solution (0.2mL/20 g/hr, s.c, Hospira) was given to replace fluid loss. Sterile eye ointment (Rugby) was used to prevent corneal drying. Surgical tools were sterilized using a hot glass bead sterilizer (Germinator 500). Following hair removal, Povidone-

iodine (Phoenix) and Lidocaine Hydrochloride Jelly (2%, Akorn) was used to disinfect and numb the scalp, respectively. The scalp and underlying connective tissue were removed to expose the parietal and interparietal bone. Lidocaine hydrochloride injectable (2%, Phoenix) was used for muscle analgesia and the right temporal muscle detached from the superior temporal line. The skull was dried using ethanol (70% in DI water) and a thin layer of Vetbond Tissue Adhesive (3M) applied. Custom-printed ABS headplates were attached using Contemporary Ortho-Jet liquid and powder (LANG) at an angle parallel to the skull. A small craniotomy (3mm diameter) was performed over the right hemisphere 2.5mm anterior and 3mm lateral lambda. Hemostatic gelfoam sponges (Pfizer) pre-soaked in sterile saline (CareFusion AirLife Modudose) were used to absorb dural bleeding. Surgery was terminated if dural tears or parenchymal hemorrhage was observed. A 4mm glass coverslip (World Precision Instruments) was placed over the exposed brain and its edges attached to the skull first with a thin layer of Vetbond and second with dental acrylic. Following surgery, mice recovered in their home cage over a warm heating pad until normal behavior resumed (~15-30 min). Postoperative care consisted of daily Carprofen injections (10mg/kg, s.c.) for one week.

Two-Photon Imaging and Laser Ablation

Fluorescence was gathered with a resonant two-photon microscope (Neurolabware, Los Angeles, CA) with 900 nm excitation light (Mai Tai HP, Spectra-Physics, Santa Clara, CA). A 16x Nikon water immersion lens (0.8 NA) or a 20x water immersion lens (Olympus, 1.0 NA) was used. Emissions were filtered using a 510/84nm and 607/70 nm BrightLine bandpass filter (Semrock, Rochester, NY). Image stacks (2.89 mm step size)

were gathered every 30-300 s using Scanbox acquisition software (Scanbox, Los Angeles, CA) at a depth of 150-250 mm below the meninges, corresponding to cortical layer 2/3. Laser ablation consisted of scanning over a small region (70x10 mm, 1.2-1.5W) at magnification 25 for 1 min.

Homeostatic and Response to Laser-Induced Ablation

Analysis All image stacks were processed and analyzed using the image processing package FIJI. Images were temporally binned down to 5 min. intervals and the resulting z stack used to analyze homeostatic activity and response to laser-induced ablation. To measure extension and retraction rates, the first 100 notable changes in process length was measured manually for each mouse. To discriminate ablation-specific motility from homeostatic extension/retraction, we restricted our measurements to long process extensions (> 20 mm) growing toward the laser ablation site. The increase in microglia processes toward the laser-ablated site is reflected by an increase in the amount of GFP fluorescence. Therefore, we measured the local microglial response to laser-induced ablation by taking the average intensity of GFP within a circle (r = 50 mm) centered at the epicenter of damage. These values were compared to the average intensity of GFP within a circle (r = 50 mm) centered 100 mm away from the epicenter of damage. The intensity at any time point (t x) was normalized using the intensity at t 5 min.

Repeat Mild Closed Head Injury (rmCHI)

2-month-old, EGFP HPC transplanted MITRG mice underwent repeat mild closed head injury (rmCHI) as described by Gold et al. (2018). Briefly, transplanted MITRG mice were randomly assigned to either sham or hit groups Sham animals received 5 days of Isoflorane anesthesia only, with no injury, 5-Hit animals received 5 days of Isoflorane anesthesia with 1 injury each day. Injuries were performed using a controlled cortical impact device (TBI-0310 Head Impactor, Precision Systems and Instrumentation, LLC, Fairfax Station, VA) Injury parameters are as follows: speed: 5 m/s; depth: 1mm; dwell time: 50ms. Following injury, animals rested until euthanized for histology 8 weeks later.

Bulk RNA-seq Data Analysis

FASTQ files were preprocessed using BBDuk to filter out ribosomal RNA and PhiX reads, trim Illumina adapters, and to quality trim any base pairs below a PHRED score of 10. FASTQC was then performed to verify the quality of the sequencing files and all files were determined to be of sufficient quality for downstream processing. Reads were then pseudoaligned to the human GRCh38.p12 transcriptome (Ensembl release 94) using Kallisto, transcripts were summarized to the gene level via tximport, and differential gene expression analysis was performed using DESeq2 after removing genes with summed counts < 10. For Kallisto pseudoaligment of samples without available library information, an average fragment length of 250 and a standard deviation of 120 were used. For TF motif analysis, RNA-seq reads were checked for quality using FASTQC. Reads were then trimmed using Trimmomatic to remove Illumina adapters and regions of reads with PHRED quality scores below 30, as well as the leading and trailing 15 base pairs of each read. Reads with a minimum length of 30

after trimming were retained. Reads were then aligned to the GRCh38.p12 transcriptome (Ensembl release 94) using Bowtie2) and summarized at the gene level using tximport. Differential expression analysis was performed using DESeq2. scRNA-seq Data Analysis FASTQ files were aligned to a dual-species transcriptome made up of the human GRCh38.p12 transcriptome (Ensembl release 95) and the mouse GRCm38 transcriptome (Ensembl release 95) using CellRanger (v2.2.0) with default commands and an expected cell count of 5,500. Following alignment, all barcodes that were identified in the mouse alignment were removed from the human dataset.

Bulk RNA-seq Data Visualization

Data were normalized and converted to a log 2 scale for visualization using DESeq2 0 s varianceStabilizingTransformation followed by batch correction using the removeBatchEffect function from limma (Ritchie et al., 2015). Heatmaps were generated using the R ‘‘Pheatmap’’ package while volcano and bar plots were generated using the ‘‘ggplot2’’ package.

scRNA data Visualization and Differential Gene Analysis

UMI count tables, for 13,597 MITRG xMGs and 11,054 5X-MITRG xMGs, were read into Seurat (v2.3.4) for preprocessing and clustering analysis. First, cells were log normalized, centered, and scaled (Default settings) followed by PCA using all genes in the dataset. PCs 1:10 were used for clustering with a resolution parameter of 0.3. Clusters identified as doublets, dividing, or gene poor (representing damaged cells) were then discarded before further analysis. Cells passing these QC parameters were

then merged by genotype (e.g., Male and Female 5X-MITRG) using the MergeSeurat function. Secondary QC cutoffs were then applied to include only cells with less than 32% ribosomal genes, 7% mitochondrial genes, greater than 800 genes but less than double the median gene count, and greater than 500 UMI but less than double the median UMI count. This resulted in 10,184 MITRG and 8,673 5X-MITRG cells with average UMI counts of 3,201 for MITRG and 3,242 for 5X-MITRG, and average genes counts of 1,583 and 1,593, respectively. Data for these cells were log normalized, centered, and scaled, using the 'negbinom' general linear model, while regressing out library size differences, percent mitochondrial genes, and sex. A second round of PCA was then performed on the cleaned data and interrogation of the PCs revealed a set of 41 highly variable genes contained across all samples, regardless of genotype or sex. These genes were present across multiple PCs and had a large effect on clustering but, as a gene set, had no discernable biological relevance. Therefore, we treated these genes as a technical artifact and removed the set from the variable gene list before repeating subsequent PCA analysis. PCA was then performed using a set of variable genes selected according to expression and dispersion cutoffs (low expression cutoff = 0.01, high expression cutoff = 3, low dispersion cutoff = 1.1). Subsequent tSNE clustering was performed using PCs 1:14 for xMGs isolated from the MITRG mouse and PCs 1:10 for xMGs isolated from the 5X-MITRG mouse, both at a resolution of 0.45. tSNE plots were generated using the same PCs used for clustering and variable genes were determined between clusters using the Wilcoxon Rank Sum Test.

Comparison of Human and Mouse DAM Genes

Differential genes analysis was performed between the DAM and Homeostatic clusters for 5X-MITRG xMGs with an FDR cutoff of 0.01 and the requirement that the gene be expressed in at least 10% of the cluster. Murine DAM genes were obtained from Keren-Shaul et al. (2017) and filtered to remove pseudogenes, genes without a verifiable official name (e.g., GM*), as well as ambiguous genes without 1:1 mouse to human homologs, as specified by either Ensembl or NCBI Homologene. The subsequent comparison utilizing qPCR, microarray, and bulk RNA-seq microglia gene lists (Kamphuis et al., 2016; Krasemann et al., 2017; Yin et al., 2017) was performed by merging the unique genes from all four lists and filtering the list for genes with 1:1 homologs.

xMG Response to Laser Ablation

All image stacks were processed and analyzed using the image processing package FIJI, a distribution of NIH ImageJ software. Stacks were temporally binned (5 min) and the average GFP intensity within a circle (r = 50mm) centered at site of damage was used to assess local microglial response to laser ablation. A second circle (r = 50mm) at least 100mm away from the site of damage was used to assess distal changes in intensity following laser ablation. The intensity at any time point (t_x) was normalized to the intensity in that area at t_{5min}. To determine differences in GFP intensity within and between groups we used a repeated-measures two-way ANOVA corrected for multiple comparison (Sidak).

Gene set enrichment analysis

Pathway analysis was performed using the Broad Institute's Gene Set Enrichment Analysis (GSEA) desktop application version 3.0 (Subramanian et al., 2005). Differential expression results, generated by comparing saline and LPS-treated samples, were taken from DESeq2 and ranked according to the sign of the fold change * -log 10 (adjusted p value). The entire list of ranked genes present in both samples was then input into GSEA's pre-ranked analysis module and the module was set to perform 1000 permutations using the weighted enrichment statistic. The gene list was compared to MSigDB's Gene Ontology database (c5.all.v6.2.symbols.gmt) consisting of the entire set of Gene Ontology terms (Ashburner et al., 2000; The Gene Ontology Consortium, 2017) and results were output, excluding any gene sets less than 15 genes or more than 5000 genes in length.

Gene Ontology Analysis

Gene ontology (GO) analysis was performed using PANTHER (Mi et al., 2017). Upregulated or downregulated genes (jlog fold changej R 2) were compared to genes with a log fold change between 2 and -2 using a statistical overrepresentation test. Significantly ($p < 0.05$) overrepresented GO terms were clustered and visualized using the EnrichmentMap plugin in Cytoscape 3.6.1.

Transcription Factor Binding Prediction and Co-Occurrence

Potential transcription factor binding sites were identified by searching the region 500bp upstream of genes using for binding motifs from the JASPAR database (2018 release). Upregulated (log fold change ≥ 2) or downregulated (log fold change ≤ -2) genes were

compared to genes with a log fold change between 2 and -2 as background. Transcription factors with putative binding sites upstream of the same gene were considered to be co-occurring. Co-occurrence frequency of a transcription factor pair was described using the Jaccard index.

Literature search

Pubmed searches were performed using the term ‘‘microglia’’ or ‘‘Alzheimer’’ plus the name of each differentially expressed gene and transcription factor of interest. At least one publication result matching both terms was considered a positive result.

Statistical Analysis

All statistical analyses were performed in either R programming language or utilizing GraphPad Prism.

Results

Human iPSC-Derived Hematopoietic Progenitor Cells Engraft and Differentiate into Cells Expressing Mature Microglia Markers

Given the developmental ontogeny of microglia, which arise from yolk-sac-derived primitive hematopoietic progenitor cells (HPCs), we hypothesized that transplantation of iPSC-derived HPCs (iHPCs), as generated in McQuade et al. (2018), which express multiple genes associated with primitive HPCs (Figure 1.1A), into the early postnatal MITRG brain would result in robust engraftment of human cells that

would differentiate into mature microglia.[9] To test this, we transplanted GFP-expressing iHPCs directly into the lateral ventricles and overlying cortex of postnatal day 1 (P1) MITRG mice (Figure 1.1B).[163] After allowing the mice to age for 2 months, immunohistochemical (IHC) analysis revealed robust engraftment of human cells throughout the forebrain that strongly expressed the homeostatic microglial marker P2RY12 (Figure 1.1C), IBA1, the myeloid transcription-factor PU.1, and the brain resident microglia-specific marker TMEM119, along with the human nuclei marker, Ku80. Further analysis revealed a high degree of concordance between the expression of GFP and P2RY12 (Figures 1.1D–1.1G) as well as the complex, ramified morphology adopted by the transplanted iHPCs (Figures 1.1H and 1.1I) strongly suggesting that the engrafted iHPCs had differentiated into microglia.

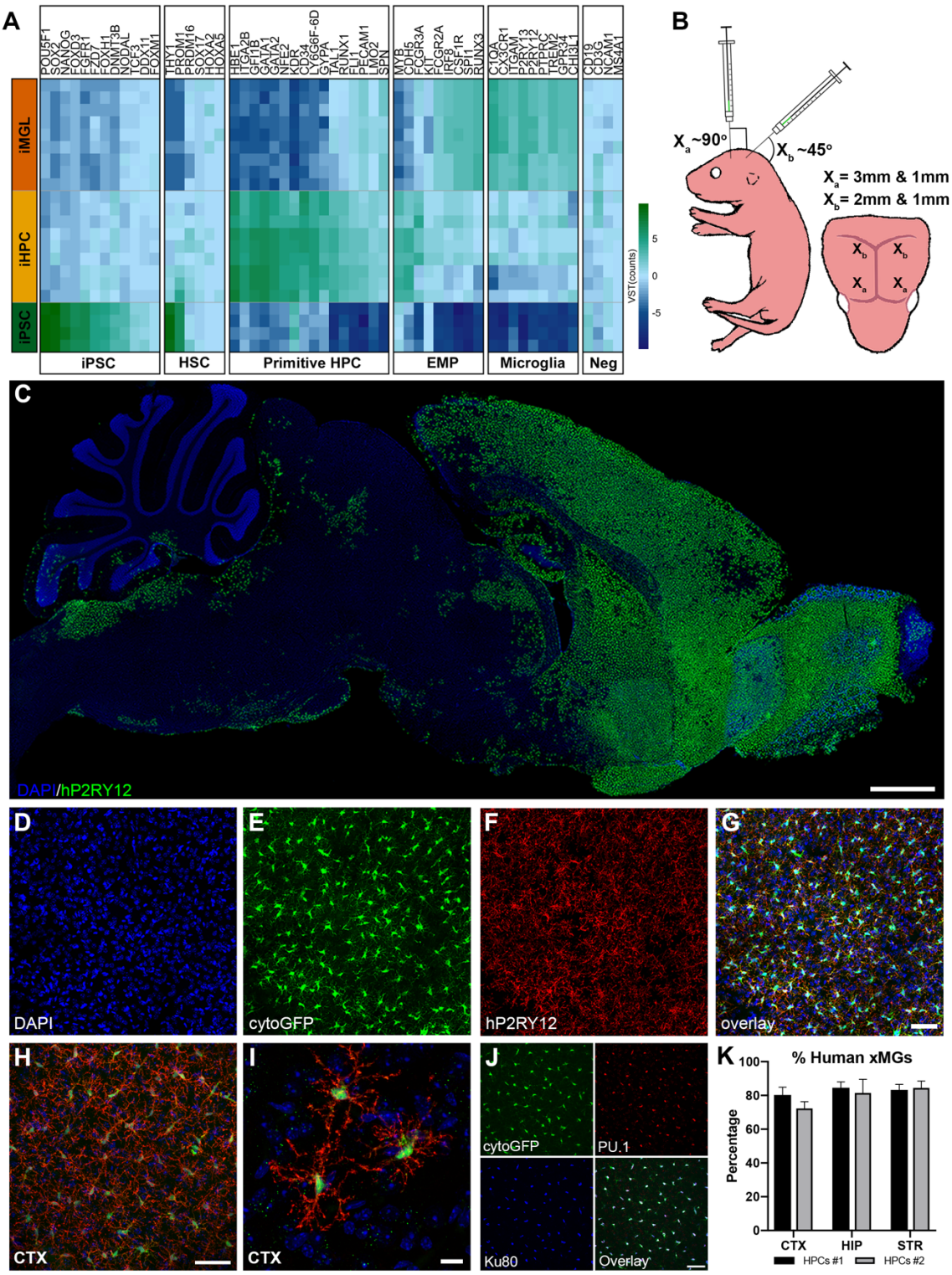

Figure 1.1. iPSC-Derived Human HPCs Differentiate into Microglia and Display Robust Engraftment within the Forebrain of MITRG Mice. (A) A heatmap comparing iPSC, iHPC, and iMGL (McQuade et al., 2018) across a sampling of genes related to iPSC, hematopoietic stem cell (HSC), primitive HPC, erythromyeloid progenitor (EMP), and microglia lineages, along with lineage negative (Neg) genes, shows that iHPCs most closely resemble primitive HPCs but also express some EMP markers. (B) Schematic of transplantation paradigm.

Assessment of the distribution of the xenotransplanted microglia (xMG) throughout the mouse brain revealed some variation depending on the distance from the site of transplantation. In areas that were directly targeted by human iHPC injection, robust xMG engraftment was observed along with very few host murine microglia (Figure 1.2A). In contrast, more distant regions displayed typical distribution and tiling of murine microglia with only an occasional xMG (Figure 1.2B). Quantification of microglia within the targeted regions, including the cortex, hippocampus, and striatum, demonstrated that ~80% of the PU.1 + microglia co-expressed the human-specific nuclear marker Ku80 (Figures 1J and 1K). Furthermore, no significant differences in engraftment were observed between different batches of iHPC transplants ($F_{1,18} = 0.6923$, $p = 0.4163$), across different brain regions ($F_{2,18} = 1.462$, $p = 0.2580$), or in the interaction between iHPC batch and region ($F_{2,18} = 0.4417$, $p = 0.6497$) (Figure 1K) demonstrating the reproducibility of this approach.

Expression of Human CSF1 Is Necessary and Sufficient for the Long-Term Engraftment of Human Microglia in the Murine Brain

We previously demonstrated that human microglia could survive for at least 2 months following transplantation into adult MITRG immune-deficient mice (Rag2 knockout [KO], interleukin-2rg [IL-2rg] KO)[25]. However, we remained curious as to whether all three humanized genes present in the MITRG; hCSF1, hCSF2, or Thrombopoietin (hTPO)) were necessary for xMG survival[163]. Given the importance of CSF1R signaling for microglia survival and previous reports that the murine CSF1 ligand cannot fully activate human CSF1R signaling, we hypothesized that expression

of humanized CSF1 alone was necessary for robust engraftment of human microglia in the murine brain[15, 164, 165]. To test this, we performed transplantations of GFP + iHPCs into MITRG mice (Figure 1.2E) and MITRG mice that had the humanized hCSF2 and hTPO genes bred out (Figure 1.2F), revealing virtually identical engraftment of human cells in both strains and confirming that expression of hCSF2 and hTPO is not necessary for xMG survival. In stark contrast, no xMGs were detected in mice that expressed hCSF2 and hTPO but lacked hCSF1 expression (Figure 1.2G). Interestingly, the necessity for hCSF1 was also dose dependent, as heterozygous hCSF1 mice exhibited partial survival of xMGs (Figure 1.2H). Last, transplantations into the parental mouse strain from which the MITRG model was developed (JAX# 017708), which includes Rag2/IL2rg deletion and hCSF1 but lacks hCSF2 and hTPO, demonstrated that human iHPCs differentiate into microglia which engraft at levels that are consistent with transplantation into MITRG mice (Figure 1.2I). Taken together, these data demonstrate that human CSF1 is both necessary and sufficient to enable the long-term engraftment and survival of human microglia in the mouse brain.

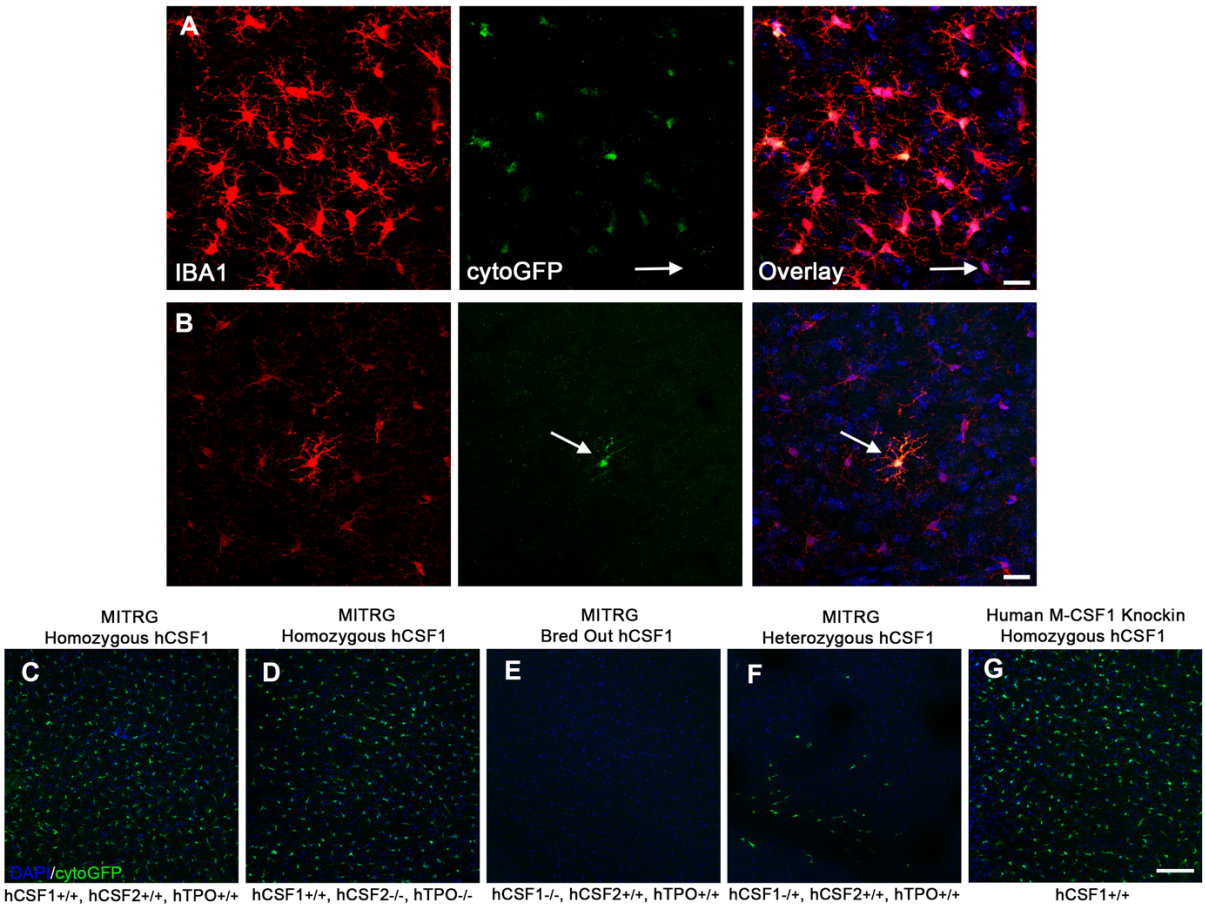

Figure 1.2. Chimeric distribution of human xMGs is influenced by age of transplantation and hCSF1 expression level. In this chimeric model, transplanted human and host murine microglia can be visualized together using the microglia marker, Iba1 (red). Differences in the intensity of Iba1 between human and murine microglia likely arise from preferential binding to the human immunogen used to produce this antibody. (A) Within targeted forebrain regions, GFP + xMGs are widely engrafted and only occasional murine microglia are detected (arrow). (B) In contrast, within areas that are not targeted with iHPC injection such as the hindbrain and midbrain, mouse microglia exhibit a typical tiling pattern that is interspersed with the occasional human cell (green cell, arrow). Scale = 20μm. (C) Human iHPCs transplanted into the MITRG mouse homozygous for all three humanized knockin genes; CSF1, CSF2, and TPO, survive and display robust engraftment (GFP: green; all nuclei, DAPI, blue). (D) Replacement of hCSF2 and hTPO expression with the murine gene, while maintaining hCSF1 expression yields equivalently robust engraftment. (E) In contrast, when hCSF1 is replaced with murine Csf1, no human cells survive. (F) The necessity of hCSF1 appears to be dose-dependent as heterozygous expression of hCSF1 dramatically reduces human microglial engraftment. (G) Human iHPCs transplanted into the parental human M-CSF1 knockin mouse strain (Rag2 - /IL2Rγ - ; JAX Stock No: 017708) which lacks hCSF2 and hTPO expression, display equivalent engraftment to the MITRG model. Scale = 20μm (A-B), 100μm (C-G).

Transplanted iHPCs Acquire Altered Morphologies and Phenotypic Signatures in a Niche-Dependent Manner

xMGs were observed throughout the forebrain and had adopted characteristic, region-specific distributions, morphologies, and marker expression levels. For example, within the cortex and olfactory bulb, xMGs created a mosaic network of ramified cells that tiled neatly with neighboring microglia, establishing distinct microdomains (Figures 1.3A–1.3C). Within the hippocampus and overlying corpus collosum, the expected contrasting morphologies were present, with ramified GFP + /P2RY12 + cells appearing within CA1, and more elongated microglia expressing lower levels of P2RY12 within the overlying white matter of the corpus callosum (Figure 1.3D). In addition, relatively few xMGs were observed within the granule cell layer (Figure 1.3E), a hippocampal subregion that exhibits the lowest number of microglia[166, 167]. Within the striatum (Figure 1.3F), xMGs engrafted predominantly within the gray matter, avoiding the white matter bundles, again consistent with the typical distribution of microglia within this region[168]. Interestingly, limited engraftment of GFP + /P2RY12 + xMGs could also be observed far from the transplantation sites, including parts of the cerebellum (Figure 1.3G) and the spinal cord, where xMGs adopted a more linear, less ramified morphology (Figure 1.3H). In addition to these varying populations of P2RY12 + xMGs, we observed subsets of human cells that expressed GFP yet exhibited a more ameboid morphology. When further examined, these cells were found to lack P2RY12 expression, instead exhibiting morphology, localization, and markers typical of other CNS-myeloid cells (Figures 1.3I–1.3T). This finding suggests that transplanted iHPCs maintain the potential to differentiate into the other yolk-sac-derived CNS-myeloid cell types: perivascular macrophages (pvMf), meningeal macrophages (mMf), and choroid plexus macrophages (cpMf). For example, GFP + /P2RY12 – pvMf-like cells were found along

the vasculature, in close opposition to GLUT1-expressing murine blood vessel endothelial cells (Figures 1.3I–1.3K). These pvMf-like cells also exhibited colocalized expression of CD163 (Figure 1.3L), an established marker of non-microglial CNS myeloid cells[169]. Whole meningeal mounts (Figure 1.3M) confirmed engraftment of more amoeboid GFP + /P2RY12 – mMf-like cells, which were also observed in sections where the meninges were preserved during cryosectioning (Figures 1.3N and 1.3O). As with the pvMf-like cells, these meningeal-localized cells also expressed CD163 (Figure 1.3P). Additionally, a small population of GFP + /P2RY12 – /CD163 + cells was found within the choroid plexus (Figures 1.3Q–1.3T). The relatively small number of cpMf-like cells is consistent with the understanding that cpMfs are maintained in the adult brain through a partial turnover from definitive bone marrow HSCs, whereas microglia, pvMf, and mMf continually self-renew[9]. Overall, these results suggest that transplantation of iHPCs into the early postnatal brain permits the context-dependent maturation of microglia and other CNS myeloid cells.

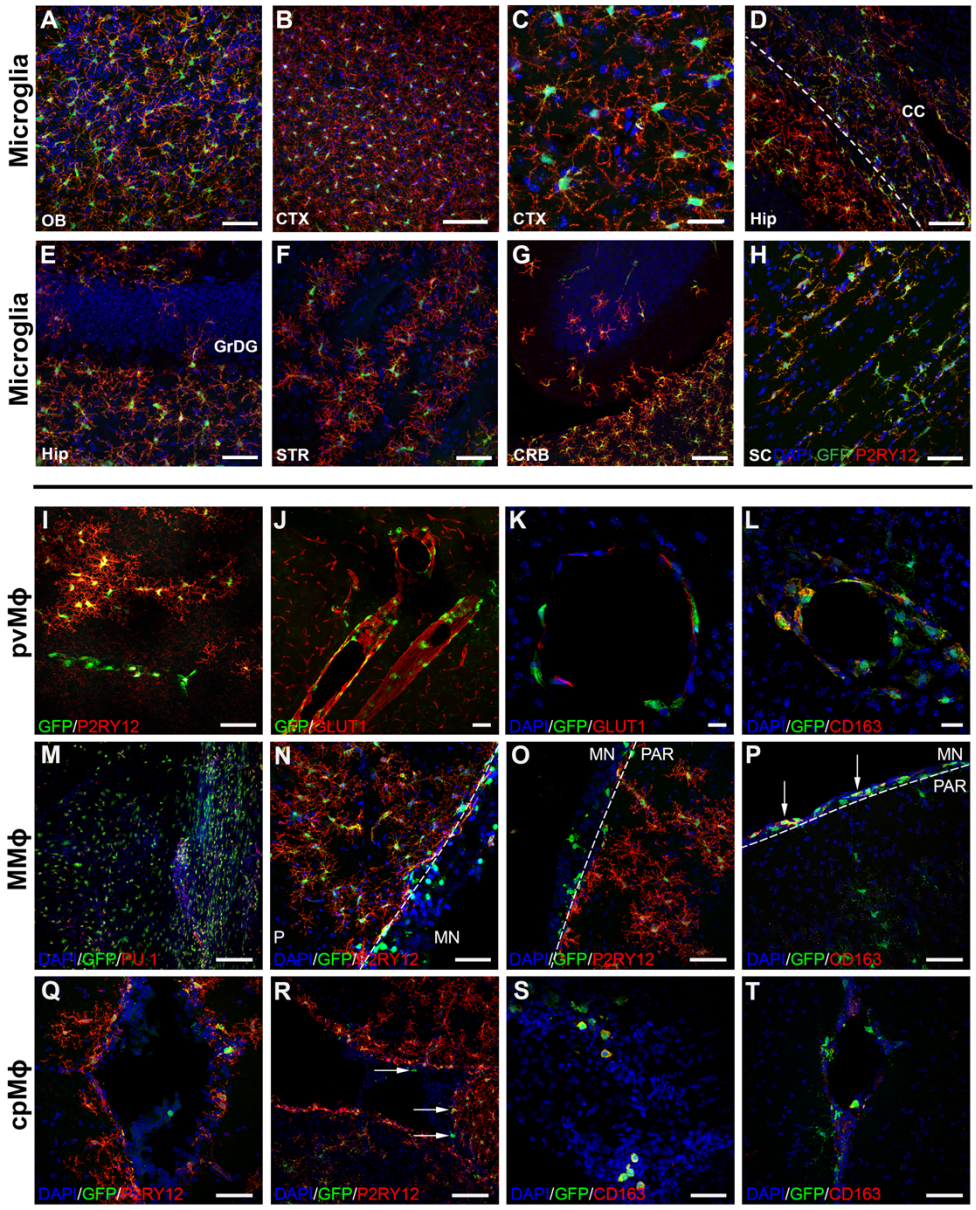

Figure 1.3. Transplanted iHPCs Adapt to Diverse Niches within the Brain and Differentiate into the Four CNS Macrophage Subtypes in a Context-Dependent Manner. (A–H) High-power images demonstrate the variety of morphological features xMGs display during homeostatic conditions, including neat tiling and complex ramifications in (A) the olfactory bulb (OB) and (B and C) the neocortex (CTX). (D) Within the corpus callosum (CC) overlying the hippocampus (Hip), xMGs exhibit a more elongated morphology with a diminished expression of P2YR12. (E and F) Consistent with normal anatomical distributions, xMGs also tend to avoid the granule cell layer of the dentate gyrus (GrDG) and the axon bundles within the striatum (STR). (G and H) Remarkably, xMGs also migrate to parts of the cerebellum (CRB) and spinal cord (SC). (I–L) A subset of GFP + cells exhibit an amoeboid morphology and linear organization and lack the homeostatic microglia marker, P2RY12 (I). These cells also encircle GLUT1 + blood vessels (J), localize to the perivascular space (K), and express CD163 (L) suggesting a perivascular macrophage (pvMf) phenotype. (M) Another population of GFP + /PU.1 + cells display robust engraftment in meningeal whole mounts. (N and O) These ameboid shaped meningeal macrophages (mMf) can also be found in sections where parts of the meninges (MN) were preserved (N) and are distinct from the fully ramified GFP + /hP2RY12 + microglia (O) within the parenchyma (PAR). (P) Similar to the pvMf, these mMf are also GFP + /hP2RY12 – /CD163 + (arrows). (Q–T) A few GFP + /hP2RY12 – choroid plexus macrophage-like (cpMf) cells can be found within the choroid plexus. Additional examples shown in (R) (arrows). GFP+ cpMf cells (S) also co-express the marker CD163 + (T). In some images, brightness and contrast settings were adjusted. Scale, 50 mm (A, D–J, N–Q, S, and T), 25 mm (C and K), 20 mm (L), 100 mm (B, M, and R).

xMGs Acquire a Transcriptomic Signature that Closely Resembles In Vivo Human Microglia

While IHC analysis revealed that xMGs expressed many microglial markers and adopted the morphology of homeostatic microglia, an in-depth transcriptomic analysis of multiple cell lines was needed to test whether xMGs fully acquire a microglial fate. Therefore, we developed methods to recover pure populations of xMGs, derived from fluorescent or non-fluorescent iPSC lines, from transplanted brains in order to perform RNA sequencing. To assess xMGs in comparison to endogenous human microglia, transcriptomes were compared between xMGs, brain-derived human microglia (ex vivo), cultured human microglia (in vitro), and iMGLs differentiated from iPSCs. To further increase the power of these comparisons, a previously published dataset that included additional ex vivo and in vitro samples was also included[19].

To explore the overall similarities and differences between these 49 human microglial samples, the studies were batch corrected and principal component analysis (PCA) was performed. This analysis revealed a clear separation of microglia groups based on environment, with a high degree of clustering between the xMGs and ex vivo microglia (Figure 1.4A). However, as we were primarily interested in determining whether transplantation had induced an in vivo transcriptomic profile, we used the dataset published by Gosselin et al. (2017) to define a list of 3,432 brain-dependent microglial genes that were differentially expressed between the ex vivo and in vitro samples. PCA analysis with this gene list further enhanced clustering of xMGs with ex vivo microglia, whereas iMGLs and in vitro microglia formed distinct, segregated

clusters, demonstrating that in vivo differentiation of iHPCs within the murine brain induces a brain-dependent microglia transcriptome (Figure 1.4B).

To perform an enhanced, gene-level analysis, the brain dependent gene list was cross-referenced to the 881-gene microglial signature published by Gosselin et al. (2017) resulting in 190 brain-dependent microglial signature genes (Figure 1.4C). Euclidean clustering of the samples mirrored the PCA clustering, with iMGLs and in vitro groups on one branch and the xMGs and ex vivo samples intermixed within the other branch. However, while the xMG profile was highly similar to the ex vivo signature, differential gene expression (DGE) analysis between xMGs and ex vivo samples demonstrated that 97 of the 881 signature genes were differentially expressed. Interestingly, Euclidean clustering of all in vivo samples using these 97 differentially expressed genes revealed that, while xMGs clustered separately from most of the ex vivo samples, three of the youngest ex vivo samples (average age 16.5 months) were intermixed with the xMG samples. This finding potentially suggests that xMGs have yet to fully mature at the examined time points. However, there were also many major histocompatibility complex (MHC) class II genes that were expressed at higher levels in the older ex vivo samples, possibly indicating an increased activation state. One explanation could be that xMGs were isolated from the healthy mouse brain whereas the ex vivo samples were isolated from patient tissue affected by epilepsy or collected from tumor margins, resulting in an activated state. Longer term aging studies may provide the evidence needed to understand these small, albeit intriguing, differences.

Further gene-level analysis showed that transplantation into the brain environment induced a number of important microglia gene sets. Key microglia-

associated transcription factors (TFs), including EGR1, FOS, FOSB, JUN, KLF2, KLF4, and SALL1 (Figure 1.4D), that were either not expressed or lowly expressed in vitro, were fully recovered following transplantation. We also focused on a number of microglia genes that have been proposed to be important for homeostasis or activation, as it has been suggested that microglia derived from transplanted cells can exhibit an ‘‘activated’’ profile[5, 6, 161]. With regards to homeostatic genes such as CX3CR1, P2RY12, SELPLG, and TGFB1, xMG expression is similar to that of the ex vivo samples, with xMGs displaying slightly elevated expression (Figure 1.4E). In contrast, xMGs do not appear to present with increased expression of genes that have been implicated in microglia activation states including CLEC7A, ITGAX, IL21R, or SIGLEC1. Additionally, whereas in vitro iMGLs express very low levels of TMEM119, transplantation fully recovers expression, consistent with the recent demonstration that TMEM119 is a brain-dependent microglia gene (Figure 1.4E)[28].

Finally, as we are interested in utilizing this model to study microglia responses to AD pathology, we compiled a list of AD risk genes to ensure that xMGs were not aberrantly expressing these transcripts. As with the previous analyses, xMGs presented with an expression profile closely mirroring that of the ex vivo samples (Figure 1.4F). Notably, genes of current interest in the field, such as APOE, TREM2, BIN1, PLCG2, MS4A4A, and MS4A6A, are expressed at ex vivo levels. These findings, in conjunction with the previously presented transcriptomic profiling, not only suggest that xMGs have the potential to be utilized in future disease studies but also, considering the human iPSC origin of these cells, offer a level of genetic similarity to human microglia that cannot currently be matched by other approaches.

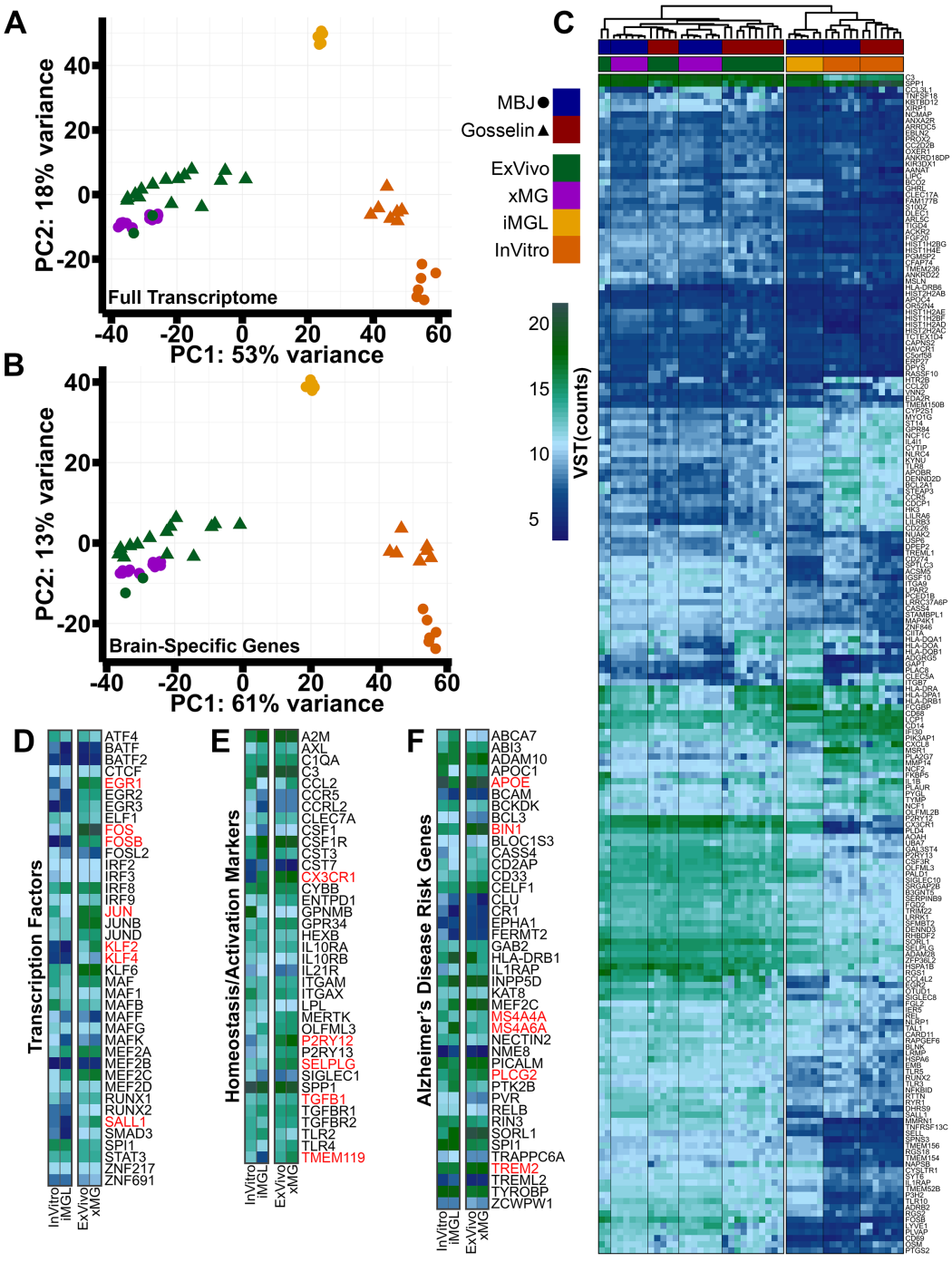

Figure 1.4. Transplantation of Human iHPCs into the Murine Brain Recapitulates an In Vivo Human Transcriptome. (A) PCA plot, including 16,413 genes, comparing freshly isolated human microglia (ex vivo, green; n = 17 patients), xMGs (purple; 3 iHPC cell lines, n = 3–6 mice per line, 13 mice total), iMGLs (yellow; n = 6 wells), and cultured human microglia (in vitro, orange; n = 13 patients) from our lab (M.B.-J., circles) or the Gosselin et al. (2017) samples (triangles). Ex vivo microglia and xMGs cluster together, while both in vitro groups (iMGLs and in vitro) cluster separately. (B) PCA comparing the 3,432 differentially expressed genes between the Gosselin et al. (2017) ex vivo and in vitro microglia (FDR =

0.05, log foldchange [LFC] cutoff = ±2). Again, xMGs cluster closely with ex vivo microglia, demonstrating that transplantation recovered a brain-dependent microglia signature. (C) Heatmap comparing sample groups from our lab (M.B.-J., blue) and Gosselin et al. (2017) (red) based on the top 190 brain-dependent microglia signature genes. Euclidean clustering shows samples cluster by environment (in vivo or in vitro), and xMG samples are intermixed with ex vivo microglia samples. (D) xMGs express TFs at levels that are comparable to ex vivo microglia, many of which were either lowly or not expressed in vitro (red text). (E) xMGs express microglia signature genes and activation markers, including P2RY12, TGFB1, and CX3CR1, at comparable levels to ex vivo microglia, suggesting that xMGs have taken on a homeostatic transcriptomic profile. xMGs also express the braindependent microglial gene TMEM119, which was not previously expressed in iMGLs. (F) xMGs express AD risk genes at levels that coincide with non-AD ex vivo microglia. This finding demonstrates that xMGs could be accurate surrogates for AD studies in mouse models. Heatmaps in (D)–(F) represent variance stabilizing transformation (VST) normalized expression values, averaged for all samples in a group.

xMGs Survey the Local Environment and Rapidly Respond to Focal Brain Injury

While validating the morphological, histological, and transcriptomic properties of human microglia within the rodent brain was critical, the utility of this chimeric approach is also dependent on whether xMGs can accurately recapitulate microglial function in vivo. Therefore, we utilized 2-photon microscopy to visualize the in vivo behavior of GFP + xMGs. Live imaging of xMGs revealed an array of neatly tiled, highly ramified human cells that were actively surveying their immediate environment (Figure 1.5A), as evidenced by constant extension and retraction of processes at rates consistent with endogenous murine microglia (Figure 1.5B). Based on previously reported descriptions of endogenous murine microglia behavior, these observations are highly consistent with the activity and morphology of homeostatic microglia[12, 170].

Since xMGs appeared to be actively surveying the brain parenchyma, we next sought to challenge that behavior with a localized, parenchymal injury. Due to the limited availability of in vivo, functional microglia data from humans, we concentrated our analysis on focal laser ablation, an approach that has been used to induce a highly reproducible microglial response in mice[11, 12]. We again used 2-photon imaging to visualize xMGs in the immediate vicinity of the damage site as well as those distally

located to the damage site and microglial response was monitored for up to 50 min post-injury (Figures 1.5C and 1.5D). In concordance with previously characterized murine microglial responses, laser damage elicited a rapid and highly localized response in which xMGs within 40 mm of the damage site immediately responded by sending processes to assess the injury, while distal xMGs showed no obvious deviations from homeostatic surveillance activity. Accordingly, quantification of mean GFP intensity within the damage site showed a steady increase for 30 min post-injury followed by a sustained intensity for up to 50 min of imaging, whereas distal GFP intensity remained consistent across all time points (Figure 1.5D). Importantly, the extension rate and magnitude of this human microglial injury response is similar to that of murine microglia (Figure 1.5E), indicating that xMGs respond to local CNS injury in a manner that is consistent with in vivo microglia[11, 12].

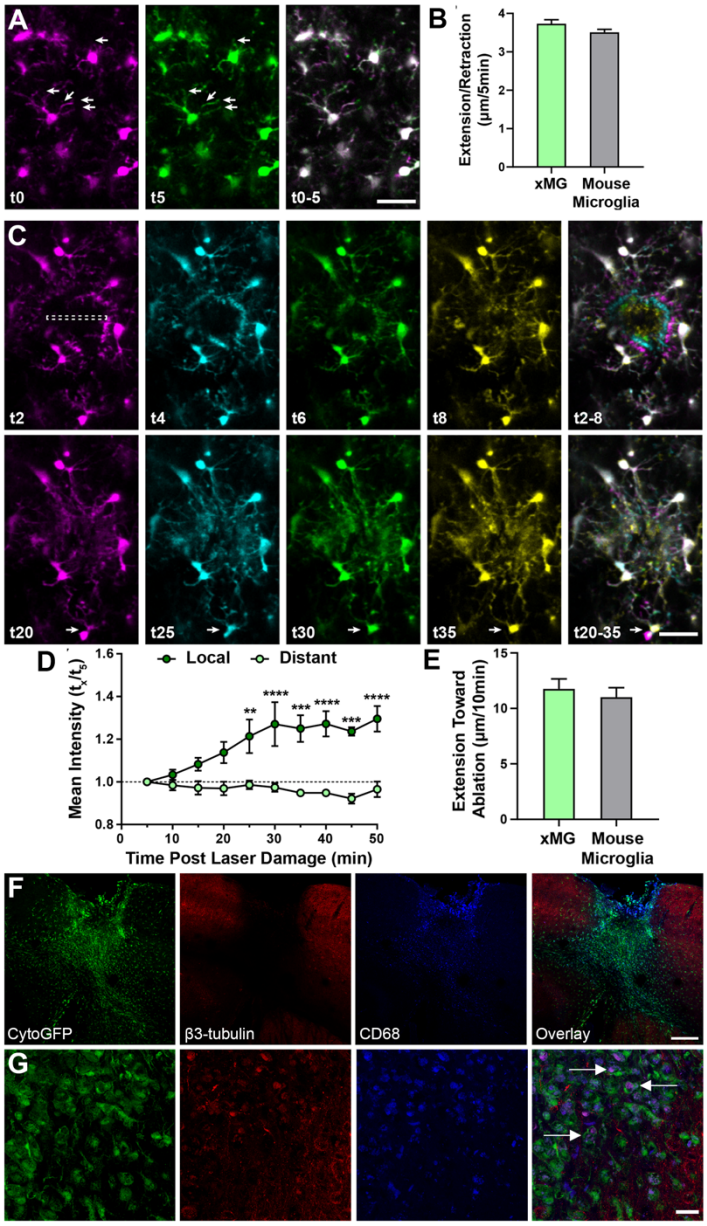

Figure 1.5. xMGs Survey Their Surroundings, Rapidly Respond to Laser Ablation and Interact with Neuronal Components after Trauma. Human microglia were visualized using multiphoton in vivo imaging in (A) homeostasis and (C) following focal, high-intensity laser exposure. (A) Time-coded colorization of homeostatic xMGs demonstrate high process motility, actively surveying their niches. Overlaid color images of t0–5 min. (right) more clearly reveals the morphological dynamics of individual cells. (B) The average length of extension and retraction in 5 min found in xMGs (3.73 ± 0.10 mm, n = 300 observations, 3 mice) was not different from those found in mouse microglia (3.51 ± 0.08 mm, n = 300 observations, 3 mice) (p = 0.25, U = 42581). (C) Time-coded colorization of microglial response to focal damage reveals that processes rapidly move toward and surround the site of injury within 8 min postlaser ablation. At later time points (t25–t35), some microglia outside the direct injury region translocate (white arrow), positioning their cell bodies closer to the injury. (D) The mean intensity at the injury site (local, dark green) is higher than the mean intensity 150 mm away (distant, light green), showing that xMG processes rapidly localize to the injury site (repeated-measures two-way ANOVA, p = 0.006. Scale, 50 mm). (E) The average length of extension toward the ablation site in 10 min by xMGs (11.76 ± 0.90 mm, n = 22 observations, 3 mice) is similar to those by mouse microglia (11.01 ± 0.87 mm, n = 37 observations, 3 mice) (p = 0.34, U = 346). (F and G) Transplanted MITRG mice underwent repeat mild closed head injury (rmCHI), and histological analysis was performed 2 months post-injury. (F) GFP + xMGs infiltrate the injury site and express increased levels of CD68 (blue). (G) Higher-power images of GFP + xMGs reveal b3-tubulin (red) and CD68 (blue) colocalized within xMGs (white arrows), indicative of microglial phagocytosis of neuronal components. All error bars reflect SEM. Scale, 200 mm (F) and 20 mm (G).

xMGs Phagocytose Neuronal Components after Brain Trauma

In several murine models, repeat mild closed head injury (rmCHI) has been shown to induce sustained microglial activation and interaction with neurons post-

injury[13, 171]. Thus, to determine whether xMGs can interact with murine neuronal components, mice were exposed to rmCHI 2 months post-transplantation and histological assessment of the injury site was performed 8 weeks later (Figures 1.5F and 1.5G). Low-power images reveal that GFP + xMGs infiltrated the injury site (Figure 1.5F), while higher-power imaging revealed that lysosomes (CD68; blue) within GFP + xMGs colocalized with b3-tubulin (red), indicative of phagocytosis of neuronal microtubule components and debris (Figure 1.5G; white arrows indicate colocalization of CD68 and b3-tubulin). Thus, xMGs can readily interact with and phagocytose degenerating neurons.

xMGs Respond Robustly to a Systemic Inflammatory Challenge

Our next functional assessment focused on characterizing the xMG response to the commonly used peripheral immune challenge lipopolysaccharide (LPS). Mice transplanted with GFP + iHPCs were aged 2 months and then administered either saline or LPS via intraperitoneal injection. Quantification of IHC images revealed a significant reduction in the homeostatic marker P2RY12 following LPS treatment and, conversely, a significant upregulation of CD45 (Figures 1.6A–1.6C), consistent with an LPS induced increase in microglial activation state. Interestingly, LPS also induced increased GFP expression, likely because of the activating effect of inflammatory stimuli on CMV-based promoters such as the CAG promoter used to drive GFP expression (Figures 1.6A–1.6C)[172].

In addition to the observed morphological and protein-level changes, xMGs were isolated from saline and LPS-treated mice in order to examine transcriptomic

alterations. DGE analysis revealed that LPS treatment resulted in 607 upregulated and 287 downregulated genes (Figure 1.6D). As anticipated, several of the highly upregulated genes (e.g., TMEM176A/B, IL21R, SPP1, MSR1, TLR2) are involved in cytokine recognition, phagocytosis, and pathogen responses, while many downregulated genes (e.g., P2RY12, P2RY13, ITGAM, SELPLG) are typical markers of microglia homeostasis. Further assessment of Gene Ontology (GO) via gene set enrichment analysis (Subramanian et al., 2005) demonstrated a coordinated upregulation of pathways related to immune response, antigen presentation, and translation initiation[173]. Additionally, examination of the differentially expressed xMG signature genes from xMG/*ex vivo* human microglia showed that many genes were normalized toward ex vivo levels following LPS treatment, including some of the previously noted MHC class II genes. This finding lends some preliminary support to our aforementioned hypothesis that, rather than being immature, xMGs transplanted into the healthy mouse brain may present with a less activated profile than microglia isolated from disease-affected human tissues.

The Human Microglia Response to Systemic Inflammation Is Not Accurately Modeled by LPS In Vitro

Many studies regarding microglia responses to LPS have been performed in vitro, by treating murine or human microglia directly with LPS[25, 174]. We therefore decided to recapitulate this approach by treating iMGLs made from the same GFP + cell line as the LPS-exposed xMGs, with LPS in vitro. RNA-seq and DGE analysis revealed 888 upregulated genes and 679 downregulated genes following in vitro LPS treatment.

Compared to the in vivo results of 607 upregulated and 287 downregulated genes, it was immediately clear that the response to LPS in a dish was more dramatic than the response in vivo. Correlation analysis between saline and LPS samples from both environments demonstrated

limited correlation between in vitro and in vivo groups, with the least correlated groups being in vivo LPS and in vitro LPS (Figure 1.6E). Unsurprisingly, the lack of correlation further manifested as a limited overlap between the DGE lists, with the LPS groups only sharing 22.7% of the upregulated genes and an abysmal 4% of downregulated genes (Figure 1.6F). To determine whether these gene-level differences also manifested at the pathway level, we performed GO analysis, which similarly revealed very little overlap between the two environments (Figure 1.6G).

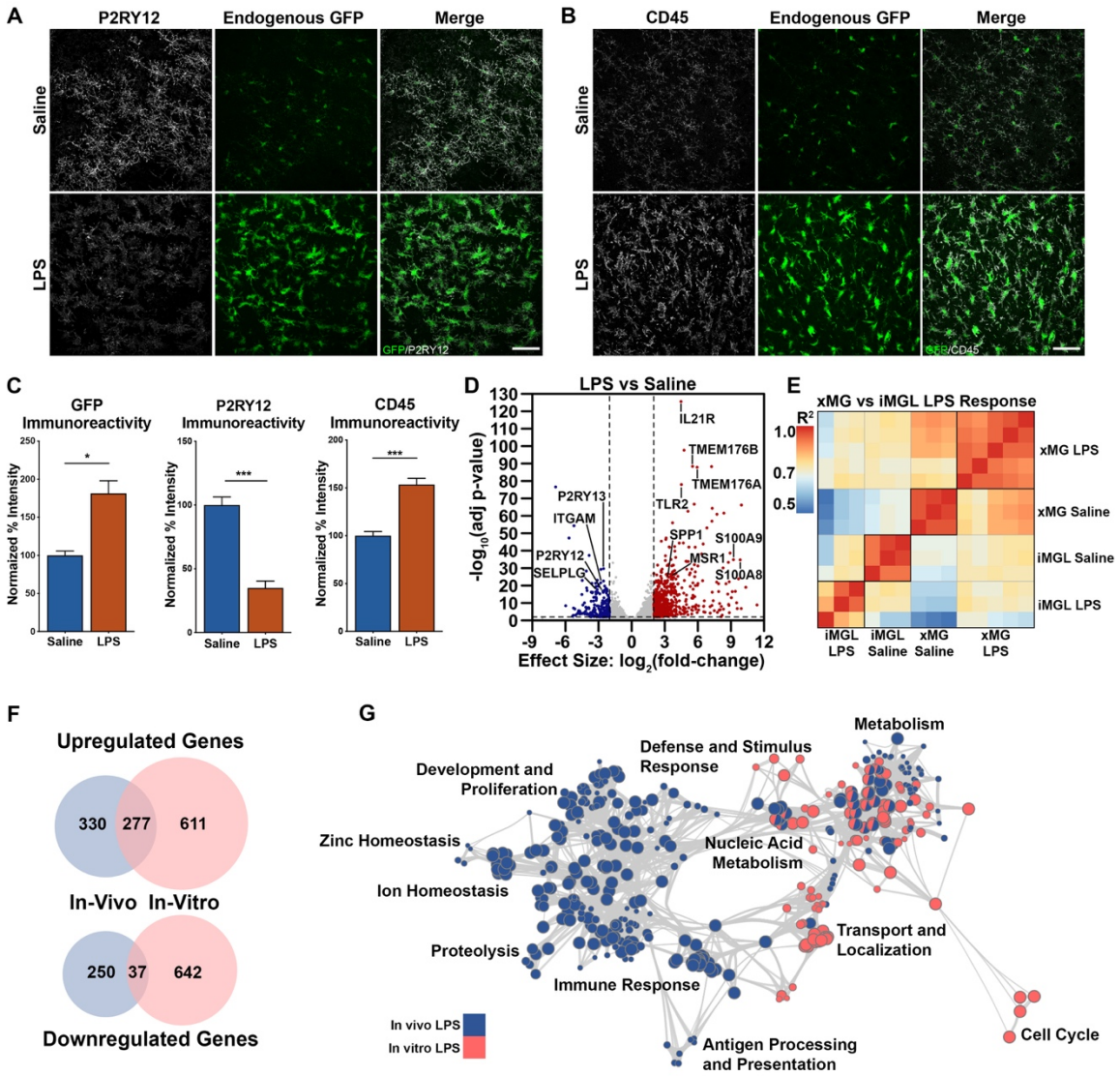

Figure 1.6. Differential Responses of xMGs and iMGLs to Lipopolysaccharide Administration. (A) xMGs treated with saline exhibit strong staining for the homeostatic microglial protein P2RY12 (pseudocolored gray) and cytosolic GFP expression (green). In contrast, LPS-treated xMGs downregulate P2RY12, whereas GFP intensity increases along with distinct alterations in microglial morphology (scale, 50 mm). (B) An upregulation of CD45 immunoreactivity (gray) can been seen after LPS treatment (scale, 50 mm). (C) Quantification of GFP reveals a significant increase in intensity with LPS stimulation (p = 0.0107) accompanied by a significant decrease in P2RY12 intensity (p = 0.0003), and a significant increase in CD45 intensity (p = 0.0004). (D) DGE analysis between microglia isolated from saline and LPS-treated animals revealed 607 upregulated genes (red, right) and 287 downregulated genes (blue, left) (FDR = 0.01, LFC cutoff = ±2; Table S4). Many upregulated genes (labeled, right) have been implicated in immune activation, while a number of downregulated genes (labeled, left) have been described as markers of microglia homeostasis. (E) Pearson correlation matrix comparing the entire transcriptome of each in vivo (xMG) saline and LPS-treated sample with each in vitro (iMGL) saline and LPStreated sample. Heatmap colors correspond to R 2 values and samples are clustered via Euclidean distancing. (F) Venn diagram comparing in vivo and in vitro LPS-induced, differentially expressed genes (FDR = 0.01, LFC cutoff = ±2), demonstrating few conserved changes. (G) Gene ontology (GO) overrepresentation analysis and GO term clustering reveals unique regulation depending on LPS treatment environment, with limited overlap between in vivo (blue) and in vitro (pink) groups. Bar plots represent mean ± SEM.

Transitions in the Expression Profile of xMGs Are Orchestrated by Well-Established Microglial Transcriptional Regulators

An overarching goal of our approach was to develop a predictive experimental model that could be used to study human microglia in vivo. Therefore, we next sought to perform an unbiased analysis of the two environmental transitions that we had exposed human microglia to: one from in vitro to in vivo and another from in vivo to peripheral stimulation with LPS. We began by performing DGE analysis, to assess how these transitions altered the transcriptional state of xMGs, and then utilized k-means clustering to identify 8 clusters of genes with expression profiles that were unique to each of the states (Figure1.7A). Exemplifying the powerful predictive potential of this approach, a subsequent literature based search of all differentially expressed genes revealed that a large majority of these genes are highly relevant to microglial biology (Figure 1.7A). Likewise, many of these genes have been implicated in AD[175]. Next, we performed GO analysis to determine which gene classes changed in response to each transition (Figure 1.7B). Comparison of GO terms revealed that, when xMGs undergo transplantation, genes related to synapse assembly, exploratory behavior, and cell-cell adhesion are strongly induced, all of which would be predicted to increase following xMG integration into the brain. In contrast, GO terms associated with genes that were upregulated following peripheral LPS stimulus were instead consistent with immune activation, interferon response, antigen presentation, and a hallmark of in vivo microglia activation: zinc homeostasis[176].

To further test whether the observed expression signatures were influenced by known microglial gene regulatory factors, we performed an unbiased search to identify TF motifs enriched within the promoter regions of all genes that exhibited differential expression with each transition state (Figure 1.7C). Using this approach, we were able to identify several TF motifs that were highly enriched during the in vitro to in vivo transition and known to be critical regulators of microglial homeostatic function (e.g., RUNX2, MEF, JUN, FOS, KLF). Similar analysis on the xMG+LPS samples identified unique TF motifs that have been implicated in the transformation of microglia to an activated state (e.g., IRF8, STAT3, RelA, CEBPA, MTF-1).

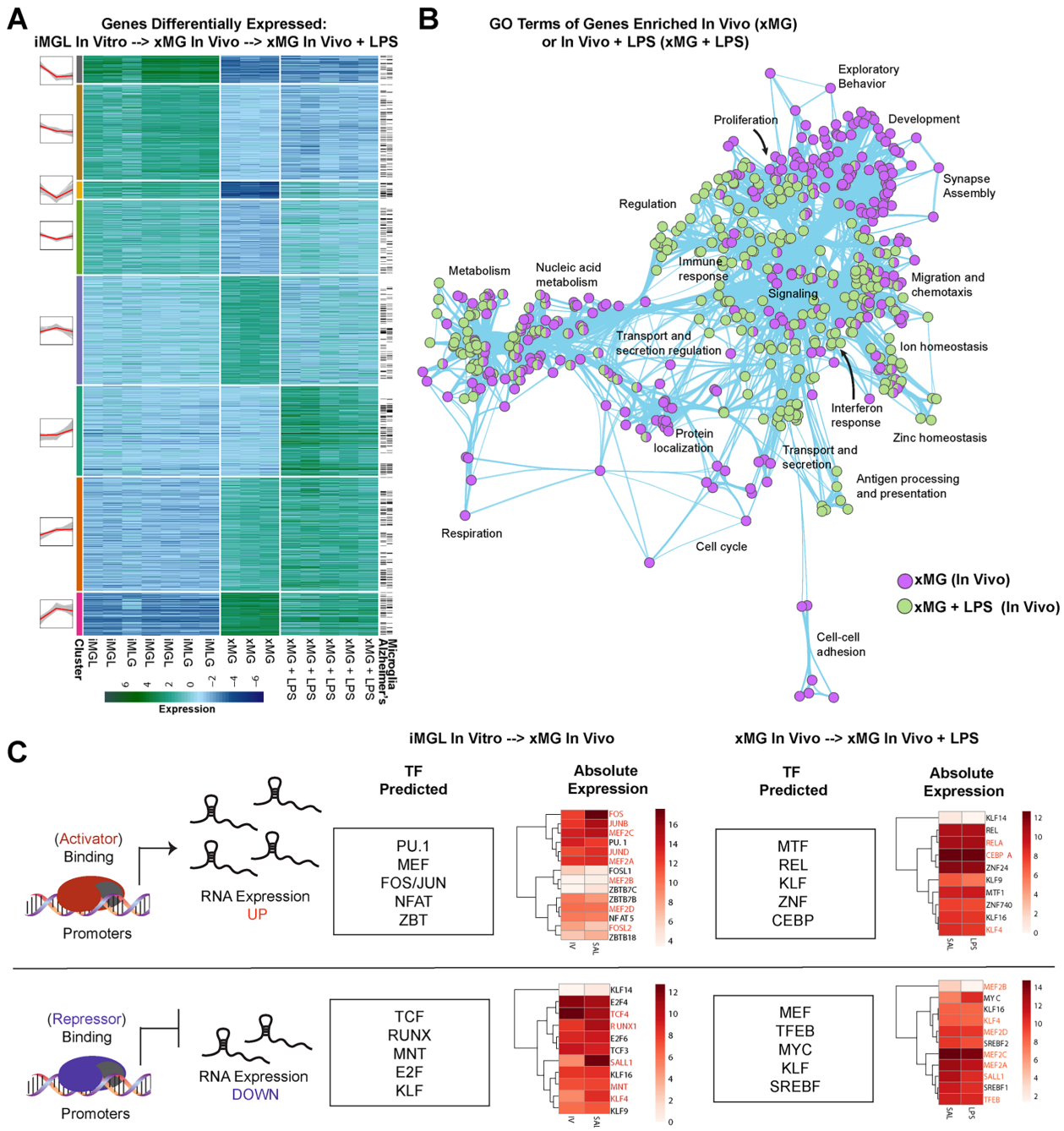

Figure 1.7. xMG Gene Expression Profiles Are Indicative of Known Microglial Activation Signatures.

(A) Heatmap of differentially expressed genes from the same GFP iPSC line differentiated into microglia in vitro versus GFP-xMGs in vivo versus in vivo GFP-xMGs activated with LPS. Black lines on the right indicate genes that have previously been implicated in Alzheimer's disease and/or microglial biology. (B) Network graph of enriched GO terms generated from (A), when comparing upregulated genes from in vitro, to in vivo, to in vivo with LPS stimulation. Nodes represent individual GO terms (gene sets), and edges represent the relatedness between them. (C) Summary of predicted TFs and their association with genes up- or downregulated between states. Heatmaps represent their expression levels at each state.

xMGs Adjacent to Beta-Amyloid Plaques Exhibit a Disease-Associated Microglia (DAM)-like Phenotype

Since we confirmed that xMGs were capable of appropriately responding to both exogenous and endogenous inflammatory insults, we next sought to determine whether xMGs could be utilized in a disease modeling application. As it was recently reported that murine microglia transition into distinct and highly specialized subpopulations upon chronic exposure to pathological beta-amyloid (Ab) in AD mouse models, we sought to verify whether a similar phenotype may occur in xMGs[5, 6]. We, therefore, transplanted GFP + iHPCs into the newly developed 5X-MITRG mouse model and allowed the mice to age for 9 months. Subsequent histological analysis revealed a clear and marked difference in the expression of numerous DAM markers in xMGs near Ab plaques (Figure 1.8). Similar to mouse DAMs and neurodegeneration-associated microglia (MGnD), xMGs in contact with plaques downregulated the homeostatic marker P2RY12 (Figures 1.8A–1.8H), adopted an activated, ameboid morphology, and occasionally phagocytosed fibrillar Ab. Additionally, plaque-associated xMGs upregulated the DAM markers CD9 (Figures 1.8I–1.8P), MERTK (Figure 1.8Q), APOE (Figure 1.8R), CD11C (Figure 1.8S), and TREM2 (Figure 1.8T).

We next sought to further test the utility of this model to study disease-relevant mutations by generating xMGs from a modified iPSC line. Deletion of TREM2 impairs the migration of murine microglia to Ab plaques, and the AD-associated R47H mutation in TREM2 has been shown to impair the association between microglia and plaques in human AD subjects and the 5XfAD mouse model of AD[99, 177-181]. To determine whether

TREM2 plays a similar role in the migration of xMGs to Ab plaques, we transplanted 5X-MITRG mice with HPCs derived from isogenic, CRISPR-edited iPSCs that carry either wild-type or R47H mutant TREM2. 9 months later, brains were examined by confocal microscopy and the association between plaques and xMGs examined by IMARIS 3D-quantification of confocal z stacks. As expected, this analysis revealed significantly less

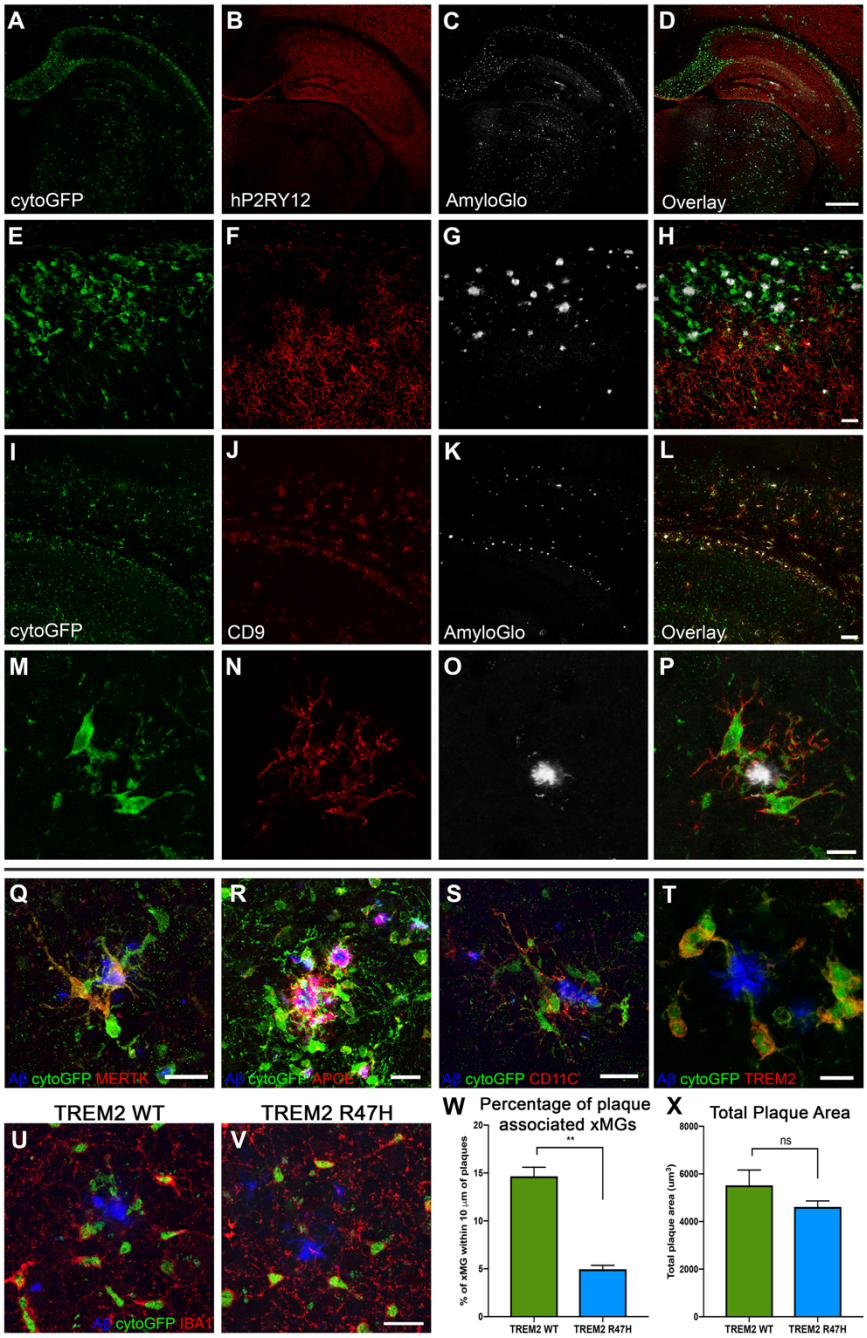

R47H xMGs clustering around Ab plaques when compared to WT xMGs (Figures 1.8U–1.8W) despite there being no significant difference in overall plaque burden across mice (Figure 1.8X). Taken as a whole, these data demonstrate that xMGs do, indeed, adopt relevant activation states in response to amyloid pathology and that the impact of disease-relevant microglial mutations can

be accurately examined with this model.

Figure 1.8. xMGs Downregulate Homeostatic Markers and Upregulate Activation Markers around Ab Plaques. Representative images of xMGs in the hippocampus and subiculum of the 5X-MITRG at 9 months. (A–H) A low power image of xMGs (A, green) reveal a dramatic downregulation of the homeostatic marker P2RY12 (B, red) within the subiculum and CA1 of the hippocampus, regions with dense beta-amyloid plaque pathology (C, gray). Overlay is shown in (D). Higher magnification demonstrates the clear distinction between GFP + xMGs (E, green) that continue to express P2RY12 (F, red) and are not adjacent to plaques (G, AmyloGlo, gray), versus plaque-associated xMGs that down-regulate P2RY12 (H). (I–P) xMGs (I, green) also display increased expression of the DAM marker CD9 (J, red), when adjacent to fibrillar amyloid plaques (K, AmyloGlo, gray), whereas distal cells do not (L, overlay). A higher power view of plaque-associated xMGs (M, green) reveal the membrane-localized expression of CD9 (N, red) in human microglia adjacent to amyloid plaques (O, AmyloGlo, gray); overlay is shown in (P). (Q–T) Additionally, plaque-associated xMGs upregulate other DAM markers, including MERTK (Q), human APOE (R), CD11C (S), and TREM2 (T). (U–X) 5X-MITRG mice were transplanted with xMGs possessing either WT TREM2 (U) or a homozygous R47H mutation (V) and aged to 9 months. Quantification of xMG migration toward Ab plaques (blue, Amyglo) revealed a significant decrease in plaque-associated R47H-expressing xMGs (green, hNuclei/Ku80; red, IBA1) but no significant difference in total plaque burden (X). **p < 0.001, scale, 500 mm (A–D), 100 mm (E–L), 20 mm (M–S, U, and V), and 10 mm (T).

Single-Cell RNA-Seq Reveals Transcriptomic Alterations in Response to AD Pathology that Are Unique to Human xMGs

While our histological analyses appeared promising, we sought to further characterize the xMG response to amyloid pathology at the transcriptomic level by isolating xMGs from the brains of aged MITRG (n = 2) and 5X-MITRG (n = 4) mice. Single-cell RNA-seq (scRNA-seq) resulted in 10,184 MITRG and 8,673 5X-MITRG cells and average gene counts of 1,583 and 1,593 per cell, respectively. t-distributed stochastic neighbor embedding (tSNE) clustering of xMGs from both MITRG and 5X-MITRG mice (Figures 1.9A and 1.9B), from male and female mice, showed similar groups of MHC class II cells (orange; HLA-DRB1, HLA-DPB1, HLA-DQA1, and CD74), cells responding to type I interferon (blue; IFI6, IRF7, ISG15, STAT1, and IFIT3), a group resembling murine DAMs (salmon; CD9, TREM2, LPL, and ITGAX), as well as a cluster that was defined by a lack of the other cluster markers, which we deemed

homeostatic (green). Additionally, the MITRG xMGs displayed a cluster defined by high levels of inflammatory chemokines (purple; CCL2, CXCL10, CCL8, and CXCL11), while the 5X-MITRG xMGs did not have a clearly defined chemokine cluster but, instead, displayed a cluster of cells defined by genes related to secretory function. Interestingly, canonical microglia markers (P2RY12, P2RY13, CX3CR1, and TMEM119) showed a relatively even distribution across most clusters but decreased expression within the DAM clusters (Figures 1.9A, 1.9B). Additionally, despite general similarities between the clusters present in the MITRG and 5X-MITRG xMGs, differences existed in the proportion of microglia within each cluster (Figure 1.9C), with the DAM and MHCII clusters being larger in the 5X-MITRG and the Interferon cluster being reduced.

We next sought to further examine the expression levels of AD risk genes within the 5X-MITRG xMGs. Analysis of the expression levels of 50 AD risk genes revealed that 39 of these genes were expressed in at least one cluster and many were differentially expressed in specific clusters (false discovery rate [FDR] % 0.01). Furthermore, analysis of the amino acid sequences of these genes demonstrated that a number of AD risk genes display low amino acid homology when compared to their human counterparts and/or ambiguous gene homologs, and with CD33 lacking any reliable homolog in the mouse.

This observation led us to investigate whether the xMG approach was capable of revealing novel human-specific aspects of the microglia response to Ab. To do so, we performed DGE analysis between the DAM and homeostatic clusters in the 5X-MITRG and compared these genes to the DAM genes published by Keren-Shaul et al. (2017), as this was the most directly comparable study published to date. This comparison

revealed a substantial number of both up- (363 genes) and down- (378 genes) regulated genes that were unique to human xMGs (Figure 1.9D). However, it is important to note that, while the study published by Keren-Shaul et al. (2017) is the only currently published study examining the 5XfAD murine microglia response to Ab pathology at the single-cell level, other studies have attempted to elucidate a similar phenotype via bulk sequencing, microarray, and qPCR in APP/ PS1 and 5XfAD mice[5, 182, 183]. Therefore, we also performed a comparison of our xMG DAM genes to an aggregated gene list composed of all the unique genes specified in these studies plus the Keren-Shaul study. While this comparison yielded slightly altered genes lists, there was still a high degree of discordance between the datasets, with 342 upregulated and 336 downregulated genes uniquely attributed to human xMGs.

In order to confirm that these differences were indeed relevant to the human microglial response to Ab, we selected two genes, HLA-DRB1 and LGALS3 (galectin 3), which have both been implicated in AD, for histological validation at the protein level in both xenotransplanted mice and AD-patient tissue[170, 184]. As shown in Figure 1.9E, both proteins are highly expressed in xMGs adjacent to murine Ab plaques, and this expression pattern bears a striking resemblance to the plaque-associated microglial labeling in AD-patient tissue. While an in-depth validation of all the unique xMG genes discovered in this analysis goes beyond the scope of the current article, this model clearly provides ample opportunity to investigate novel aspects of the in vivo microglial response to amyloid pathology. We, therefore, propose that xMGs are not just capable of recapitulating general in vivo microglia behavior but that utilizing xMGs in conjunction

with disease models provides a method of uncovering new genetic insights into human neurological disease.

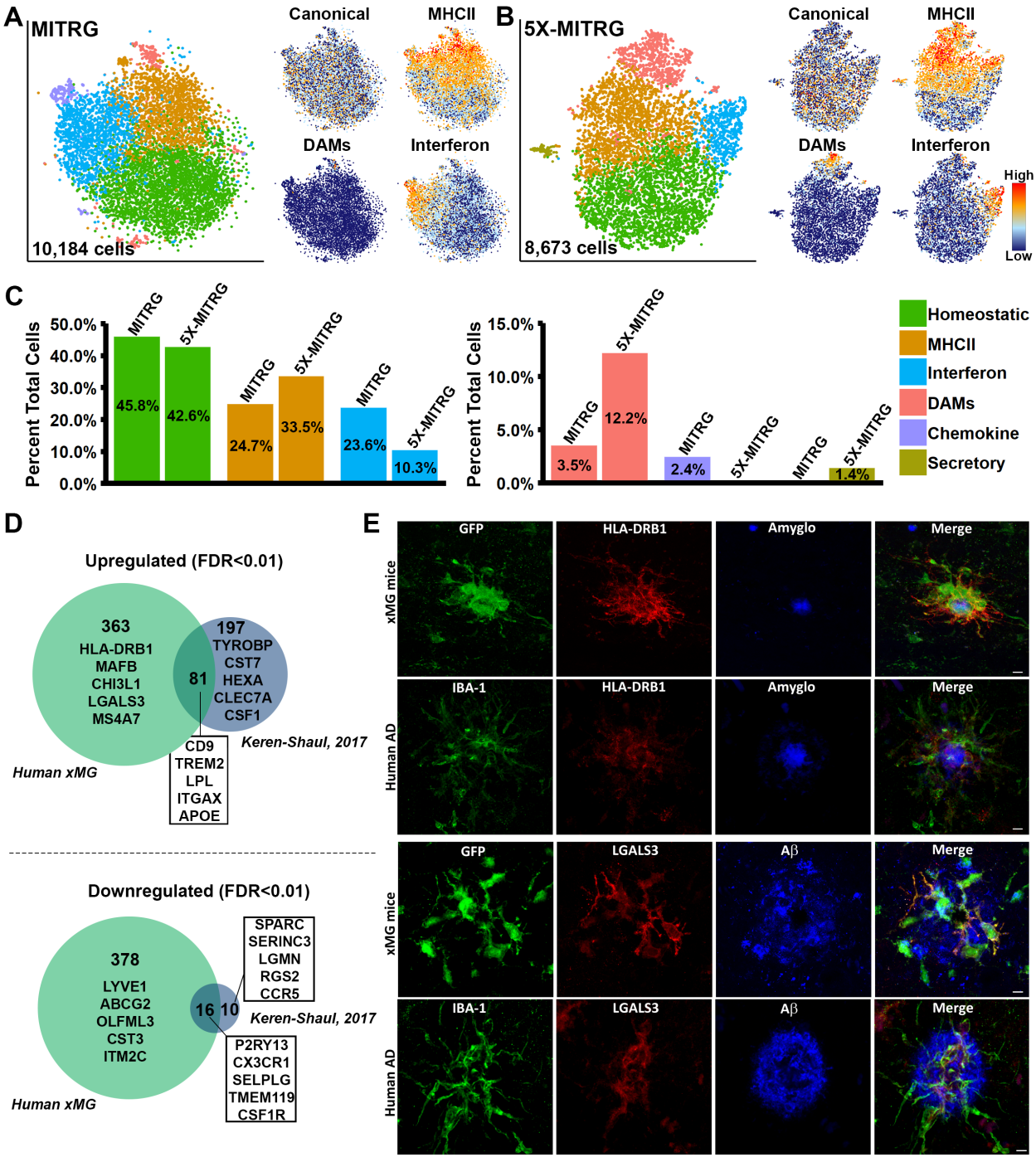

Figure 1.9. Single-Cell Sequencing of xMGs from MITRG and MITRG-5X Mice Reveals Altered Population Distributions and Human-Specific Genetic Responses. (A) tSNE plot of 10,184 xMGs isolated from 10.5-month-old MITRG mice (n = 2) reveals multiple clusters defined by genes related to

MHC class II (orange; HLADRB1, HLA-DPB1, HLA-DQA1, and CD74), type I interferon (blue; IFI6, IRF7, ISG15, STAT1, and IFIT3), DAMs (salmon; CD9, TREM2, LPL, and ITGAX), inflammatory chemokines (purple; CCL2, CXCL10, CCL8, and CXCL11), and a ‘‘homeostatic’’ cluster (green) that was mainly defined by a lack of activation markers. Additionally, canonical microglia markers (P2RY12, P2RY13, CX3CR1, and TMEM119) showed a uniform distribution across all clusters besides DAMs. (B) tSNE plot of 8,673 xMGs isolated from 10.5- and 12-month-old 5X-MITRG mice (n = 4) reveals similar clusters to the MITRG xMGs. Exceptions include the addition of a secretory cluster (olive; ANAX3, AGR2, PLAC8, and PLA2G7) the loss of a clearly defined chemokine cluster. (C) Bar plot comparing the percentage of total cells making up each cluster in WT MITRG and 5X-MITRG tSNE plots. (D) DAM genes, reported by Keren-Shaul et al. (2017), from 5XfAD murine microglia were filtered to contain only genes defined by Ensembl or NCBI Homologene to have 1:1 human orthologs. Remaining genes were then compared to the differentially expressed genes between DAM and homeostatic xMGs (FDR %0.01) demonstrating that limited overlap exists between the human xMG and mouse DAM genes. (E) Protein-level validation of human-specific DAM genes HLA-DRB1 (top) and LGALS3 (bottom) in both 5X-MITRG and human AD brain sections.

Discussion

Over the last decade, the field has increasingly recognized the importance of microglia in both homeostatic brain function and neurological disease. As our understanding has grown, so too has the need to develop more predictive models of human microglia to study these highly adaptable cells. Traditionally, this has meant collecting and culturing microglia from postmortem or surgically resected tissue or trusting that rodent microglia faithfully recapitulate human microglial phenotypes. While these approaches continue to be fundamental to our understanding of microglial biology, recent advancements have led to a more widely applicable toolkit. With the development of the first protocols to generate microglia from patient-derived stem cells in vitro, researchers are now able to model and manipulate the complex, polygenic landscapes that potentially underlie human microglia function and dysfunction. However, the field has also recently recognized that, despite these exciting new capabilities, the plasticity that makes microglia so fascinating represents a double-edged sword that complicates our attempts at in vitro modeling.

To address this challenge, we turned to transplantation of human iHPCs into the humanized, immune-deficient mouse brain. This paradigm induces robust microglial engraftment and differentiation of the complete complement of CNS macrophage subtypes. Additionally, microglia arising from this approach recapitulate the complex expression profile that is characteristic of their endogenous human counterparts, dynamically react to local and peripheral insults, and robustly respond to Ab pathology on both the morphological and transcriptomic levels. Taken together, these results support the conclusion that xMGs serve as suitable surrogates for endogenous human microglia, enabling new and informative in vivo studies of this important cell type.

Furthermore, similar approaches to ours have been published by two outside labs in Mancuso et al., 2019 and Svoboda et al., 2019 and submitted to BioRxiv by Xu et al., 2019 (doi:https://doi.org/10.1101/594721)[185, 186]. These papers used iPSC derived human microglia or progenitor cells transplanted into an immunodeficient mouse humanized for CSF1 at an early postnatal stage and all report that these cells will migrate and differentiate into mature human microglia. These papers also report a similar transcriptomic signature to freshly isolated human microglia and touch on the differences and similarities between human and murine gene signatures in homeostatic and inflammatory conditions. These experiments further validate the utility of our model and suggest our approach can reproduce healthy human microglial and allow us to study their responses and interactions with pathology.

Despite the many potential advantages of this chimeric model, it is important to note that xMGs expectedly come with caveats of their own, the most prominent being the requirement of an immune-deficient recipient organism. With recent studies

demonstrating the interactive relationship between microglia and peripheral immune cells, especially in the context of neurodegeneration, this deficiency is important to acknowledge[148]. While this problem is by no means unique to this model, as in vitro models inevitably suffer from the same pitfall, determining the most effective method of rectifying this shortcoming will require many additional studies. Additionally, it is wildly known that mouse CSF1 is not homologous enough to promote survival and differentiation of human microglia so it is possible that other less lethal non-homologies are present, either emerging from the host brain environment, or produced by the transplanted human cells[15].

Our hope is that the assessments herein provide sufficient demonstrations of the utility of this model that will encourage further studies examining the complex in vivo interactions between human microglia and neurological disease. The experiments utilizing the 5X-MITRG model and subsequent single-cell analysis have already revealed a substantial genetic response to Ab plaques that appears to be unique to human microglia. Additionally, our combination of this approach with an isogenic TREM2 mutant line has highlighted the potential use of this model to interrogate the impact of individual risk genes on human microglia function. By leveraging CRISPR technology and the growing availability of patient iPSC lines, our hope is that this approach can be broadly used to examine the impact of mutations, genetic diversity, and polygenic risk on human microglial function, thereby improving our understanding of these complex and fascinating cells.

CHAPTER 2

Using Chimeric Models to Study the Interactions Between Human Microglia and Alzheimer's Disease Pathology *in vivo*

Morgan A. Coburn, Whitney England, Jonathan Hasselmann, Amanda McQuade, Katherine Picard, Victor Lau, Jorge Silva, Alex Tamburino, Methodios Ximerakis, Jaclyn Beck, Sepideh Kiani Shabestari, Rebecca Mathews, Marie-Ève Tremblay, Robert C. Spitale, Hayk Davtyan, and Mathew Blurton-Jones

Introduction

Alzheimer's Disease (AD) is a progressive neurodegenerative disease, characterized pathologically by the accumulation of insoluble amyloid beta (Aβ) plaques and neurofibrillary tangles composed of hyperphosphorylated Tau. Alzheimer's can generally be subcategorized into two types, familial or fAD—where dominantly inherited mutations in three key genes: β-amyloid precursor protein (APP), presenilin 1 (PSEN1), and presenilin 2 (PSEN2) lead to early-onset AD, and the far more prevalent late-onset AD (LOAD) which is influenced by many genetic and environmental risk factors that in combination drive the development and progression of LOAD[18, 187, 188]. These genetic factors can occur with varying frequency and impact on disease risk; for instance, although fAD mutations are quite rare they are fully penetrant. In contrast, LOAD is generally associated with relatively common polymorphisms, many of which occur in loci that have been implicated in innate immunity and microglial functions[189, 190]. While these LOAD-associated risk genes confer relatively small individual effects, together they combine to confer a greater overall polygenic risk of disease[67, 191]. Yet understanding the collective functional consequences of these AD risk genes remains challenging, in large part because homology of these AD risk genes between human and mouse microglia is often poor[55]. Therefore, studies that examine how human microglia respond to and interact with a Aβ and tau pathologies could offer important new insight into the role of microglia in AD pathogenesis.

Microglia are the primary immune cell of the Central Nervous System (CNS) and intimately involved in numerous developmental, homeostatic, and neurodegenerative processes. Microglia arise from primitive hematopoietic progenitors (HPCs) that migrate

from the fetal yolk sac and begin to colonize the CNS at embryonic day 9.5 in mice[10]. Once mature, microglia use their highly motile processes to survey the entirety of the brain parenchyma every few hours[12]. *In vitro*, the inherent responsiveness of microglia to their environment underlies an important experimental confound as these cells dramatically shift transcriptional profiles upon isolation from the brain and *in vitro* culturing[19, 36]. Given the incredible environmental sensitivity that microglia display, we previously developed a chimeric model that introduces human microglial progenitors into the brains of early postnatal, immunodeficient, hCSF1 knockin mice[36]. This model achieves ~80% human chimerism within the murine forebrain by adulthood and has proven to be a useful tool to examine the transcriptional and function responses of human microglia to Aβ plaque pathology and the impact of AD risk genes on these reposes[36, 192, 193]. Given the considerable genetic divergence between humans and mice, especially as they pertain to AD, this chimeric approach further serves as an important way to assess the uniquely human response of microglia to AD pathology.

The transcriptional responses of murine microglia to neurodegenerative conditions have been well established, especially in regard to their interactions with Aβ plaques. Disease Associated Microglia (DAM), Microglial Neurodegenerative (MGnD) signatures, and Activated Response Microglia (ARM), signatures have been consistently characterized by a downregulation of homeostatic genes (P2RY12, P2RY13, CX3CR1, and CSF1R etc.), and a corresponding upregulation of genes implicated in phagocytosis, lipid metabolism, and neuroinflammation (i.e. TREM2, CD9, LPL, HLA-DR, ITGAX, etc)[5, 6, 45]. Interestingly, many of the microglia AD risk genes identified by GWAS exhibit altered expression in these DAM/MGnD/ARM

subpopulations. In addition, amyloidopathy leads to an enrichment of microglial subpopulations that express antigen presentation genes, transcripts upregulated in response to Type 1 Interferons, as well as genes that promote microglial proliferation. Our group previously demonstrated that human xenotransplanted microglia (xMG) will likewise also upregulate key DAM, antigen presentation, and IFN genes identified in mice, as well as many uniquely human transcripts, highlighting the importance of studying human microglial responses to AD pathology *in vivo*[36].

Although considerably less is known about the microglial response to Tau pathology, recent studies have begun to identify murine microglial populations that emerge in response to Tau phosphorylation and neuronal death. For example, in the CK-p25 mouse model of tau hyperphosphorylation, early microglial responses are characterized by upregulation of genes related to cell cycle and DNA replication, whereas late-stage responses during the neurodegenerative phase involve antigen presentation, interferon responsive genes, antiviral transcripts, and canonical DAM genes[194]. Exciting recent progress in the examination of human tauopathies including Frontotemporal Dementia (FTD), Progressive Supranuclear palsy (PSP), and AD have identified progressive stages of microglial activation[110]. Specifically, tauopathy-responsive microglia transition from responding to peptide activators with radical oxidative species and IL-1β transcripts, to lipid activators that initiate phagocytosis, to exocytosed nucleotide activators that induce Type 1 Interferons, to final late-stage Type 2 Interferon responses elicited by dying neurons and infiltrating leukocytes. These varying stages can be split into opposing ontogenetic forces, where an “activation” microglia subpopulation involves expression of antigen presentation and NLRP3

inflammasome genes which proceeds a more “suppressive” phenotype characterized by Type 1 Interferon responsive genes. Interestingly, “activation” microglia can be stimulated by Aβ and expresses genes that inhibit IFNβ production, whereas treatment with IFNβ suppresses this “activation” phenotype[110]. Single Cell RNA Sequencing (scRNA Seq) of human AD patients similarly highlights the emergence of a Type 1 Interferon responsive cluster of microglia that emerge[137].

Studies of specific human AD brain regions that exhibit high amyloid and/or tau loads have similarly described divergent microglia populations. For example, where regions high in amyloid pathology but low in tau are characterized by an “activation” phenotype that includes genes associated with ‘cell migration’ (*ITGAX*, *GPNMB* and *FLT1*), ’phagocytosis‘ (*COLEC12*, *MSR1*, *AXL*) and ’lipid localization’ (*SPP1*, *LPL*, *PPARG*). In contrast, the addition of tau pathology leads to a preferential shift to a population with possible neurotrophic functions, such as “synapse organization” (*GRID2*, *ADGRB3*, *GPM6A*) and “axonogenesis” (*UNC5C*, *SLIT2*, *NRXN1*)[195]. Though Gerrits and colleagues (2021) report substantial divergence between amyloid- and tau-responsive human microglia populations, an earlier paper described a similar network of co-expressed genes within the hippocampus of amyloid and tau transgenic mice, where one major exception was a critical TREM2 hub that occurred in amyloid mice alone. This prior analysis suggests that murine microglial responses to AD pathologies may be more homogeneous than that of human microglia[109]. Interestingly, in combined amyloid and tau models, expression of TREM2 can restrain the progression of tau pathology, but only in the presence of amyloid[196].

Although recent studies have begun to shed light on microglial responses to amyloid and tau pathology and the relationship between tau and amyloid in this response, much remains unknown. The considerable genetic divergence between humans and mice, especially in microglial AD risk genes, and the many technical and physical challenges of collecting and examining human postmortem microglial samples, makes interpreting these findings challenging. It also remains unclear how agonal state or common comorbidities, many of which involve inflammation, impact the microglial signature observed in postmortem samples[197]. To further address this important area of research we have generated and examined novel chimeric models of AD that develop neurofibrillary tangle pathology, amyloid pathology, or combined amyloid and tau pathologies. By transplanting human microglial progenitors into each of these models and examining the transcriptional and histological responses of human microglia to varying disease states, we sought to further our collective understanding of the role of microglia in AD.

Materials and Methods

Animals. All animal procedures were conducted in accordance with the guidelines set forth by the National Institutes of Health and the University of California, Irvine Institutional Animal Care and Use Committee. The human M-CSF knockin mouse model was purchased from Jackson Laboratories (stock #017708) and includes deletions of Rag2-/- and (Il2rg-/y, and humanized CSF1. hCSF1-PS19 mice were generated by backcrossing PS19 mice (B6;C3-Tg(Prnp-MAPT*P301S)PS19Vle/J JAX stock #008169) onto the hCSF1 background and restoring homozygosity for hCSF1, RAG2, and il2rg

alleles while maintaining hemizygosity for the PS19 tau transgene The hCSF1-5xfAD model was previously generated using a similar strategy of backcrossing 5XFAD mice with hCSF1 mice[36]. To generate all four of the genotypes examined in the current study (WT, 5XFAD, PS19, PS-5X), hCSF1-5xfAD were crossed with hCSF1-PS19 mice. All mice were age and sex matched and group housed on a 12h/12h light/dark cycle with food and water ad libitum.

Acquisition and maintenance of iPSC lines. GFP-expressing iPSC line (Coriell, AICS-0036) was purchased from Coriell and previously generated by CRISPR modification of the line WTC11 to insert a monoallelic mEGFP into the AAVS1 safe harbor locus under a CAGG promoter. Maintenance of iPSC lines involved culturing in feeder-free conditions in complete mTeSR E8 medium (StemCell Technologies, Inc.), in a humidified incubator (5% CO_2, 37°C), with medium changed daily. Passaging was performed every 7-8 days using ReLeaSR (StemCell Technologies, Inc.) and cells were plated onto 6-well plates (Corning), coated with growth factor-reduced Matrigel (1mg/mL; BD Biosciences), in mTeSR E8 medium, supplemented with 0.5uM Thiazovivin (StemCell Technologies, Inc.) for the first 24 h post-passage. All cell lines were tested for mycoplasma on a monthly basis, and confirmed to be negative, and normal 46XY karyotyping was confirmed every ten passages.

Differentiation of Hematopoietic Progenitor Cells and Microglia from iPSCs. iPSCs were differentiated into hematopoietic progenitor cells (iHPCs) and iPSC-microglia following our previously published protocol[27]. Briefly, iPSCs were

passaged in mTeSR1 to achieve a density of 40 colonies of ~100 cells each per 35 mm well on Matrigel-coated plates (1 mg/plate). On day 0, cells were transferred to Medium A from the STEMdiff Hematopoietic Kit (Stem Cell Technologies Cat #05310). On day 3, flattened endothelial cell colonies were observed and media was changed to Medium B. On day 10-12, medium and floating cells were carefully removed with a serological pipette to collect non-adherent CD43+ iHPCs. At this point, d10-d12 iHPCs were frozen in Bambanker (Wako) to avoid batch differences throughout the study. Cells used for early-postnatal iHPC transplantation were thawed in iPS-Microglia medium (DMEM/F12, 2X insulin-transferrin-selenite, 2X B27, 0.5X N2, 1X glutamax, 1X non-essential amino acids, 400 mM monothioglycerol, and 5 mg/mL human insulin freshly supplemented with 100 ng/mL IL-34, 50 ng/mL TGFβ1, and 25 ng/mL M-CSF (Peprotech)) and allowed to recover for 24-48 hours, then resuspended at 62,500 cells/μL in 1X DPBS (low Ca 2+, low Mg 2+). To continue differentiation of iHPCs to iPSC-microglia for *in vitro* studies, media was added to thawed or fresh iHPCs every 48 hours for 28 days with extra cytokines CD200 and CXCL1 added for the last 3 days in culture.

Treatment of in vitro Microglia and Incucyte imaging. Mature iPSC-microglia were plated at 30% confluence onto fibronectin (StemCell Technologies) coated glass imaging plates (Corning). Cells were allowed to settle before treatment for 24 hours with IFNα-2A (100 ng/mL), IFNβ (100 ng/mL), a combination of IFNα/β (50 ng/mL each), IFNγ (100 ng/mL), or IL-1β (100 ng/mL). Inflammasome activation followed a classical LPS+ATP paradigm; 100 ng/mL LPS for 3 hours, followed by addition of 10 uM ATP and then immediate imaging. Cell eccentricity was examined using the Essen IncuCyte S3 with

four images per well, n=4 wells per condition. Phase masks were calculated using IncuCyte 2020B software.

Early Postnatal Intracerebroventricular Transplantation of iHPCs. On P0, pups were tail clipped for overnight PCR to probe for sex, PS19, and 5XFAD genotypes, at this point pups were also tattooed for later identification. P1-P3 hCSF1-PS5x mice received bilateral intracerebroventricular transplants of 500K total iHPCs according to our protocol published by Hasselmann & Coburn et al. (2019). In brief, pups were placed in a clean cage over a heating pad with a nestlet from the home cage to maintain the mother's scent. Pups were then placed on ice for 2-3 min to induce hypothermic anesthesia. Free-hand transplantation was performed using a 30-gauge needle affixed to a 10 mL Hamilton syringe, mice received 1 ml of iHPCs suspended in sterile 1X DPBS at 62.5K cells/ ml at each injection site (8 sites) totaling 500K cells/pup. Bilateral injections were performed at 2/5th of the distance from the lambda suture to each eye, injecting into the lateral ventricles 3mm down from the surface of the skull and into the overlying anterior cortex at 1 mm down, and into the posterior cortex in line with the forebrain injection sites, and perpendicular to lambda at a 45° angle. Transplanted pups were then returned to their home cages and weaned at P21.

Immunohistochemistry, Immunocytochemistry, and Confocal Microscopy. Animals were administered Euthasol and monitored for loss of consciousness. Once animals no longer responded to toe pinch, mice were intracardially perfused with ice cold 1X DPBS. xMGs were isolated from ½ brains (see detailed methods below), and the remaining half

brain was drop fixed in 4% (w/v) PFA for 48 h. Samples were then cryoprotected in 30% (w/v) sucrose and then cut coronally at 40 mm on a freezing sliding microtome. Tissue sections were collected and stored as free-floating sections in PBS with 0.05% sodium azide. For staining, tissue was blocked for 1 h in 1X PBS, 0.2% Triton X-100, and 10% goat or donkey serum. For Ab plaque visualization sections were stained with Amylo-glo (1:100; Biosensis Cat #TR-300-AG) for 20 min. Immediately following blocking and Amylo-glo staining if applicable, sections were placed in primary antibodies diluted in 1X PBS and 1% goat or donkey serum and incubated overnight on a shaker at 4°C. Primary antibodies used include: GFP (1:500; Millipore Cat# Ab16901), MC-1 (1:1000; generous gift of Dr. Peter Davies), HT7 (1:1000; Thermo Fisher), MAP2 (1:500; Abcam Cat# ab5392), P2RY12 (1:1000 withCitrate antigen retrieval, Sigma Cat# HPA014518, Ku80 (1:250; Invitrogen Cat#MA5-12933), MX1 (1:200; Cell Signaling Cat# 37849), CD9 (1:200; Biolegend Cat# 312102), IRF3 (1:200; Cell Signaling Cat# 11904T), IRF4 (1:200; Cell Signaling Cat# 15196T), IRF5 (1:200; Cell Signaling Cat# 20261T), HLA-DR (1:200; Invitrogen Cat# 14-9956-82), MerTK (1:200; Abcam Cat# ab52968), and ASC-TMS1(1:200; Cell Signaling Cat# 13833T). Following overnight primary antibody incubation sections were placed in appropriate Alexa Fluor conjugated secondary antibodies (Life Technologies) for 1 h, before rinsing and mounting on microscope slides with Fluoromount G (Southern Biotech). For *in vitro* studies, iPS Microglia were fixed with prewarmed 4% PFA for 7 minutes, washed 2x with DPBS. For immunocytochemistry, cells were blocked for 1 h in 1X PBS, 0.2% Triton X-100, and 10% goat or donkey serum then incubated in primary antibodies diluted in 1X PBS and 1% goat or donkey serum and for 1hr at room temp or overnight at 4°C. Cells were then incubated in Alexa-

conjugated secondary antibodies for 1 h, before washing and bathing in PBS for imaging. Immunofluorescent brain sections and fixed in vitro microglia were then imaged using an Olympus FX1200 confocal microscope. Images collected for quantitative analysis were captured at 40X using identical parameters within a given analysis group. Representative confocal Z stacks were also captured at 40X or 60X. In some cases, brightness and contrast settings were slightly adjusted to reveal fine structures and morphology and pseudocolored for clarity and consistency. Such adjustments were only made to representative images, non-quantified and applied equally across groups.

Imaris Quantification and Statistical Analysis. All quantification of confocal images was performed blinded to genotype or treatment. To examine human microglial interactions with Ab plaques and neurofibrillary tangles, sections were stained with antibodies against GFP (to amplify endogenous expression in xMGs), AmyloGlo (fibrillar Aβ), and MC-1 (misfolded tau). IMARIS 9.7.0 based quantification of Aβ plaques and Tau pathology was performed using the ‘‘Surfaces’’ function to provide information on area. For further analysis of Rod microglia, additional sections were stained with antibodies against MC-1 (tangles), CD9 (Disease Associated Microglia), and MX1 (IFN responsive microglia) and the IMARIS “Surfaces” function used to quantify area and intensity. To assess *in vivo* microglial elongation, z-stacks were first processed using a median filter in order to better define edges and subtract autofluorescence, then the “Surfaces” function was performed on GFP positive cells and Object-Oriented Bounding Box lengths A, B, and C were assessed. To assess *in vitro* microglial elongation, single plane images were first processed using a median filter, followed by gamma correction, and then background

subtraction to ensure cell edges were distinct and to minimize the software categorizing two neighboring cells as one, then the “Cells” function was performed on GFP positive cells and Objection Oriented Bounding Box length “C” was divided by “B” to obtain a length to width ratio on cells images on a single plane (Axis “A” represented the z axis in the single stack images). Analysis of distributions of elongated *in vivo* and *in vitro* microglia was performed using a Kolmogotov-Smirnov test. Total plaque and MC-1 area, were tested for statistical significance ($p < 0.05$) though unpaired t tests. CD9 and MX1 expression and microglial elongation were tested for statistical significance ($p<0.05$) through 2way ANOVA with multiple comparisons using Prism 9. All data sets were analyzed for outliers prior to running t tests or ANOVAs using a ROUT outlier test (Q = 1%). To assess the total length and numbers of filopodia present on treated in vitro microglia, the ImageJ plugin, FiloQuant, was used[198]. When indicated, numbers and lengths of filopodia were normalized to total GFP+ cells as determined by IMARIS “Surfaces" described above. Numbers and lengths of filopodia were tested for statistical significance ($p<0.05$) through 2way ANOVA with multiple comparisons using Prism 9.

Tissue preparation for electron microscopy. Sections from male and female hCSF1-PS5X containing the dorsal hippocampus (Bregma -1.46 mm to -2.18mm) were used for electron microscopy. Sections were rinsed in phosphate buffer (PB, 0.1M, pH 7.4), and then post-fixed in a 0.6% glutaraldehyde (Electron Microscopy Sciences) solution in 4% paraformaldehyde (PFA) in PB for 1h, then sections were further incubated in 4% PFA in PB for another 1 hour. Sections were washed with phosphate-buffered saline (PBS, 50 mM, pH 7.4) and immersed in a 0.3% H_2O_2 in PBS solution for 5 minutes. Sections were

then washed in PBS and incubated in a 0.1% $NaBH_4$ solution in PBS for 30 minutes. Sections were subsequently washed again in PBS and immersed in a blocking buffer solution (10% donkey serum, 3% bovine serum albumin, 0.01% Triton X-100 in PBS) for 1 hour. Sections were incubated at 4°C overnight with chicken anti-GFP antibody in blocking buffer ([1:5000], Aves Lab, cat. #GFP-1020). The next day, sections were washed with PBS for 5 times 5 minutes, and then incubated in a biotinylated donkey anti-chicken secondary antibody ([1:200], Jackson ImmunoResearch, cat. 703-005-155) in Tris-buffered saline (TBS, 50mM, pH 7.4) for 90 minutes. Sections were subsequently washed in PBS and incubated in avidin-biotin complex solution (Vectastain, cat. #VECTPK6100) in TBS. Following additional PBS washes, sections were stained with 0.05% 3,3'-diaminobenzidine (DAB), 0.015% H_2O_2 solution in Tris-HCl (0.5M, pH 8). After DAB incubation, sections were washed in PB and incubated in an equal volume of 3% potassium ferrocyanide in PB and 4% aqueous osmium tetroxide (Electron Microscopy Sciences). Following washes in PB, tissues were incubated for 20 minutes in warm 1% thiocarbohydrazide solution in double distilled water (ddH_2O) and then washed in ddH_2O. A 30 minute incubation of 2% osmium tetroxide was performed afterwards. Brain sections were then washed in ddH_2O and dehydrated with an increasing concentration of ethanol (5 minutes each): 2x35%, 1x50%, 1x70%, 1x80%, 1x90%, 3x100%. After ethanol dehydration, the sections were immersed three times for 5 minutes in propylene oxide and submerged overnight in Durcupan resin (Sigma Canada). The following day, tissues were placed between 2 fluoropolymer sheets (ACLAR, Electron Microscopy Sciences), covered with a thin layer of resin and placed 4 days at 55°C to polymerize.

Ultramicrotomy and transmission electron microscopy. The dorsal hippocampus CA1 was excised from the fluoropolymer sheet with a razor blade and glued onto a resin block. Ultrathin sections were cut at 70nm using a Leica ARTOS 3D Ultramicrotome. and pictures were acquired using a JOEL JEM-1400 transmission electron microscope operated at 80 kV and equipped with a Gatan SC-1000 digital camera. Pictures of xMG cell bodies and processes, identified by their GFP immunoreactivity, were acquired at magnifications ranging between x6000 and x10000. Lipid bodies were identified by their round and homogeneous shape and dark outline. Lysosomal inclusions were recognized by their ovoid-like shape, irregular pattern and dark appearance. Endoplasmic reticulum were considered dilated when the closer gap per two opposing membranes presented a distance greater than 100 nm. between the closer gap per two opposing membranes. Mitochondrial ultrastructural alterations were identified by the dilatation of their cristae. Pre-synaptic axon terminals were identified by their synaptic vesicles and post-synaptic dendritic spines were identified by their post-synaptic density. Neurons were recognized by their pale, large and round nucleus, and distinctive heterochromatin pattern[199-201].

Tissue dissociation and magnetic isolation of xMGs for scRNA-seq. N=4, 6 month old male mice per genotype were killed using Euthasol and perfused with ice cold PBS, where immediately half brains were dissected, and the cerebellum was removed. Tissue was stored briefly in RPMI. Tissue dissociation was then performed using a Dounce homogenizer. Briefly, ½ brains were added to a 7mL Dounce homogenizer containing 4mLs of RPMI, tissue was homogenized by first performing 10 strokes using the “A” pestle, followed by another 10 strokes using the “B” pestle. At this point, homogenate was

then passed through a sterile 70mm filter and pelleted by centrifugation (10 min, 400xg, 4°C). Myelin and debris were removed by resuspending the pellet in 8mL 30% Percoll, overlaid with 2mL of 1X DPBS, spinning at 400xg for 25 min at 4°C, with acceleration and brake set to 0, and discarding the myelin band and supernatant. Dissociated cell pellets were resuspended in 80uL FACS buffer (0.5% BSA in 1X DPBS) + 20uL Mouse cell removal beads (Miltenyi) to remove all mouse cells and incubated at 4°C for 15 min. Samples were then separated using LS columns and the MidiMACs separator (Miltenyi) and the human cells were collected in the flow through. Purified human cells were then pelleted via centrifugation (10 min, 400xg) and dead/apoptotic cells were removed using the EasySep Dead Cell Removal (Annexin V) kit (Miltenyi; cat# 17899). Cell pellets were resuspended in 70uL of Dead Cell Removal (DCR) buffer (2% BSA and 1mM CaCl2 in PBS) followed by the addition of 5uL of the DCR Cocktail and 5uL of the Biotin Selection Cocktail. Samples were then incubated at room temperature for 3 min. After incubation, 10mL of DCR beads were added immediately followed by 2.4mL of DCR buffer and incubated for at RT for 10 minutes on the EasyEights EasySep magnet (StemCell Technologies; cat #18103). Keeping the sample on the magnet, the supernatant was collected and pelleted by centrifugation (10 min, 400xg, 4°C). Cells were then resuspended at ~1,000 cells per microliter in FACS buffer, according to counts performed on a hemocytometer. Two PS-5X samples were excluded due to a high debris content, and one 5XFAD sample was excluded due to low viability. Two samples from each group, unless otherwise stated were then pooled together for 10X single cell sequencing.

Single-cell sequencing via 10X. scRNA-seq library preparation was performed according to the 10X Genomics Chromium Single Cell 3' Reagents kit v3 user guide except that sample volumes containing 25,000 cells were loaded onto the 10X Genomics flow cell in order to capture ~10,000 total cells. The 10X Genomics workflow was then followed according to the manufacturer protocol and libraries were pooled at equimolar concentrations for sequencing on an Illumina NovaSeq 6000, targeting ~50,000 reads per cell. FASTQ files were aligned to the human GRCh38 transcriptome using the CellRanger v3.0.2 count command, with the expected cells set to 10,000 and no secondary analysis performed[202].

scRNA-seq Data Visualization and Differential Gene Analysis. UMI count tables were read into Seurat (v3)[203] for preprocessing and clustering analysis. Initial QC was performed by log normalizing and scaling (default settings) each dataset followed by PCA performed using all genes in the dataset. Seurat's 'ElbowPlot' function was used to select principal components (PCs) to be used for clustering along with a resolution parameter of 0.5 and clusters identified as being doublets, gene poor, or dividing were removed from the dataset prior to downstream analysis. Secondary QC cutoffs were then applied to retain only cells with less than 20-25% ribosomal genes, 12.5% mitochondrial genes, greater than 500 genes but less than double the median gene count, and greater than 500 UMI but less than double the median UMI count. At this point one PS19 and one PS-5X sample were discarded due to a failed 10X run. Cells passing QC for each sample were then merged using Seurat's 'merge' function and datasets were processed using Seurat's integrated analysis workflow[204]. Briefly, samples from individual mice were

integrated using the 'FindIntegationAnchors' and 'IntegrateData' commands using dimensions 1:25. Datasets were then scaled and sources of technical variation were regressed out (number of genes, percent ribosomal genes, and percent mitochondrial genes) and PCA was performed using Seurat's 'RunPCA' command. A shared nearest neighbor (SNN) plot was generated using Seurat's 'FindNeighbors' function using PCs 1:40 as input, clustering was performed using the 'FindClusters' function and a resolution parameter of 0.3, and dimension reduction was performed using the 'RunUMAP' function with the same PCs used for generating the SNN plot. Differentially expressed genes were determined between clusters using the 'FindAllMarkers' function, which employs a Wilcoxon Rank Sum Test, with and FDR cutoff of 0.01, an LFC cutoff of 0.25, and the requirement that the gene be expressed in at least 10% of the cluster and clusters were labeled according to manual curation of the differential gene lists.

DPA analysis. To assess potential differences in cluster proportions between genotypes we utilized a modified version of scDC[205]. Briefly, we used stratified bootstrap resampling as described in [scDC paper] to generate additional imputed populations. We initially attempted to re-cluster each bootstrapped population using Seurat's *FindNeighbors()* and *FindClusters()*[203, 206, 207]. However, our original clustering contains one very large cluster and multiple clusters that are at least ten times smaller in cell count. This, in addition to the heterogeneity of the population as a whole, made it difficult for *FindClusters()* to fully partition out all cell types in the bootstrapped samples even with a high resolution parameter. Therefore we opted not to recluster after bootstrapping, and instead used the alternative *scDC_NoClustering()* library method

provided by the authors [cite scDC paper]. This method performs bootstrap resampling a total of 10,000 times, and calculates new proportions and cell counts from the original cluster identities attached to the cells in each sample.

We then fit a generalized linear model to each set of imputed cell populations using the following formula: *glm(cellCount ~ cellType*genotype, family = poisson(link=log))* where *cellCount* is the number of cells identified as a certain cell type for a certain genotype. Before fitting the model, total cell counts were normalized across samples and genotypes, while maintaining the proportion of cells for each cell type within each sample. Statistics from each GLM were pooled as in [scDC paper] using the R package *mice*'s *pool()* function[208]. Significance of the pooled estimates was determined by the univariate Wald test. As we found significant interactions between multiple cell types and genotypes, we also conducted post-hoc pairwise comparisons. For each GLM, we ran the *multcomp* function *glht(fit, linfct=emm(pairwise~genotype|cellTypes, adjust="tukey"))*, which generated pairwise comparisons between genotypes within each cluster[209]. Estimates from each GLM for each comparison were pooled using *mice*'s *pool.scalar()* function, and significance for the pooled estimates was calculated using Tukey's test to adjust for multiple comparisons.

Pseudotime and Pseudobulk analyses. Pseudotime analysis was performed using Monocle 3[210]. Variable features used for dataset integration and PCA and UMAP embeddings from the Seurat analysis were used for trajectory analysis. The graph was constructed using Monocle's learn_graph function with default parameters. The graph vertex closest to the set of cells in the homeostatic cluster was used as the earliest point

in pseudotime. For Pseudobulk analysis differentially expressed genes between genotypes were identified using Seurat's FindMarkers function with an FDR cutoff of 0.01, an LFC cutoff of 0.10, and an expression cutoff of 10% of cells per genotype.

Gene Ontology Network and Transcription Factor Analysis. Overrepresented biological process GO terms were identified using PANTHER with an FDR cutoff of 0.05[211]. Genes with significantly increased or decreased expression in 5XFAD, PS19, or PS5X cells versus WT controls were compared to the full set of human genes. Identified GO terms were visualized as a network using the Enrichment Map 3.3.2 plugin for Cytoscape 3.8.2[212, 213]. For Transcription factor analysis binding sites within 500bp upstream of genes differentially expressed in 5XFAD, PS19, or PS-5X cells versus WT controls were identified using blerr (github.com/englandwe/blerr), using the JASPAR 2018 set of transcription factor binding sites with a Z-score cutoff of 2[214].

Subclustering of DAM, IL-1β, and IFN Clusters. Cells in the DAM, IL-1β, or IFN cluster were extracted from the full dataset, and independent sets of variable features were identified using Seurat's FindVariableFeatures function, RunPCA, FindNeighbors, and RunUMAP were run on each cluster as described above. Subclustering was performed using the FindClusters function at a resolutions of 0.3 for IFN and IL-1B and 0.5 for DAM. Differentially expressed genes between clusters were identified as described above. Subclusters were named using the GO Biological Processes 2021 output generated by inputting up to the top 20 upregulated genes in each subclusters into Enrichr.

Results

Development of novel chimeric mouse models to study the interactions between human microglia and amyloid and tau pathologies. We recently demonstrated that iPSC-microglial progenitors can be engrafted into an immune-deficient mouse model of AD to examine human-specific microglial responses to beta-amyloid pathology and the impact of *Trem2* mutations or deletion on these findings[27, 36, 193]. However, the interactions between human microglia and neurofibrillary tangles and the combined impact of amyloid and tau pathologies on these cells remains unclear. We therefore developed two additional chimeric mouse models to specifically examine these questions. We began by backcrossing the well-established PS19 model of neurofibrillary tangle pathology onto a hCSF1/Rag2$^{-/-}$/il2rg$^{-/-}$ background. PS19 mice express a human tau transgene carrying the frontotemporal dementia (FTD)-linked P301S mutation and develop progressive tau hyperphosphorylation and tangle formation. While the P301S tau mutation leads to FTD, not AD, these mice develop neurofibrillary tangle pathology that closely mimics that of human AD patients. As wild-type human tau expression fails to induce tangle formation in mice, the PS19 model is routinely used to examine both FTD- and AD-related aspects of tau pathology[104, 215-217].

Next, we crossed the resulting hCSF1-PS19 mice with an equivalent hCSF1-5XFAD mouse model which we previously generated and described[36]. hCSF1-5XFAD mice expresses mutant transgenes for amyloid precursor protein (APP) and Presenilin-1 (PSEN1) on the hCSF1/Rag2$^{-/-}$/il2rg$^{-/-}$ immunodeficient background. As both PS19 and 5XFAD transgenes are maintained in a hemizygous state and the hCSF1, Rag2, and

il2rg genes are maintained in a homozygous or (-/y) state, this F1 cross produces four specific genotypes: 1) hCSF1-WT mice, 2) hCSF1-5XFAD mice, 3) hCSF1-PS19 mice, and 4) hCSF1-PS19-5X mice.

Human microglia interact with amyloid and tau pathology *in vivo*. To examine the potential interactions between human microglia and amyloid and tau pathologies, mouse pups from each of the four genotypes (WT, 5XFAD, PS19, PS-5X) were transplanted on postnatal day 1-3 (P1-3), with GFP-expressing iPSC-derived microglial progenitors as described in Hasselmann and Coburn et. al (2019)[36]. Mice were then aged to 6 months and then euthanized to enable both immunohistochemical (IHC) and single cell RNA sequencing analyses. Immunohistochemical (IHC) analysis of GFP expression (green) revealed robust engraftment of xenotransplanted human microglia (xMGs) throughout the forebrain, including the hippocampus (**Figure 2.1A-E**) and cortex (**Figure S2.1A-F**) of all 4 genotypes: WT, 5XFAD, PS19, and PS-5X. To examine the potential interactions between microglia and amyloid and tau pathologies, GFP immunoreactivity (green) was combined with Amylo-Glo labeling of fibrillar Aβ (white) and MC-1 immunolabeling of misfolded pathological tau (red). Quantification of Aβ area revealed no differences between 5XFAD and PS-5X mice within CA1 of the hippocampus (**Figure 2.1F**), on the other hand, MC-1 positive Tau immunoreactivity was significantly increased in CA1 of PS-5X mice as compared to the PS19 mice (**Figure 2.1G**), consistent with prior reports that amyloid can accelerate the accumulation of pathological tau[196, 218-220]. Within the cortex we detected a significant increase in Aβ area in PS-5X mice as compared to the 5XFAD, whereas MC1+ Tau

pathology remained unchanged between PS19 and PS-5X mice in this region (**Figure S2.1A-F**). Similar changes in amyloid load in AD models have previously been described, although the impact of tau co-expression on Aβ varies considerably across differing bigenic models[221-224].

Most interestingly, imaging of GFP-expressing human microglia within CA1 of the hippocampus of PS-5X mice revealed many cells that exhibited a distinct elongated 'Rod-Like' morphology. Given the location of these Rod microglia within the Stratum Radiatum of CA1, we next utilized MAP2+ immunolabeling to examine the apical dendrites of CA1 pyramidal neurons in relation to GFP+ microglia. High power confocal imaging of this region revealed many Rod-shaped microglia (green) closely paralleling and interacting with MAP2+ dendrites (red). Notably, many small processes could also be seen extending from the main linear cell body of human microglia onto adjacent MAP2+ dendrites (**Figure 2.1H**). Whereas Rod-Like microglia have previously been described in varying pathological states, including Alzheimer's, Huntington's, and models of Traumatic Brain Injury (TBI), the transcriptional and functional significance of this highly distinct phenotype is largely unknown[119, 225, 226].

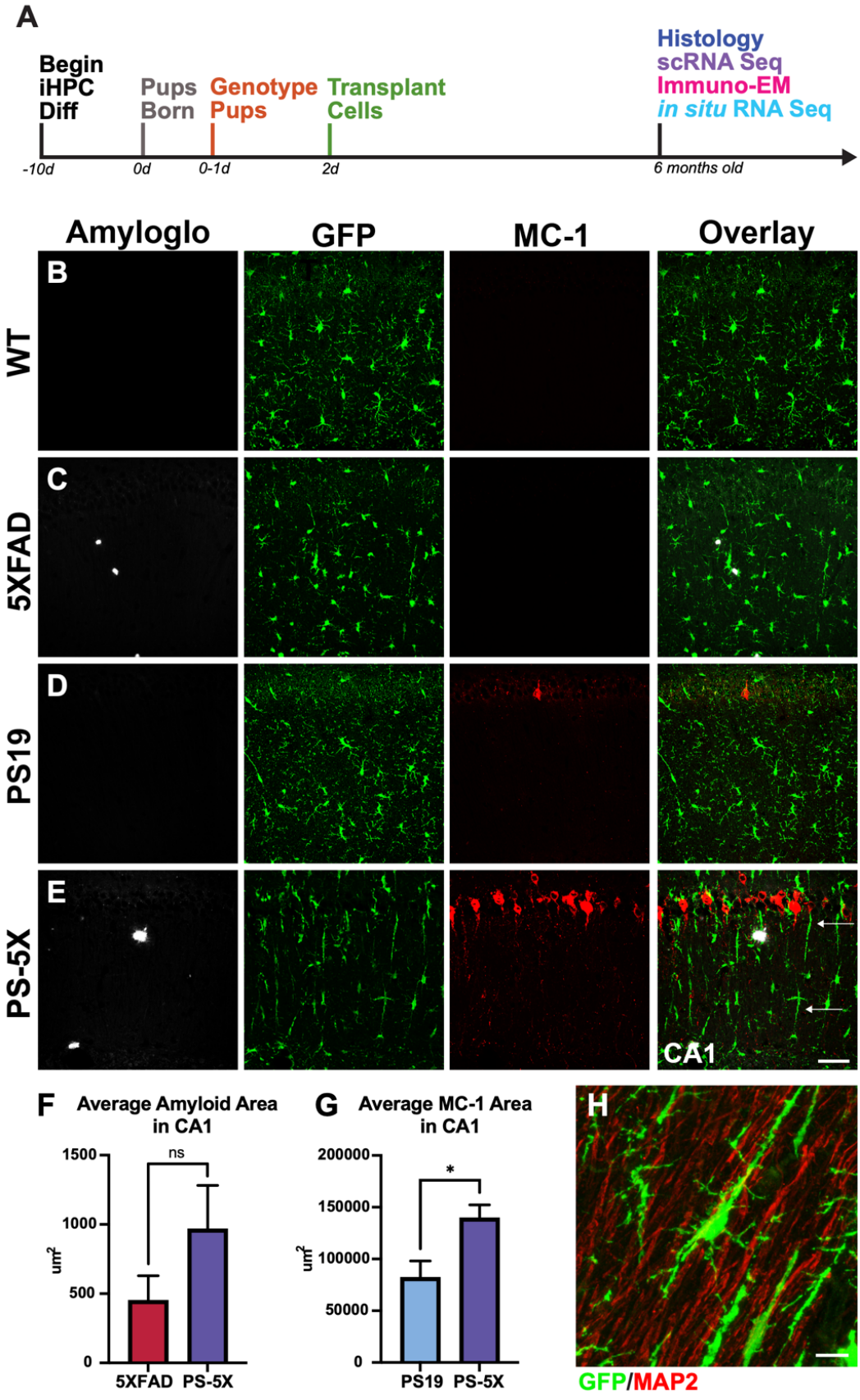
A
Begin iHPC Diff
Pups Born
Genotype Pups
Transplant Cells
Histology
scRNA Seq
Immuno-EM
in situ RNA Seq
-10d
0d
0-1d
2d
6 months old
Amyloglo
GFP
MC-1
Overlay
B
C
D
E
WT
5XFAD
PS19
PS-5X
CA1
F Average Amyloid Area in CA1
ns
1500
1000
500
0
um2
5XFAD
PS-5X
G Average MC-1 Area in CA1
*
200000
150000
100000
50000
0
um2
PS19
PS-5X
H
GFP/MAP2

Figure 2.1. Xenotransplanted human microglia differentially interact Amyloid and Tau Pathologies in vivo. Representative confocal Z-stacks captured within CA1 of the hippocampus of 6-month old chimeric mice. **(A)** Simplified experimental timeline. **(B)** Xenotransplanted microglia (xMGs, green, GFP) exhibit a typical tiled pattern of distribution within the hippocampus of wild-type mice. **(C)** In chimeric 5XFAD mice a subset of human microglia are observed adjacent to beta-amyloid plaques (amyloglo, white). **(D)** At 6-months of age PS19 mice exhibit only sparsely labeled MC-1+ neurofibrillary tangles (red) within the pyramidal cell layer of CA1. **(E)** In contrast, combined bigenic PS-5X mice exhibit greater numbers of MC1+ tangles, and xMGs surround and interact with both plaques and tangles. Whereas plaque-associated xMGs exhibit a more ameboid morphology, microglia adjacent to tau immunoreactive CA1 dendrites (MC1, red) exhibit an elongated Rod-like appearance (arrows). **(F)** Average CA1 amyloid area within CA1 remains unchanged between 5XFAD and PS-5X mice ($p = 0.1847$). **(G)** In contrast, MC-1 area is significantly higher in bigenic PS-5X hippocampus than PS19 mice ($p = 0.0207$) **(H)** GFP+ Rod microglia (green) are frequently observed in close apposition to MAP2+ dendrites (red). Scale A-D = 50μm, Scale G = 10μm.

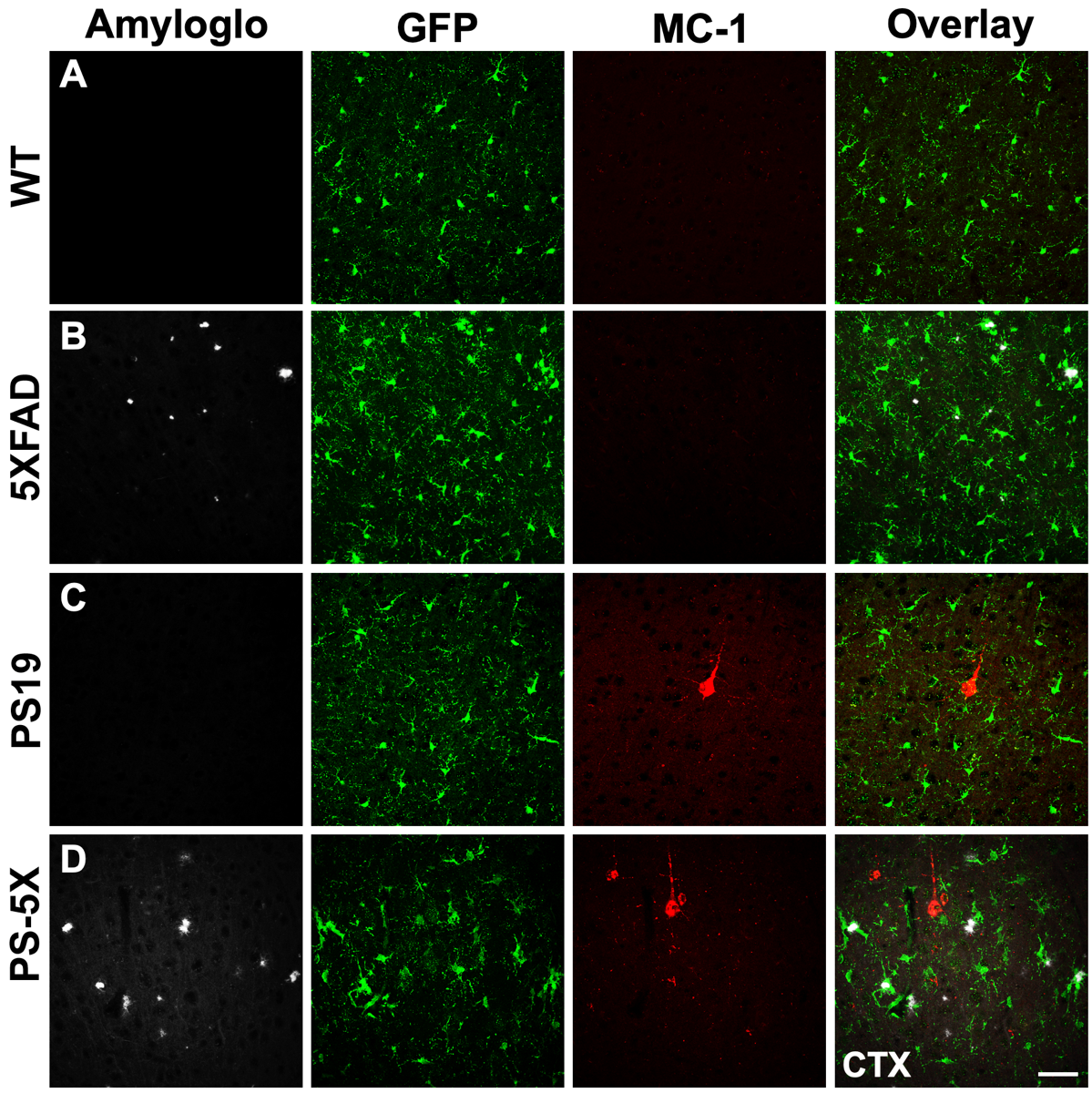
Amyloglo
GFP
MC-1
Overlay
A
WT
B
5XFAD
C
PS19
D
PS-5X
CTX

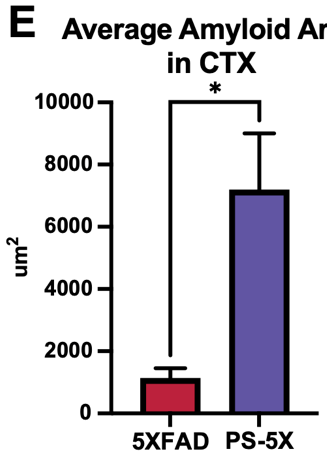
E
Average Amyloid Area in CTX
*
10000
8000
6000
4000
2000
0
um2
5XFAD
PS-5X

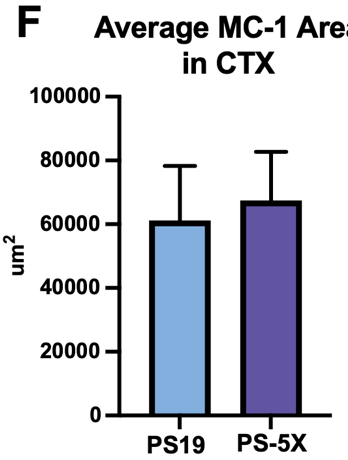
F
Average MC-1 Area in CTX
100000
80000
60000
40000
20000
0
um2
PS19
PS-5X

Figure S2.1. Human microglia interact with both amyloid and tau pathology within the cortex. Representative confocal images captured from the cortex overlying the dorsal hippocampus of 6-month old chimeric mice. **(A)** Human GFP-expressing microglia (green) are seen uniformly tiling the WT murine cortex (CTX). **(B)** In 5XFAD mice, xMGs are observed in close proximity to amyloid beta plaques (white). **(C)** xMGs in the PS19 cortex show little interaction with MC-1+ tangles (red). **(D)** xMGs approach and surround amyloid beta plaques in the PS-5X cortex. **(E)** Average amyloid area within the cortex is significantly increased in the PS-5X mice compared to 5XFAD mice ($p = 0.0157$). **(F)** In contrast, average MC-1 immunoreactive area is unchanged in PS-5X mice compared to PS19 mice. Scale = 50μm.

Human microglia adopt rod and satellite morphologies in chimeric mice and AD subjects. Given the unique Rod-shaped phenotype observed within CA1 of PS-5X mice (**Figure 2.1H**), we sought to better characterize morphology and examine canonical microglia markers in chimeric mice and human AD hippocampal samples. GFP-expressing xMGs adopt a striking Rod-like phenotype in CA1 of PS-5X mice that closely mimics the morphology of a subset of Iba1+ microglia within the hippocampi of pathology-confirmed human AD samples (**Figure 2.2A&B**). Upon further investigation we found that xMGs can also adopt a 'Satellite' phenotype wherein they closely associate their somas' with the somas of resident tau-expressing murine neurons (**Figure 2.2C**). A similar Satellite phenotype is also detected in human AD tissue, where Iba1+ microglia (green) can be seen interacting with tau immunoreactive (HT7+, red) tangles in the hippocampus (**Figure 2.2D**). This intriguing Satellite phenotype has previously been associated with loss of synapses in rodent models of TBI[227].

Along with the Satellite phenotype, Rod xMGs align next to tau+ dendrites in CA1 of PS-5X mirroring that of Rod microglia in human AD hippocampal tissue proximal to neurofibrillary tangles (**Figure 2.2E&F**). To further understand the phenotype of Rod microglia we began by examining expression of P2RY12, a purinergic receptor and canonical 'homeostatic' microglia marker. P2RY12 mRNA and protein levels are

typically diminished in ‘activated’ microglia including plaque-adjacent disease-associated microglia (DAMs). In contrast, Rod xMGs are nearly all immunoreactive for hP2RY12 (cyan) and can be seen closely abutting long-axis neuronal processes (red) and extending numerous fine filipodia onto MAP2+ dendrites (**Figure 2.2G&H**). As staining procedures for P2RY12 requires antigen retrieval that quenches the xMG GFP signal, the P2RY12 antibody was further confirmed to be human enriched by co-staining with the human-specific nuclear marker Ku80+ (**Figure S2.2**).

To quantify the prevalence of Rod microglia across each genotype we next utilized IMARIS image analysis to compare the long versus short axis of human microglia within each genotype. This analysis revealed that PS-5X xMGs have a significantly higher length to width ratio than WT, 5XFAD, and PS19 xMGs (**Figure 2.2I**). Indeed, by using a numerical cutoff for Rod xMGs (set to the WT mean ratio + standard deviation), Rod microglia were found to represent 35% of all PS-5X CA1 microglia and to be more than twice as abundant in PS-5X mice than other genotypes (**Figure 2.2J**). Nevertheless, it is clear that xMG morphology in PS-5X CA1s is not deterministic, as plaque associated xMGs within CA1 still retain a more ameboid DAM-like phenotype (**Figure S2.2C**).

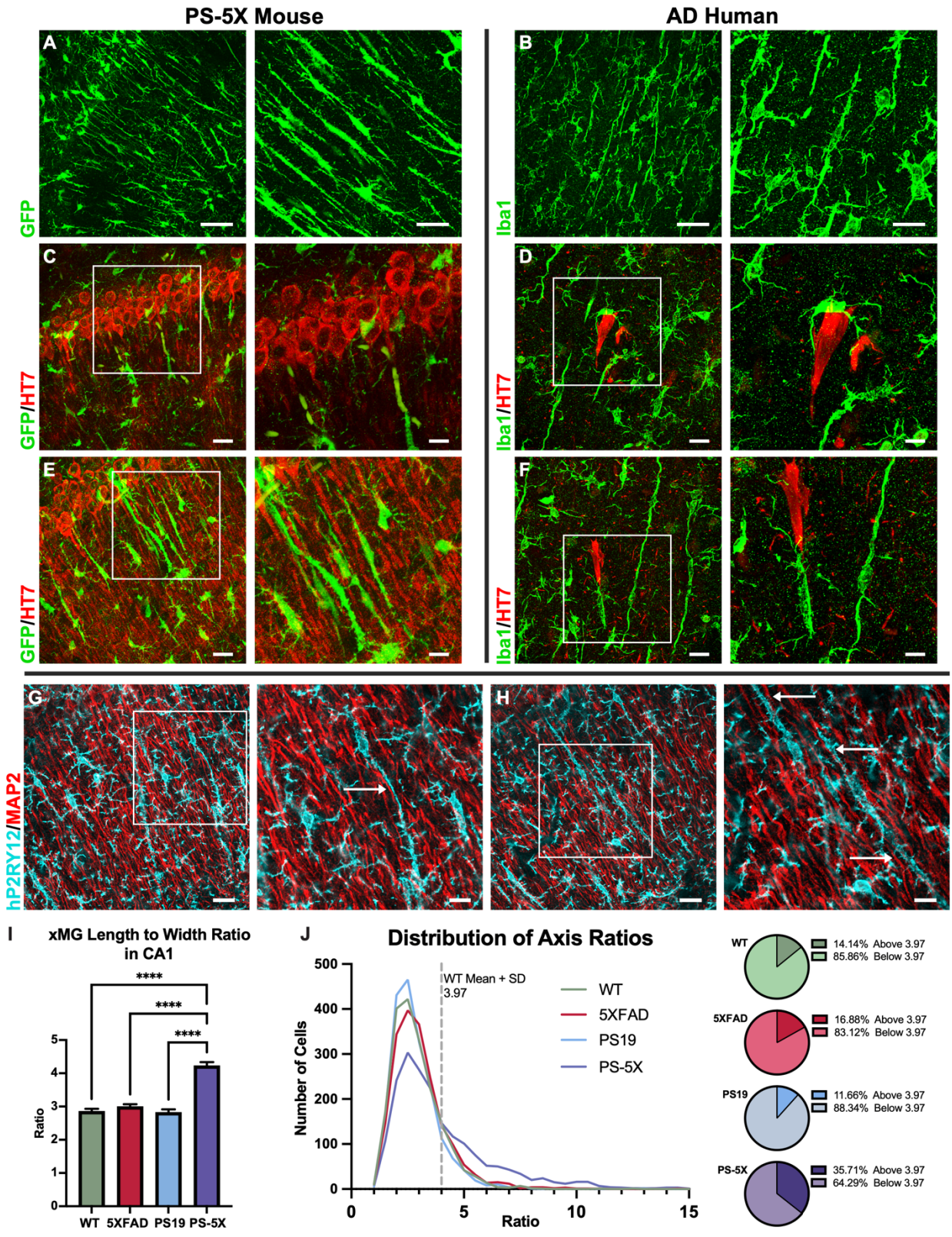

Figure 2.2. Human microglia adjacent to tau+ neurons adopt Rod and Satellite morphologies in chimeric PS-5X mice and AD patient samples. (A) xMGs adopt a striking rod phenotype in CA1 of PS-

5X mice (green, GFP). **(B)** A similar elongated morphology is observed within the hippocampus of pathology confirmed human AD tissue samples (Iba1, green). **(C)** Satellite xMGs can also be seen adjacent to the somas of tau+ murine neurons withing the pyramidal cell layer (GFP; green, Tau-HT7; red) and within Human AD tissue **(D)** (Iba1; green, HT7; red). **(E)** Rod xMGs align next to Tau positive dendrites in CA1 (GFP; green, Tau-HT7; red). **(F)** Likewise, Rod microglia in human AD hippocampal tissue are observed proximal to HT7+ tangles (Iba1; green, HT7; red). **(G)** Rod xMGs are nearly all positive for hP2RY12 (blue) and can be seen closely abutting long-axis neuronal processes (MAP2; red, arrow) **(G;** white arrow), microglial cell bodies **(H;** central white arrow), and extending fine processes toward MAP2+ dendrites **(H**; upper and lower arrows). **(I)** Imaris based quantification of GFP+ microglia show that PS-5X xMGs have a significantly higher length to width ratio than WT, 5XFAD, and PS19 xMGs (One-Way ANOVA with multiple comparisons; adjusted p<0.0001). **(J)** Distribution of length to width ratios of GFP+ XMGs, the grey dotted line represents a cutoff for Rod-Like xMGs set to the WT mean ratio + standard deviation. PS-5X mice have a higher percentage of cells that surpass this Rod morphology cutoff (purple; 35.71%), compared to WT (green; 14.14%), 5XFAD (red; 16.88%), and PS19 (blue; 11.66%) mice. A Kolmogotov-Smirnov test shows that PS-5X and WT groups (p < 1.00E-15; D = 0.2226) have the largest difference in distributions, whereas the 5XFAD (P = 6.48E-5; D = 0.07384) and PS19 (P = 0.0337; D = 0.04641) distributions are more similar to WT. Boxed regions in G and H are shown in 2X zoom right of their corresponding 1X images. Scale A & B left = 50µm, Scale A & B right, C-H left, = 20µm, Scale C-H right = 10µm.

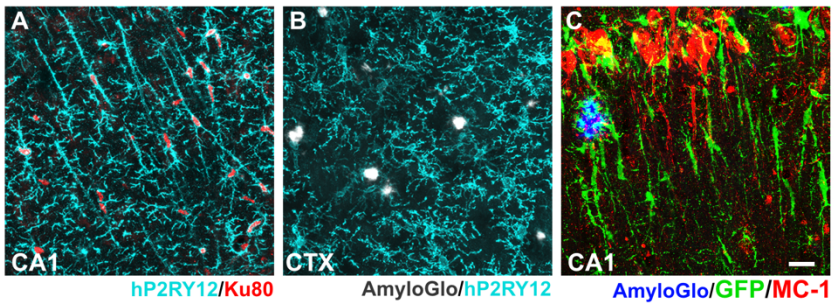

Figure S2.2. P2RY12 expression is downregulated around beta amyloid plaques. (A) P2RY12+ Rod microglia within CA1 of PS-5X mice co-label with the human nuclei-specific marker Ku80. **(B)** As expected, P2RY12 expression is downregulated in plaque associated DAM xMGs within the cortex. **(C)** xMGs (green) adopt differing morphologies in response to amyloid plaques (blue) and neurofibrillary tangles (red) within CA1 of PS-5X mice. Scale A-C = 20µm

Immuno-electron microscopy reveals ultrastructure of human microglia interacting with hippocampal neurons. P2RY12 is an ADP receptor and plays important roles in neuronal-microglial interactions and the microglial response to neuronal injury[112, 113]. Given the high expression of P2RY12 in Rod microglia, we sought to more closely examine the physical interactions between Rod microglia and hippocampal neurons by electron microscopy (EM). Immuno-electron microscopy was

performed to define and examine the ultrastructural interactions between human GFP-expressing microglia (dark electron-dense labeling of GFP) and CA1 neurons of 6-month-old PS-5X mice. This analysis revealed numerous examples of both Rod microglia and Satellite microglia that were closely interacting with neuronal dendrites and soma respectively **(Figure 2.3)**. Interestingly, in some examples. neuronal cell bodies exhibited dilated endoplasmic reticulum (ER), providing evidence of neuronal dysfunction. In many cases neuronal synapses or axon terminals were observed immediately adjacent to human microglia or microglial processes, suggesting that xenotransplanted microglia can directly interact with murine synapses.

Recent studies have shown that both aging and neuropathology can promote the accumulation of lipid droplets within microglia[193, 228, 229]. Our ultrastructural analysis likewise revealed examples of lipid accumulation within human microglia (**Figure 2.3C**). In some xMGs subcellular morphology indicative of cellular stress and dysfunction can be observed with the detection of dilated ER and dilated golgi (**Figure 2.3D**). In other examples, xMG processes can be seen enveloping a murine dendrite (**Figure 2.3E**), contacting a dendritic spines (**Figure 2.3G**), or extending a phagocytic cup (**Figure 2.3H**). Additionally, areas of extracellular degradation are visible in various frames, which may be the result of post fixation processing or Matrix Metalloproteinases (MMPs) secreted by nearby microglia[230].

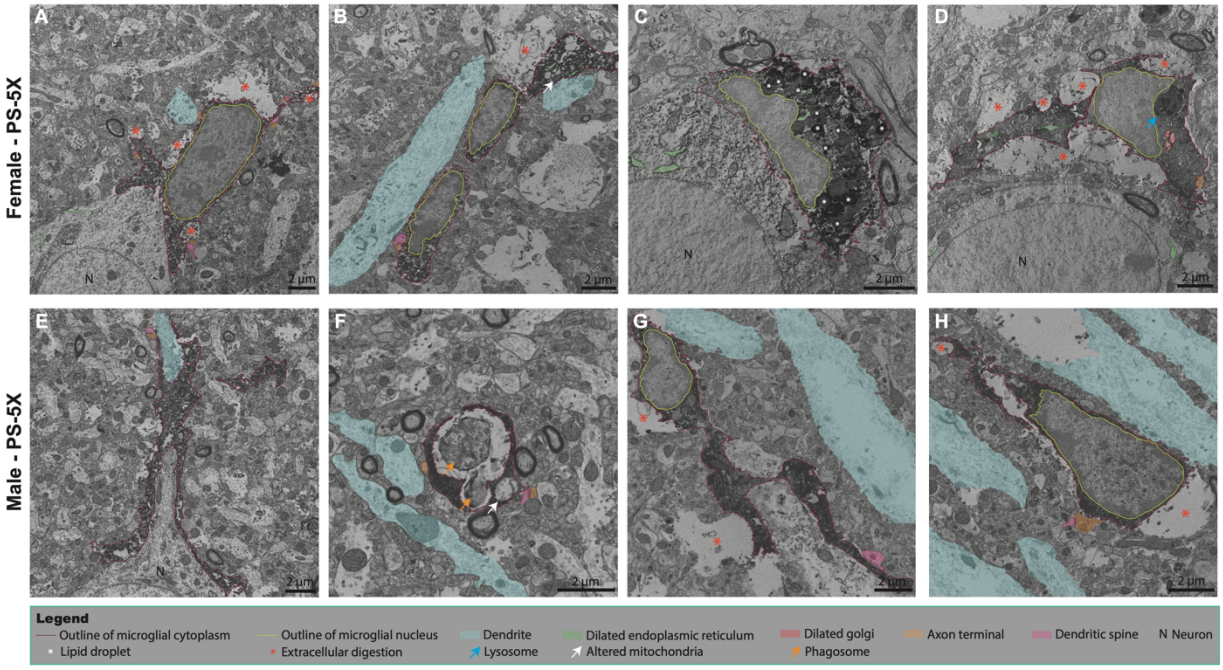

Figure 2.3. Immuno-Electron Microscopy reveals Ultrastructure of Human Microglia Interacting with Murine Neurons. Representative immuno-electron microscopy images of GFP+ xMGs engrafted in the stratum radiatum and stratum pyramidale of 6mo Female (A-D) and Male (E-H) PS-5X mice. A) A Satellite xMG (cytosol; outlined burgundy, nucleus; outlined yellow) is seen closely associating with a murine neuronal cell body (nucleus; labeled "N") with dilated endoplasmic reticulum (ER; green), as well as with several synapses (axon terminal, orange; dendritic spine, pink). The cross-section also reveals that the xMG is in close association with an axon terminal. Extracellular digestion (red asterisks) can also be observed adjacent to the xMG. B) Two Rod-Like xMGs are closely associated with murine dendrites and a synapse. Both xMGs show signs of cellular stress, such as ultrastructurally altered mitochondria (white arrows) and dilated ER. C) A Satellite xMG is closely associated with a murine neuron with dilated ER. The satellite xMG also contains multiple lipid droplets (white asterisks). D) Two xMGs extend processes to a nearby murine neuronal cell body and to each other, with one closely juxtaposing an axon terminal. Parenchymal areas surrounding the xMG display signs of extracellular digestion. Within the xMGs, dilated ER, dilated Golgi (red), and a lysosome (blue arrow) can all be visualized. E) xMG processes can be seen overlapping a murine neuronal axon hillock, extending down a dendrite. F) xMG processes encircle a phagosome (orange arrows), while an altered mitochondrion is visible within the process. G) A xMG has its cell body interacts with a murine dendrite, while its process contacts a dendritic spine. H) A Rod-Like xMG is situated between multiple murine dendrites. Extracellular digestion is seen near the xMG cytoplasm . Scale A-H = 2µm.

Amyloid and Tau pathologies differentially impact the transcriptional states of human microglia. To further characterize the response of xMGs to amyloid and/or tau pathologies we isolated engrafted cells from 6-month-old WT, 5XFAD, PS19, and PS-5X chimeric mice. Single-cell RNA-seq (scRNA-seq) was performed and following quality control filtering identified 12422 WT, 11045 5XFAD, 18599 PS19, and 5797 PS-

5X microglia with average gene per cell counts of 1661, 1658, 1137, and 1512 respectively. A uniform manifold approximation and projection (UMAP) plot of the combined 47,863 xMGs isolated from all four genotypes reveals multiple clusters of human microglia that are defined by genes related to MHC class II (MHCII; Orange; HLA-DRB1, HLA-DPA1, and HLA-DRB5), Type I Interferon Responsive (IFN: Salmon; IFI6, ISG15, and IFIT1), DAMs (Blue; CD9, CD83, and APOC1), Humanin-Like (Olive Green; MTRN2L10 and MT3), IL-1β (Purple; CXCL10, CCL4, and IL-1β), Degranulation (Lilac; AGR2 and ANXA3), Boarder Macrophages (Macros, red; CD163 and CD28) and a “homeostatic” cluster (Green) that was mainly defined by a lack of activation markers (**Figure 2.4A-C**). Both Dotplot (**Figure 2.4B**) and gene UMAP (**Figure 2.4C**) analyses revealed additional heterogeneity and some overlap of individual genes between clusters. For example, high expression of IFI6 is observed within the IFN cluster but also within subsets of the DAM and IL-1β clusters. Likewise IL-1β expression is most highly enriched in the IL-1β cluster but also within a subset of DAM microglia. To more clearly depict potential differences in cluster distributions across genotypes, UMAPs were down-sampled revealing, broadly, that the DAM, IFN, and/or IL-1β clusters are expanded in the 5XFAD, PS19, and PS-5X genotypes in comparison to WT mice (**Figure 2.4D**).

Next, pseudotime analysis was performed to better understand the potential progression from one transcriptional state to another. By setting an origin point in the homeostatic cluster, xMGs are found to follow two distinct paths. One trajectory moves upward and towards the right from the homeostatic state to induce the expression of MHCII genes before transitioning into a DAM state (**Figure 2.4E**). In contrast, a second

trajectory moves from the homeostatic state into an INF-enriched gene expression state that then proceeds to give rise to the IL-1β cell cluster. Similar evidence that murine microglia can follow distinct pathways toward specific activation states has been described before by Sala Frigerio et al., 2019[45]. However, to our knowledge this is the first evidence that human microglia can similarly follow distinct activation trajectories.

In order to compare cluster distributions between genotypes we next performed Differential Proportion Analysis (DPA), revealing that PS-5X mice have significantly fewer human microglia within the homeostatic cluster compared to WT (p = 8.27E-11), 5XFAD (p = 1.18E-10), and PS19 mice (p = 8.99E-08). Additionally, 5XFAD mice have slightly less cells in the MHCII cluster (p = 0.03256) compared to WT mice. PS-5X mice also exhibit significantly more IFN-enriched xMGs then WT (p = 0), 5XFAD (p = 1.09E-12), and PS19 mice (p = 3.28E-07). Interestingly, tau pathology alone has no effect on the number of microglia expressing DAM genes but does lead to significantly heightened expression of IFN-responsive transcripts in comparison to WT mice (p = 9.45E-06). Thus, the DAM phenotype is predominantly associated with amyloid pathology, whereas IFN genes can be induced independently by either tau or amyloid pathologies. PS-5X also exhibit significantly more DAMs than WT (p = 6.34E-09), 5XFAD (p = 0.01044), and PS19 mice (p = 4.72E-07). 5XFAD mice additionally have more DAMs than WT (p = 0.00236) and just missed significance over PS19 (p = 0.05622). PS-5X also exhibit a specific induction of IL-1β enriched microglia that is significant greater than both WT (p = 5.75E-05) and PS19 (p = 0.04481) (Figure 2.4F). To further examine which genes define each of these cluster and how these genes

differ across genotypes, heatmaps were generated to compare the relative gene expression of the top 20 differentially expressed genes (DEGs) within the Homeostatic, MHCII, IFN, DAM, and IL-1β clusters compared to every other cluster (**Figure 2.4G**). Across the board, the relative expression of DEGs associated with activation are generally increased in PS-5X mice compared to WT, 5XFAD, and PS19 mice. Interestingly PS-5X mice also show increases in MHC class I and II genes within the Homeostatic cluster as well--which is generally characterized by low levels of activation genes--suggesting that even the Homeostatic cluster within PS-5X mice is slightly more activated.

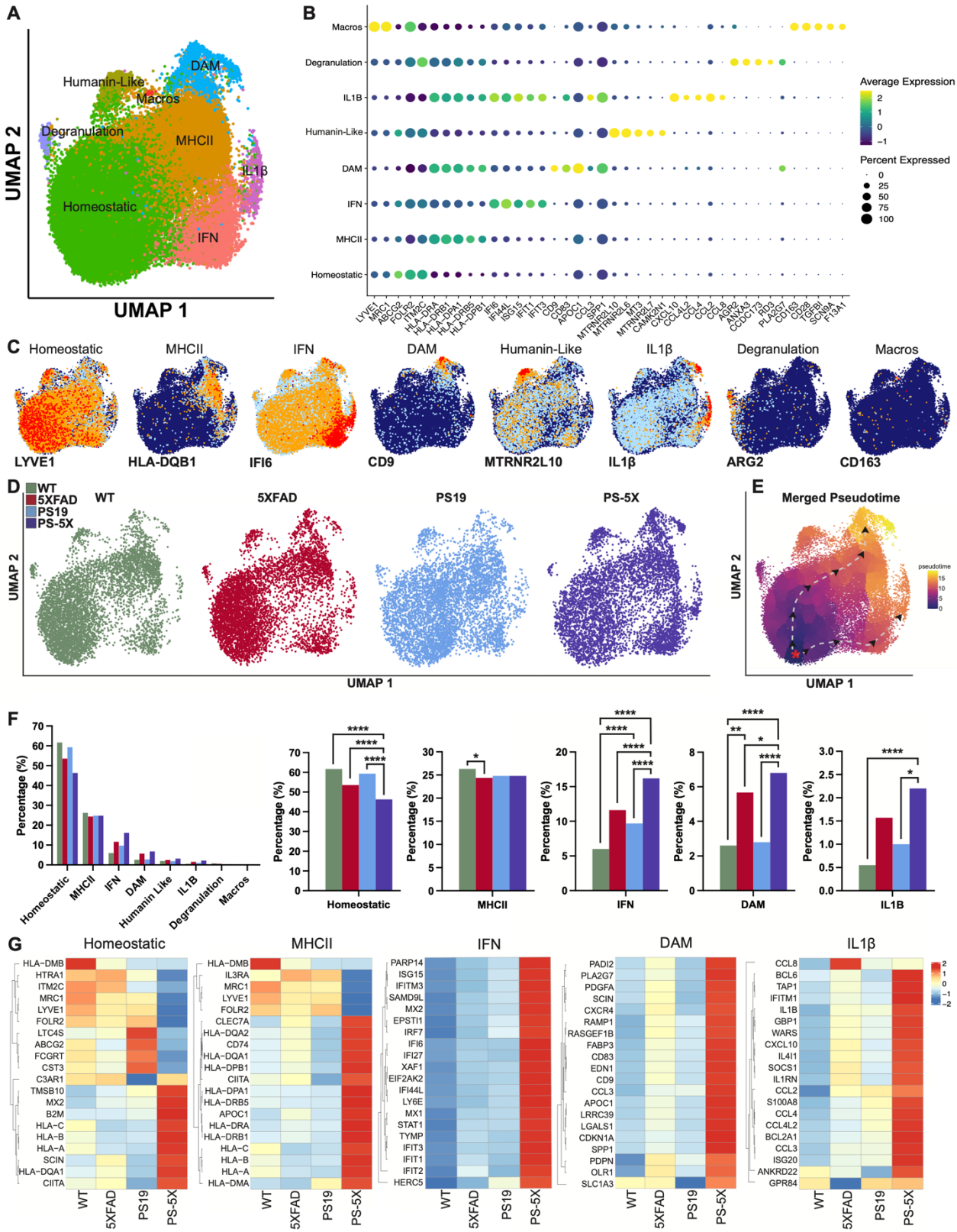

Figure 2.4. Single-cell sequencing reveals altered population distributions and gene expression as Human Microglia respond to combined amyloid and tau pathologies . **(A)** UMAP plot of 47,863 xMGs isolated from 6-month-old male WT, 5X, PS19, and PS-5X chimeric mice reveals eight distinct

clusters defined by genes related to MHC class II (MHCII), Type I Interferon Responsive (IFN: Salmon), DAMs (Blue), Humanin-Like (Olive Green;), IL-1β (Purple), Degranulation (Lilac;), Macros (red) and a "homeostatic" cluster (Green). **(B)** A dotplot of the top 5 upregulated DEGs for each cluster, the size of the dot indicates percent of cells expressing a given gene, color indicates relative expression levels. **(C)** Individual heatmaps of representative genes for each cluster; LYVE1 is expressed highly in the homeostatic cluster, HLA-DRQ1 is expressed highest in the MHCII cluster, IFI6 is expressed highest in the IFN cluster, CD9 is restricted to the DAM cluster, MTRNR2L10 is highly expressed in the Humanin-Like cluster, IL-1β is expressed highest in the IL-1β cluster but also within a small subset of DAMs, ARG2 is expressed highest in the Degranulation cluster, CD163 is expressed highest in the Macros cluster. **(D)** Individual UMAPs for each genotype (Green; WT, Red; 5XFAD, Blue; PS19, Purple; PS-5X) were down-sampled to show equivalent numbers of cells per genotype. **(E)** Pseudotime analysis displays the trajectory of xMG activation states, origin is delineated by a red asterisk and two general paths leading toward the DAM and IL-1β states via MHCII and IFN clusters respectively are outlined with grey dashed lines and black arrows. **(F)** Bar plot comparing the percentage of total cells within each cluster. Individual cluster bar plots for Homeostatic, MHCII, IFN, DAM, and IL-1β are displayed to more clearly demonstrate cluster differences. DPA reveals PS-5X mice have significantly less cells in the homeostatic cluster compared to WT ($p = 8.27E-11$), 5XFAD ($p = 1.18E-10$), and PS19 mice ($p = 8.99E-08$). Additionally, 5XFAD mice have less cells in the MHCII cluster ($p = 0.03256$) compared to WT. PS-5X mice have significantly more IFNs then WT ($p = 0$), 5XFAD ($p = 1.09E-12$), and PS19 ($p = 3.28E-07$) and PS19 have significantly more IFNs then WT ($p = 9.45E-06$). PS-5X have significantly more DAMs than WT ($p = 6.34E-09$), 5XFAD ($p = 0.01044$), and PS19 ($p = 4.72E-07$), 5XFAD mice additionally have more DAMs than WT ($p = 0.00236$) and just missed significance over PS19 ($p = 0.05622$). Finally, PS-5X mice have significantly more IL-1βs then WT ($p = 5.75E-05$) and PS19 ($p = 0.04481$). **(G)** Heatmaps comparing relative gene expression of the top 20 DEGs in Homeostatic, MHCII, IFN, DAM, and IL-1β clusters between WT, 5XFAD, PS19, and PS-5X mice reveal a robust induction of many activation genes in PS-5X mice

Pseudobulk analysis reveals both similarities and differences in the microglial response to amyloid and tau pathologies. To further understand whether human microglia exhibit differing responses to amyloid and tau pathology or the combination of both of these hallmark AD pathologies, we next performed pseudobulk analysis of our scRNA-seq datasets. Numerous DEGs were identified when comparing each individual genotype to WT controls (FDR<0.01, LFC>0.10, and expression cutoff of 10% of cells per genotype). Specifically, we detected 72 DEGs in response to amyloid pathology alone, 344 significantly altered genes in PS19 mice, and 672 DEGs when microglia interact with both AD pathologies in PS-5X mice. Interestingly, Venn diagram comparisons of upregulated and downregulated genes across each AD genotype in comparison to WT mice reveals varying degrees of overlap (**Figure 2.5A&B**). For

example, 55 upregulated genes are shared between PS19 and PS-5X groups whereas only 26 genes are shared between 5X and PS-5X groups. A similar difference between these groups is observed for downregulated genes. Thus, it appears that the microglia response to tau pathology is greatly heightened in the combined PS-5X model, whereas the response to amyloid pathology becomes more nuanced in the PS-5X model. Another interesting observation from this pseudobulk analysis is the finding that AD risk genes are greatly enriched in these comparisons (**Figure 2.5A&B, red text**)[231-235]. Upregulation of OAS1 in the PS-5X mice is particularly noteworthy, as recent reports have linked OAS1 variants with worsened COVID-19 outcomes along with AD risk; OAS1 is a key antiviral factor induced by IFNs that can sense exogenous nucleic acids[236-238]. Extracellular nucleotides have been previously reported to initiate Type 1 IFN responses and linked to amyloid and tau pathology in mice and humans[110, 138-140].

To better understand the functional implications of these transcriptional changes, we next performed Gene Ontology (GO) network analysis (**Figure 2.5C**). xMGs within 5XFAD mice are predominantly characterized by an upregulation of genes related to ’Response to Stimulus‘ and ’Response to Type 1 Interferon‘ while downregulating genes related to ’Cellular Response to Stress‘ and ’Protein Folding’. The ’Response to Type 1 Interferon‘ in 5XFAD mice also shared to some extent by PS19, and PS-5X xMG, but appears further expanded in PS-5X mice. PS19 and PS-5X xMG also share alterations in ’Metabolism‘ and in PS-5X mice ’Mitochondrion Organization, and Cristae Formation‘ are upregulated, which may explain the altered mitochondria ultrastructure observed by electron microscopy (Figure 2.4). Furthermore, nodes under ’Metabolism‘ include GO

terms surrounding RNA and DNA catabolism, which may explain the overall skew towards downregulated genes in both PS19 and PS5X xMG. Additionally, interactions between pathogenic tau and RNA binding proteins that lead to altered and diminished gene expression patterns have been described by multiple groups and may explain the patterns of downregulation seen in PS19 and PS-5X but not 5XFAD xMG[239-242]. To better understand the transcriptional landscape that may underlie these gene expression patterns, we next examined the frequency of transcription factors (TF) motifs within the 500bp upstream promoter regions of all DEGs (**Figure 2.5D**). Most notably, this analysis showed that upregulation of many of the genes observed PS-5X xMG, and to a lesser extent 5XFAD xMGs, are predicted to be largely driven by Interferon Responsive Factors (IRF9, IRF4, IRF8, IRF3, IRF5 and IRF2). This finding is particularly intriguing given that Interferon signaling has previously been implicated in the adoption of Rod-like morphology in murine microglia following traumatic brain injury[119].

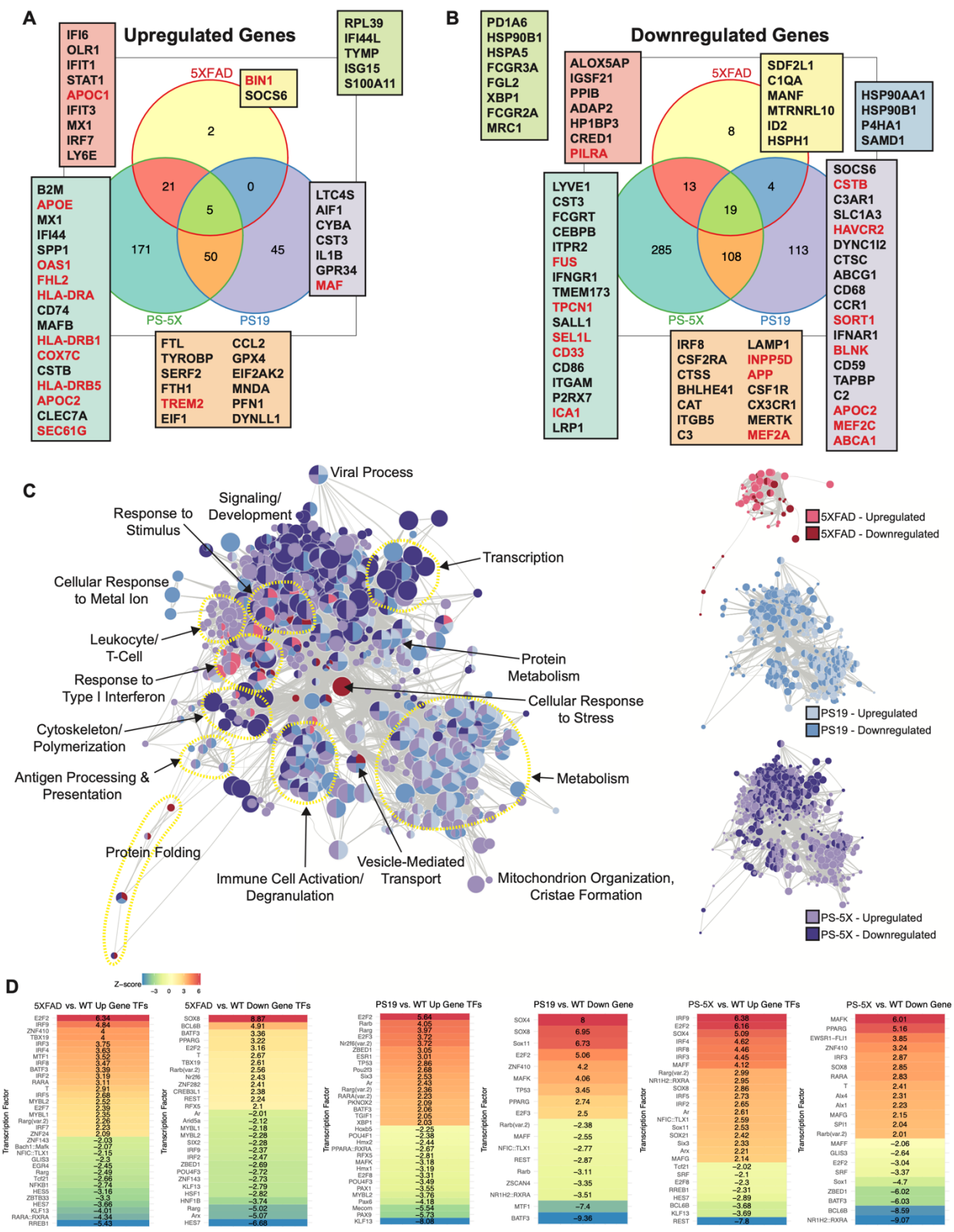

Figure 2.5. Pseudobulk analysis reveals both similarities and differences in the microglial response to amyloid and tau pathologies. (A) Overlapping Upregulated and **(B)** Downregulated xMG genes of each genotype compared to WT, genes of interest are highlighted in boxes in corresponding

colors, AD risk genes are inscribed in red. **(C)** Gene Ontology network analysis generated from all pseudobulk DEGs, nodes represent individual GO terms, whereas the size represents the number of cells within a node, and the distance between nodes represents similarity. For clarity, similar nodes are encircled with yellow dashed lines labeled with arrows. **(D)** Predicted transcription factor analysis of up and down-regulated genes in each genotype as compared to WT.

Subclustering of human microglia reveals additional genotype-dependent heterogeneity. To further examine the potential heterogeneity within each transcriptionally distinct clusters and to begin to explore which cluster Rod-xMGs may lie, we performed subclustering of xMG within the DAM, IL-1β, and IFN clusters (**Figure 2.6**). DAM Subclustering reveals 5 distinct subclusters: Homeostatic, MHCII, IL-1β, Lipid Metabolism, and IFN; defined by inputting upregulated genes into Enrichr and examining the resulting Biological Pathway ontology terms[243-245]. UMAPs of representative genes that are enriched within key subclusters are shown including HLA-DRB5 within the MHCII subcluster, LIPA within the Lipid Metabolism subcluster, IL-1β within the IL-1β subcluster, and ISG15 within the IFN subcluster (**Figure 2.6A**). Each of these DAM subclusters were then mapped back onto the original complete dataset UMAP to visualize where they fall relative to the original primary clusters. To determine whether certain subclusters are overrepresented in one genotype versus another, color coded UMAPs displaying each genotype reveal variation in cell populations especially within the DAM-IFN cluster (circled), which appears absent in WT and enriched in PS19 and PS-5X mice (**Figure 2.6A**). Subclustering of the IFN cluster also revealed 5 distinct subclusters: Homeostatic, DNA Modification, IFN, MHCII/IFN, and MHCII. Whereas some genes are relatively restricted to a given subcluster, others are expressed within two or more subclusters (i.e. HLA-DRB1 is enriched in both MHCII/IFN and MHCII alone) (**Figure 2.6B**). Color coded genotype UMAPs show differences in the MHCII/IFN

cluster which appears expanded in PS19 and PS-5X mice (**Figure 2.6B**). Finally, IL-1β subclustering reveals 3 distinct subclusters: IFN, Chemokine/Cytokine, and DNA Modification/Cell Cycle with representative subcluster enriched genes shown (**Figure 2.6C**). Interestingly, the IL-1β—IFN subcluster is largely absent in WT compared to 5XFAD, PS19, and PS-5X. Taken together, subclustering analysis revealed additional microglia transcriptional states that further differentiate between the WT, 5XFAD, PS19, and PS-5X genotypes. Strikingly in each of these subclusters, genotype-dependent differences in populations were most apparent microglia that express high levels of INF-responsive genes. Thus, it appears that INF signaling drives much of the differential responses to amyloid and tau pathology as well as the induction of Rod microglial morphology.

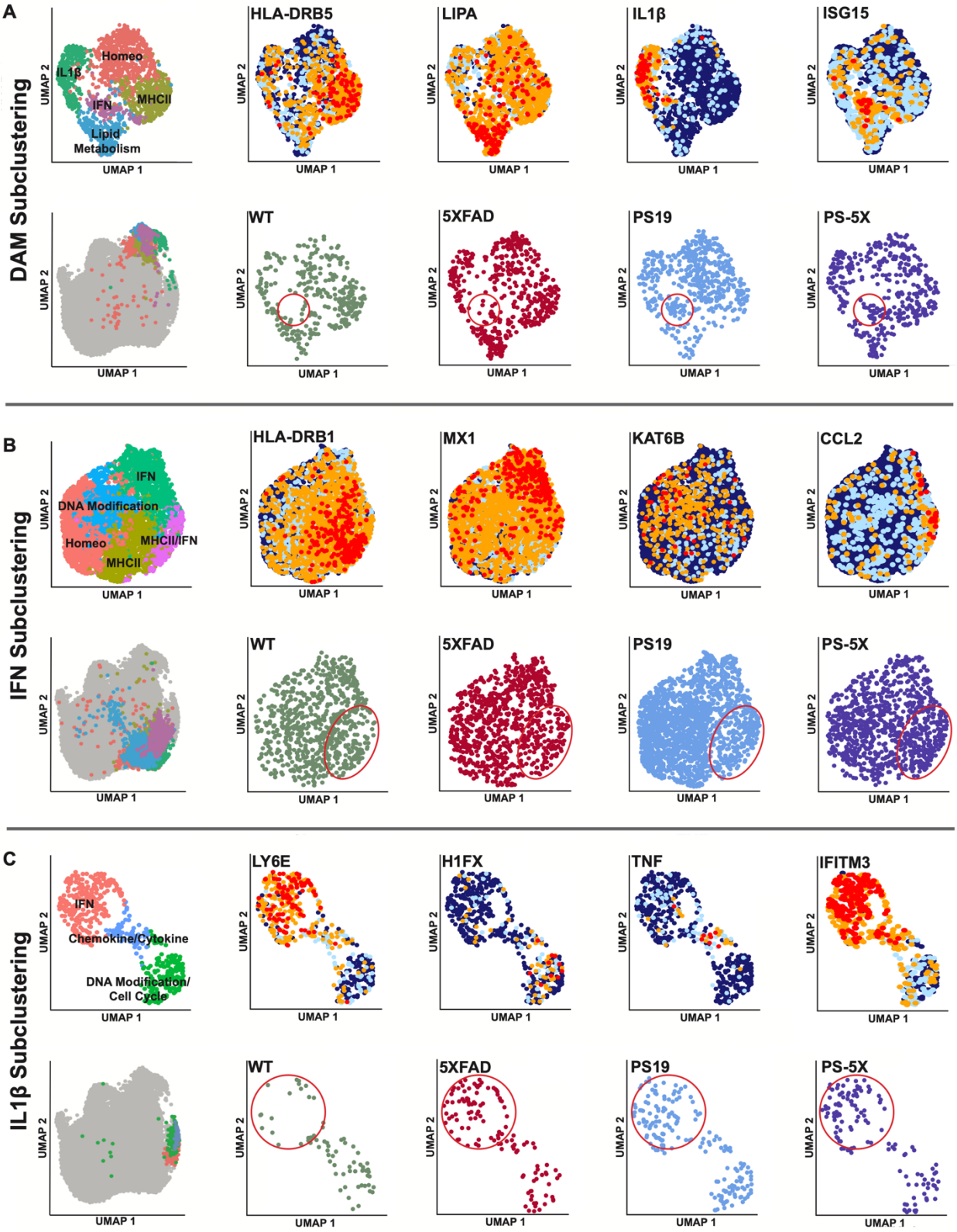

Figure 2.6. Subclustering of human microglia reveals additional genotype-dependent heterogeneity within DAM, IL-1β and INF clusters. (A) DAM xMGs can be further divided into 5 distinct

subclusters (Homeo; pink, MHCII; olive, IL-1β; green, Lipid Metabolism; blue, and IFN; purple). UMAPs of 4 representative genes enriched within each subcluster are displayed to the right. The DAM subclusters are then back-mapped onto the original UMAP (Fig 4A) to display where each clusters aligns within the broader population of xMGs. Color coded UMAPs displaying each genotype (WT; green, 5XFAD; red, PS19; blue, PS-5X, purple) reveal variation in cell populations across genotypes, a red circle highlights the DAM-IFN subcluster which is mostly absent in WT mice but enriched in PS19 and PS-5X groups. **(B)** IFN subclustering reveals 5 distinct subclusters (Homeo; pink, DNA Modification; blue, IFN; green, MHCII/IFN; purple, MHCII; olive). UMAPs of representative genes enriched within 4 of these subcluster are displayed to the right. The IFN subclusters are then back-mapped onto the original UMAP. Color coded UMAPs displaying each genotype reveal variation in cell populations across genotypes, a red circle highlights the MHCII/IFN cluster which appears expanded in PS19 and PS-5X. **(C)** IL-1β xMGs can be further divided into 3 distinct subclusters (IFN; pink, Chemokine/Cytokine; blue, DNA Modification/Cell Cycle; green). Gene UMAPs of 4 key genes are displayed to the right. The IL-1β subclusters are then back-mapped onto the original UMAP and color coded clustering for each genotype reveal variation in cell populations across genotypes, a red circle highlights the IFN cluster which is largely absent in WT xMGs.

Rod microglia express multiple interferon-responsive proteins. Given the heterogeneity of IFN genes across genotypes revealed by subclustering, and increases in PS-5X IFN cluster, we sought to probe for expression of Type 1 Interferon Responsive proteins. As Rod microglia are predominantly observed in PS-5X mice and our TF analysis and prior reports implicate interferon signaling in this morphology we looked here first. We began by examining MX1, a Type 1 IFN Responsive protein that is implicated in antiviral responses and upregulated in AD microglia[246]. MX1 was examined in combination with the DAM marker CD9 (**Figure 2.7A-J, Figure S2.3A-J**). Histological assessment of xMGs in the WT CA1 and CTX show very low expression of either MX1 or CD9 along with a typical ramified homeostatic morphology (**Figure 2.7A, Figure S2.3A**). Within the stratum radiatum of 6-month-old 5XFAD mice, occasional amyloid plaques are observed and adjacent microglia exhibit an upregulation of CD9 expression and a subtle induction of MX1 (**Figure 2.7B)**. Similar findings are observed within the cortex which exhibits greater numbers of amyloid plaques **(Figure S2.3B**). In PS19 CA1 and cortex, xMGs exhibit morphologies that closely resembling WT xMG

labeling and likewise exhibit minimal expression of MX1 and CD9, (**Figure 2.7C, Figure S2.3C**). In contrast, xMGs associated with plaques in PS-5X mice strongly express both CD9 and MX1. Interestingly, in CA1, MX1 is expressed in most Rod-xMGs, whereas CD9 expression is only observed in a small subset of Rod microglia (**Figure 2.7D, Figure S2.3D**). To better understand the potential impact of varying pathologies on xMG numbers GFP+ cells were quantified using IMARIS, revealing no differences in the number of cells in CA1, and a subtle but significant ($p = 0.0404$) increase in xMGs within the cortex of PS-5X mice (**Figure 2.7E, Figure S2.3E**). We previously reported that GFP expression via the CAG promoter is increased in response to inflammatory stimuli (Hasselmann and Coburn et al., 2019). Here we show a similar effect, with GFP intensity elevated in PS-5X CA1 xMGs compared to all genotypes and significantly increased within the cortex of PS-5X mice compared to WT and PS19 groups (**Figure 2.7F, Figure S2.3F**)

To further assess potential differences in MX1 and CD9 expression, we performed IMARIS based quantification of both area and intensity. Average MX1 area in CA1 is significantly higher in the PS-5X compared to all other groups. In addition, average MX1 intensity within GFP+ xMGs in CA1 is also significantly higher in PS-5X mice (**Figure 2.7G&H**) Similar findings are observed within the cortex, where Average MX1 area is significantly higher in the PS-5X compared to PS19 and WT mice, although MX1 intensity normalized to GFP+ cell number shows only a trend towards increased levels in PS-5X and 5XFAD cortices (**Figure S2.3G&H**). Interestingly, MX1 mRNA expression is also increased, specifically within PS-5X mice in both the IFN and IL-1β clusters, as

well as a slight increase within Homeostatic, MHCII, DAM and Humanin-Like clusters, suggesting that PS-5X xMGs on a whole exhibit heightened Type 1 Interferon responsiveness (**Figure S2.3K**). Similar to MX1, average CD9 area and average intensity is significantly higher in the PS-5X compared to all other groups in the hippocampus (**Figure 2.7I,J**)., Within the cortex, MX1 area is also significantly increased in PS-5X mice versus WT, 5XFAD, and PS19 groups (**Figure S2.3I,J**). Consistent with our prior findings that CD9 is strongly induced in DAM XMGs, CD9 mRNA expression is greatly enriched within the DAM cluster of 5XFAD, PS19, and PS-5X mice (**Figure S2.3D**).

Given the high expression of MX1 within PS-5X Rod-xMGs we next sought to probe for expression of additional Type 1 Interferon responsive proteins as well as other markers of microglial activation. Interestingly, Rod-xMGs are nearly all positive for the interferon responsive transcription factors IRF3, IRF4, IRF5; all of which were predicted to be enriched in PS-5X mice via our TF motif analysis **(Figure 2.5D)**. Labeling with an antibody against HLA-DR, which recognizes the AD risk genes HLA-DRB1 and HLA-DRB5, revealed an unusual perinuclear expression pattern specifically within Rod microglia. This perinuclear pattern has previously been described in response to Interferon stimulation further supporting the notion that Rod morphology may be induced as part of an interferon-responsive program. Many of these Rod xMGs were also immunoreactive for MerTK, a TAM receptor implicated in synaptic pruning and amyloid phagocytosis, as well as partially positive for Apoptosis-associated speck-like protein containing a CARD (ASC), a critical component of the inflammasome that

mediates maturation of IL-1β and has been implicated in both amyloid and tau pathogenesis (**Figure 2.7K-P**)[97, 146, 247-250].

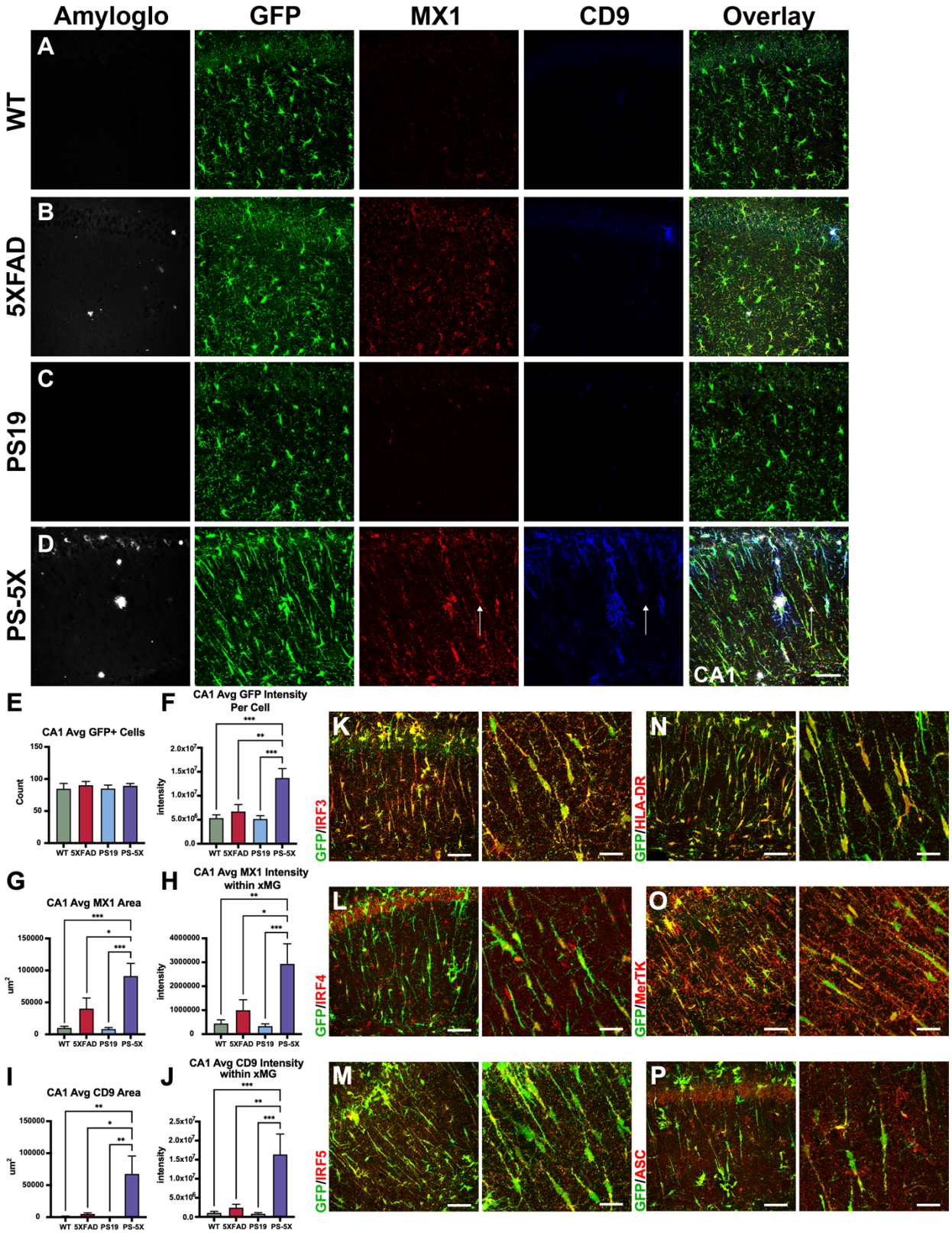

Figure 2.7. Rod microglia express several IFN responsive proteins. (A) xMGs (green, GFP) within CA1 of WT mice exhibit little to no expression of either MX1 (red) or CD9 (blue). **(B)** In contrast, xMGs in

association with amyloid beta plaques in 5XFAD mice upregulate CD9. **(C)** xMGs within CA1 of the PS19 mice show little expression of either Mx1 or CD9. **(D)** In PS-5X mice, xMGs exhibit a substantial increase in both MX1 and CD9 immunoreactivity. Interestingly, whereas CD9 is predominantly enriched in plaque-adjacent xMGs, MX1 is expressed in both plaque associate and rod microglia. Arrows highlight examples of $MX1^{high}/CD9^{low}$ rod microglia. **(E)** No differences between groups in the total number of GFP+ Cells in CA1 are observed. **(F)** However, the average intensity of GFP per cell is significantly increased in PS-5X mice compared to all other genotypes (WT, $p = 0.0002$; 5XFAD, $p = 0.0028$; PS19, $p = 0.0001$), consistent with prior findings that inflammatory stimuli can activate the CAG promoter used to drive GFP. **(G)** Average MX1 area in CA1 is significantly higher in the PS-5X mice compared to 5XFAD ($p = 0.0438$), PS19 ($p = 0.0005$) and WT ($p = 0.0009$). **(H)** Average MX1 intensity within GFP+ xMGs is also significantly higher in PS-5X mice compared to WT ($p = 0.0015$), 5XFAD ($p = 0.0237$), and PS19 ($p = 0.0009$). Average CD9 area **(I)** and intensity **(J)** is significantly higher in the PS-5X compared to WT (area, $p = 0.0039$; intensity, $p = 0.0005$), 5XFAD (area, $p = 0.0118$; intensity, $p = 0.0028$), and PS19 (area, $p = 0.0048$; intensity, $p = 0.0004$) CA1. **(K)** Rod xMGs within CA1 of PS-5X mice are nearly all positive for IRF3 **(K)**, IRF4 **(L)**, IRF5 **(M)**, HLA-DR **(N)** and MerTK **(O)**. A subset of Rod xMGs are also positive for the inflammasome component ASC **(P)**. Scale A-D, K-P Left Image= 50μm, K-P Right Image= 20μm

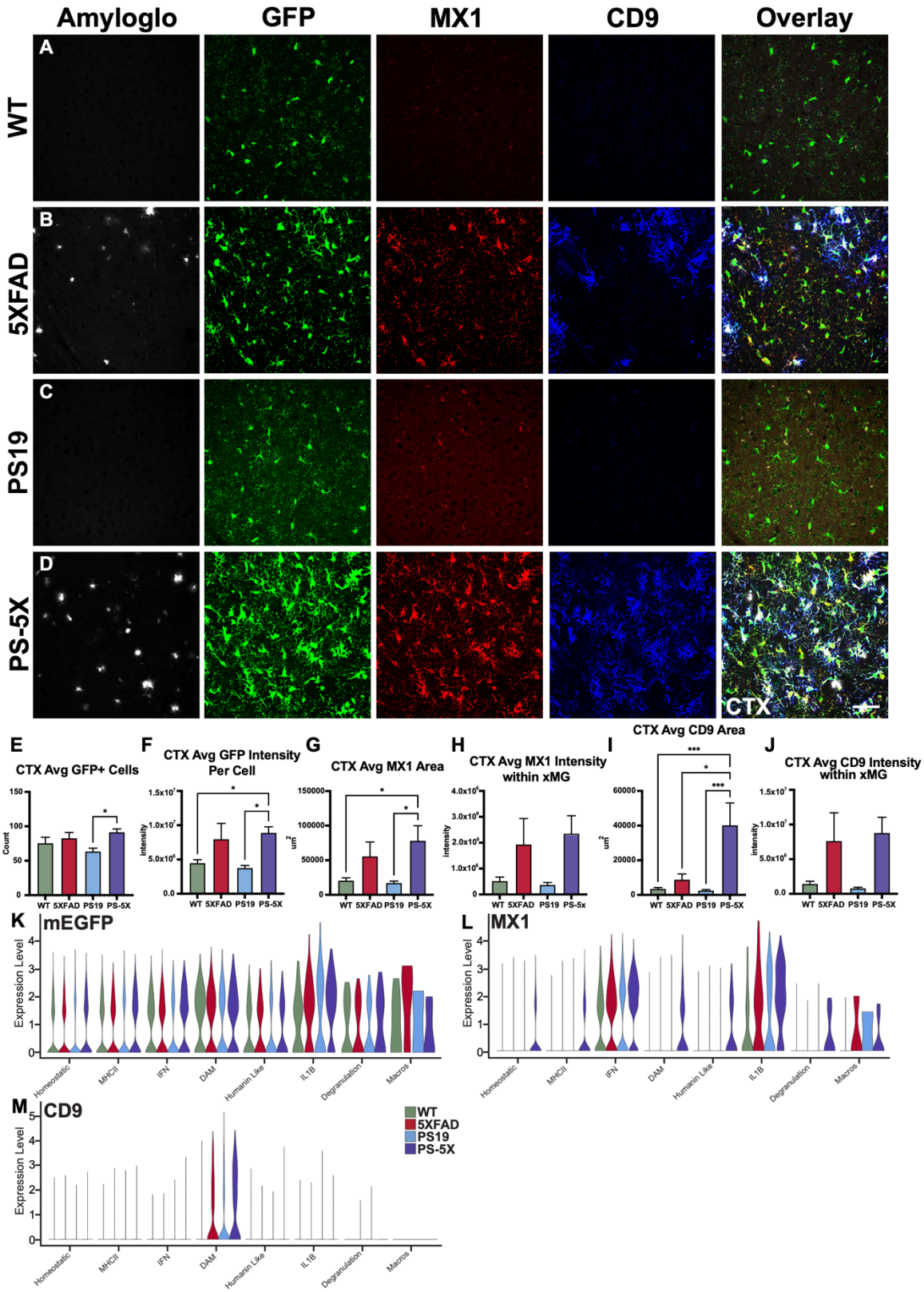

Figure S2.3. MX1 and CD9 immunoreactivity are significantly increased within the cortex of PS-5X mice. (A) xMGs within the cortex of wild type mice exhibit a typical tiled and homeostatic appearance. **(B)** In contrast, xMGs within 5XFAD mice interact with amyloid plaques and upregulate both MX1 and CD9 in

plaque proximal regions. **(C)** xMGs in the PS19 cortex exhibit little to no CD9 or MX1 expression. **(D)** In PS-5X mice, xMGs surround amyloid plaques and greatly upregulate expression of both CD9 and MX1 **(E)** Significantly more GFP+ microglia are detected within the cortex of PS-5X mice compared to PS19, but no other differences in microglia number are observed between genotypes ($p = 0.0404$). **(F)** GFP intensity is also significantly higher in PS-5X microglia in comparison to both WT ($p = 0.0476$) and PS19 ($p = 0.0221$) mice. **(G)** Average MX1 area is significantly higher in PS-5X mice compared to both PS19 ($p = 0.0253$) and WT ($p = 0.0371$) groups. **(H)** Average MX1 intensity within GFP+ xMG is not significantly different between genotypes, although there is a strong trend towards increased MX1 immunoreactivity within PS-5X and 5XFAD microglia. **(I)** Average CD9 area is significantly higher in PS-5X mice compared to all other groups (WT, $p = 0.0009$; 5XFAD, $p = 0.0110$; and PS19, $p = 0.0006$). **(J)** Average CD9 intensity is significantly higher in the PS-5X compared to WT, 5XFAD, and PS19 CTX. **(K)** Violin Plot of mEGFP expression in xMGs reveals slightly elevated expression in DAM and IL-1β clusters. **(L)** Violin Plot of MX1 expression in xMG reveals elevated expression in IFN and IL-1β clusters across genotypes and also within the DAM cluster of PS-5X mice. **(M)** Violin Plot of CD9 expression in xMG reveals elevated expression in the DAM cluster within 5XFAD, PS19, and PS-5X mice. Scale = 50μm

Rod microglia morphology can be induced with Type 1, but not Type 2 Interferons. Given the high expression of IFN responsive proteins within Rod-xMG, as well as the expanded IFN cluster in PS-5X mice, we wondered whether a similar Rod-Like phenotype could be elicited *in vitro* by exposure to interferons or other stimuli. Although elongated microglial morphology can be elicited *in vitro* via a scratch assay, the potential molecular cues that underlie this phenotypic change remain unknown[251, 252].

In order to assess whether human iPS-Microglia could be induced to adopt a Rod-Like morphology *in vitro*, cells were cultured and treated with various stimuli and Incucyte-based quantification was performed (**Figure 2.8**). 24 hours after control treatment, iPS Microglia maintain a slightly ameboid morphology typical of cultured microglia (**Figure 2.8A**). In contrast, treatment with 100ng/mL of the Type 1 Interferons IFNα, IFNβ, or a combination of IFNα and IFNβ, led to adoption of a striking Rod-Like morphology *in vitro* (**Figure 2.8B-D**). Interestingly, this elongation is not driven by a Type 2 Interferon, as 100ng/mL of IFNγ does not elicit a Rod-Like morphology (**Figure 2.8E**). Likewise, neither induction of the inflammasome via a classical paradigm (LPS + ATP), nor

treatment with IL-1β, induced a Rod-Like morphology (**Figure 2.8F&G**)[253, 254]. To quantitatively assess the degree to which cells had elongated, a ratio of long to short axis was calculated for all cells. This analysis further demonstrated that treatment with IFNα and/or IFNβ produced significantly more elongated microglia than control treatments. In contrast, treatment with LPS/ATP elicited a more ameboid morphology ($p<0.0001$), while IFNγ and IL-1β produced no significant changes in microglia length (**Figure 2.8F&G**). Given the high level of MX1 expression observed in Rod-xMGs *in vivo*, we next examined the expression of this Type 1 Interferon Responsive protein along with the DAM marker CD9, via confocal microscopy. MX1 expression was almost undetectable in control-treated cells whereas treatment with IFNα, IFNβ, and IFNα/β greatly increased MX1 immunoreactivity while eliciting little to no change in CD9 expression (**Figure 2.8I-Q**). In contrast, treatment with IFNγ, LPS/ATP, and IL-1β had little effect on either MX1 or CD9 expression (**Figure 2.8M-O**).

Interestingly, microglia treated with Type 1 Interferons alone also extended many fine processes along the main cell body (**Figure 2.8J,K,L;** white arrows) that were highly reminiscent of the P2RY12 immunoreactive filipodia observed in PS-5X xMGs *in vivo* (**Figure 2.2G,H**). Quantification of these filopodia revealed that though all conditions were able to change at least one aspect of filopodia length or numbers, treatment with Type 1 Interferons alone elicited significantly more medium length filopodia on *in vitro* Microglia as determined by total length divided by numbers. Changes were also observed in cells treated with LPS and ATP, where they develop significantly fewer filopodia that are far longer, and with IL-1β treatment which conversely triggers

abundant, but very short filipodia (**Figure 2.8R&S**). Representative images of iPS-microglial filopodia in Control and IFNα/β treated cells as well as the skeletonization process are shown in **Figure 2.8T&U**. To further determine whether Type 1 Interferon exposure skews iPS Microglia toward a Rod-Like phenotype, we assessed the distributions of length to width ratios. As with our *in vivo* analysis, we used a cutoff for the Rod microglia set to the Control mean ratio + standard deviation. Treatment with Type 1 Interferons leads to a dramatic shift in elongation in at least half of the iPS Microglia, which is an even greater change than observed *in vivo* (**Figure 2.8V&W**).

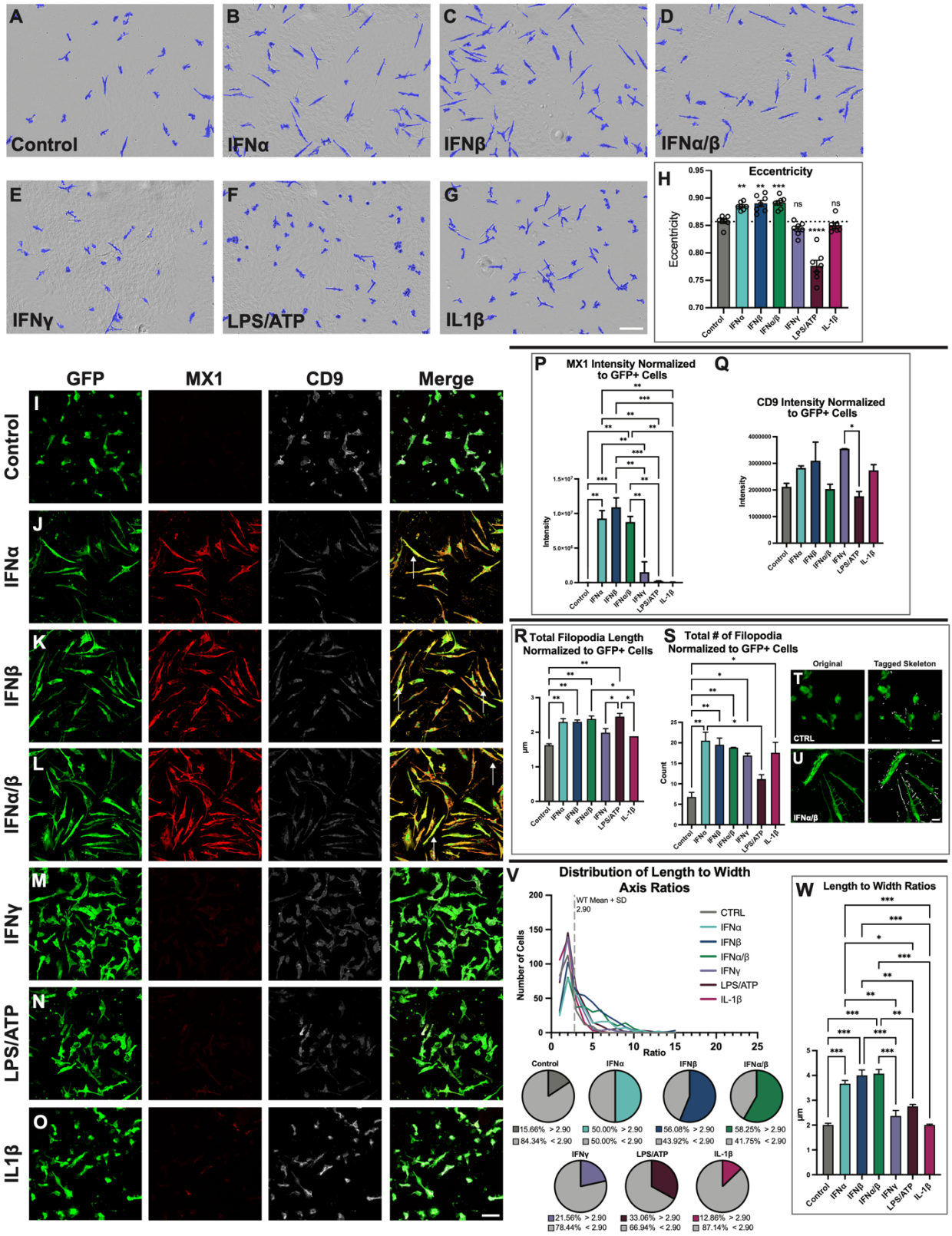

Figure 2.8. Rod microglia can be induced *in vitro* with Type 1, but not Type 2 Interferons.
Representative pseudocolored phase contrast images of iPS microglia cultured *in vitro* and treated with recombinant protein or LPS/ATP. **(A)** iPS Microglia are largely non-adherent and maintain a slightly

ameboid morphology typical of cultured microglia. 24 hours after treatment with 100ng/mL IFNα **(B)** or IFNβ **(C)**, microglia adopt a striking Rod-Like morphology *in vitro*. Combined treatment with 50ng/mL each of IFNα and IFNβ similarly elicits Rod morphology. In contrast, treatment with 100ng/mL of IFNγ **(E)** does not elicit a Rod-Like phenotype. **(F)** To induce inflammasome activation, a classical paradigm of 100ng/mL of LPS followed by 10μM ATP was utilized. This approach failed to elicit a Rod-like phenotype in iPS-microglia. **(G)** Likewise, 100ng/mL of IL-1β does not elicit a Rod morphology. **(H)** The degree of eccentricity was quantified showing that treatment with IFNα and/or IFNβ significantly increased the adoption of a rod-like morphology in comparison to control microglia (IFNα $p = 0.0071$; IFNβ $p = 0.0013$; IFNα/β $p = 0.0008$). In contrast, treatment with LPS/ATP elicits a more ameboid morphology ($p<0.0001$), whereas IFNγ and IL-1β are not significantly different from control. **(I-O)** Confocal microscopy reveals the expression of GFP, MX1, and CD9 in iPS microglia. MX1 is low in untreated cells **(I)** whereas treatment with IFNα **(J)**, IFNβ **(K)**, and IFNα/β **(L)** increases MX1 immunoreactivity but has little effect on CD9 levels. Treatment with IFNγ **(M)**, LPS/ATP **(N)**, and IL-1β **(O)** does not elicit increased MX1 expression and CD9 expression is also equivalent to controls, aside from IFNγ. Arrows highlight Rod microglia with many fine processes along the main cell body. **(P)** Treatment with Type 1 Interferons lead to a significant increase in MX1 expression normalized by GFP+ cell counts and compared to all other conditions (IFNα vs Control $p = 0.0023$; IFNα vs IFNγ $p = 0.0064$; IFNα vs LPS/ATP $p = 0.0026$; IFNα vs IL-1β $p = 0.0023$, IFNβ vs Control $p = 0.0008$; IFNβ vs IFNγ $p = 0.0021$; IFNβ vs LPS/ATP $p = 0.0009$; IFNβ vs IL-1β, $p = 0.0008$, IFNα/β vs Control $p = 0.0032$; IFNα/β vs IFNγ $p = 0.0094$; IFNα/β vs LPS/ATP $p = 0.0037$; IFNα/β vs IL-1β $p = 0.0033$). **(Q)** Treatment with IFNγ leads to a slight significant increase in CD9 expression normalized by GFP+ cell counts compared to LPS/ATP, all other conditions show no significant differences. **(R)** Treatment with Type 1 Interferons, as well as LPS/ATP elicit greater combined filopodia lengths when normalized to GFP+ cell counts compared to controls (IFNα $p = 0.0043$; IFNβ $p = 0.0042$; IFNα/β $p = 0.0021$; LPS/ATP $p = 0.0012$). Additionally combined filopodia length is longer in IFNα/β compared to IL-1β ($p = 0.0026$), and treatment with LPS/ATP leads to longer combined filopodia than IFNγ ($p = 0.0322$) and IL-1β treatments ($p = 0.0113$). **(S)** Treatment with Interferons and IL-1β also leads to significantly more filopodia per cell than control (IFNα $p = 0.0035$; IFNβ $p = 0.0055$; IFNα/β $p = 0.0076$; IFNγ $p = 0.0195$; IL-1β $p = 0.0138$). Additionally, filopodia per cell is significantly increased in IFNα compared to LPS/ATP. **(T&U)** Representative original and tagged skeleton images of Control **(T)** and cells treated with IFNα/β **(U)** used for filopodia quantification**. (V)** Distribution of length to width ratios of GFP+ in vitro Microglia, the grey dotted line represents a cutoff for Rod in vitro Microglia set to the Control mean ratio + standard deviation (2.90). Treatment with Type 1 Interferons leads to the highest percentages of cells that surpass this Rod morphology cutoff (IFNα, teal; 50.00%. IFNβ, navy; 56.08%. IFNα/β, green; 58.25%) compared to Control (dark grey; 15.66%), IFNγ (purple; 21.56%), and IL-1β (fuchsia; 12.86%). Cells treated with LPS/ATP (maroon; 33.06%) additionally had a slight increase compared to control. A Kolmogotov-Smirnov test shows Type 1 Interferon treated cells have the largest difference in distributions (IFNα $p < 1.00E-15$; $D = 0.4559$, IFNβ $p < 1.00E-15$; $D = 0.4650$, IFNα/β $p < 1.00E-15$; $D = 0.4599$), followed by LPS/ATP ($p = 6.55E-6$; $D = 0.2064$), whereas treatments with IFNγ ($p = 4.20E-3$; $D = 0.1484$) and IL-1β ($p = 0.6440$; $D = 0.0629$) distributions are more similar to Control. **(W)** Treatment with Type 1 Interferons leads to a significant increase in length to width ratios compared to all other conditions (IFNα vs Control $p = 0.0007$; IFNα vs IFNγ $p = 0.0031$; IFNα vs LPS/ATP $p = 0.0223$; IFNα vs IL-1β $p = 0.0007$, IFNβ vs Control $p = 0.0002$; IFNβ vs IFNγ $p = 0.0008$; IFNβ vs LPS/ATP $p = 0.0040$; IFNβ vs IL-1β, $p = 0.0002$, IFNα/β vs Control $p = 0.0002$; IFNα/β vs IFNγ $p = 0.0006$; IFNα/β vs LPS/ATP $p = 0.0028$; IFNα/β vs IL-1β $p = 0.0002$). Scale A-G = 100μm, I-O = 20μm

Discussion

Genetic studies continue to highlight the importance of microglia in the development and progression of Alzheimer's Disease. These findings have in turn motivated a growing investigation and appreciation of how murine microglia respond to

beta-amyloid and tau pathologies [6, 36, 110, 137, 196, 215]. However, many of the candidate microglial AD risk genes implicated by GWAS exhibit limited homology between mouse and humans[55]. Thus, there is pressing need to further understand the interactions between human microglia and AD pathologies. We previously developed a chimeric approach to examine the impact of beta-amyloid plaque pathology on human iPSC-microglia *in vivo,* finding that amyloid plaques induce a DAM-like transcriptional state that differs substantially from that of murine microglia[36]. Recent single nuclei sequencing (snSeq) studies of postmortem human samples have likewise shown relatively limited overlap in microglial gene expression profiles between mouse models and human disease, further highlighting the need to study human microglial responses to AD pathology[7].

While our understanding of the interactions between microglia and amyloid pathology continues to grow, far less is known regarding how human microglia respond to neurofibrillary tangle pathology or the combination of these two pathognomonic AD lesions. In the current study we sought to address this shortcoming by developing and examining new chimeric models of tau pathology and combined amyloid and tau pathologies.

Here, we show in 6 month old chimeric mice that tau pathology alone is insufficient to induce a DAM-like transcriptional state in human microglia but instead leads to the induction of Type 1 Interferon Responsive genes. More importantly, when amyloid and tau pathologies are combined, mimicking both hallmark pathologies of AD, human microglia exhibit numerous changes in transcriptional and morphological state. Specifically, we find that combined plaque and tangle pathologies further promote the

induction of Interferon Responsive programs, lead to a significant expansion of DAM microglia, and induce of a proinflammatory IL-1β-enriched phenotype. In addition, the combination of amyloid and tau pathology leads to the adoption of a distinct Rod-Like morphology within CA1 of the hippocampus. Both confocal and electron microscopy further demonstrate the intimate interactions between Rod microglia and tau-laden neurofibrillary tangles in chimeric PS-5x mice.

Rod-Like microglia have previously been described in varying human pathological states, including AD and Huntington's disease, and in experimental traumatic brain injury[119, 225, 226, 255]. In fact an initial reference to Rod Cells or “Staebchenzellen” in German, dates back to the early 1900’s, with their description in brains from dementia patients, paresis, epilepsy, glioma, and meningitis. Interestingly, whether or not Staebchenzellen were glial in origin was often debated by Franz Nissl and Alois Alzheimer[256, 257]. Here we show that Rod xMGs surprisingly express P2RY12, a purinergic receptor that is commonly used as a marker of ‘homeostatic’ microglia[247]. Yet, Rod microglia also co-express a variety of activation markers including multiple interferon responsive proteins and MHCII antigen presentation molecules such as HLA-DR. Importantly, we find that Rod microglia are similarly observed in close proximity to neurofibrillary tangles in human AD subjects. Furthermore, this phenotype can be induced in human iPSC-microglia by type I interferons, but not other inflammatory stimuli. Precisely what role Rod microglia play in the pathogenesis of AD remains unclear. Are these cells neuroprotective, attempting to support or preserve the function of tau-laden neurons? Alternatively, could they instead contribute to or exacerbate tau pathology by producing proinflammatory cytokines that promote tau

hyperphosphorylation[250, 258, 259]? Additional studies are clearly needed to address these remaining questions and further define and understand this intriguing microglial phenotype. However, the transcriptional, histological, and morphology datasets provided herein will likely continue to provide important new clues to guide these next set of studies.

CONCLUSION AND FUTURE DIRECTIONS

Morgan Coburn, Mathew Blurton-Jones

The field of neuroscience has expanded dramatically in the past century since Alios Alzheimer first described the neurodegenerative disease that now shares his name[260]. Neuroimmunology, in particular, has experienced a wave of interest as we've come to understand that the brain is not as "immune privileged" as we had once believed. A Pubmed search for "microglia" exemplifies how rapidly the field of neuroimmunology has grown. In the mid-90s and early 2000's searches for 'microglia' yielded hits numbering in the double digits. In contrast, before, and rising near exponentially since, in 2020, 4,392 "microglia" articles were published, demonstrating the near exponential rise in productivity and interest in this field. And yet, early papers on microglia mirror in some ways some of the papers published today, that continue to utilize histological protocols to better identify microglia and answer questions about their alterations in morphology that occur in response to disease pathology. However, many new approaches are now also being brought to bear on these important questions. For example, recent publications have developed and presented novel *in vitro* methods to generate human microglia from induced pluripotent stem cells (iPSCs). With the advent of next generation sequencing, researchers have also been able to probe the varying transcriptional profiles that these highly plastic cells adopt as they respond to pathology. Both microglial biologists of the past and today understand that developing better methods to studies these cells has been critical to ask deeper and more insightful questions about their role in health and disease. It is my sincere hope that the studies I have pursued in my thesis research and presented here, will bolster this exciting field, and provide better tools, datasets, and insight into the uniquely human microglial responses to pathology.

Many prior studies have examined the morphological and transcriptional responses of murine microglia as they interact with and respond to amyloid plaques. These disease-associated microglia (DAMs) typically adopt amoeboid morphologies and exhibit heightened expression of various activation and lipid-responsive genes including TREM2, CD11c, CD9, LPL, SPP1, and APOE[2, 6]. Other groups have referred to these plaque proximal microglia as neurodegenerative microglia (MGnD) or Activated response microglia (ARMs). Regardless of the nomenclature, microglial activation states in the context of AD have predominantly been examined in relation to beta-amyloid plaque pathology. Most recently, Lee and colleagues (2021) and colleagues extended our understanding of murine microglial responses to AD pathology by also examining a transgenic model of tangle formation and the combined impact of amyloid and tau pathologies with and without TREM2 expression[196]. They show an expanded "DAM2" phenotype within 20-month old tau and amyloid expressing mice that gives way to an Interferon Responsive population when TREM2 is deleted, indicating that TREM2 allows the DAM activation state to override other microglial fates. Thus, in the midst of a sea of amyloidopathy, tauopathy may only provide a late-stage impact or induce a more tenuous pull towards IFN responsive states. Others groups have reported similar IFN responsive microglial subpopulations in human AD and FTD patient samples, in the latter, as disease progresses early neuronal injury triggers a pro-inflammatory microglial phenotype through Pathogen-associated molecular pattern (PAMP) receptors, but later release of nucleotides from neurons leads to a chronic Type 1 Interferon responsive microglial phenotype[110, 137]. DNA damage can induce type 1 interferon production, which in turn can prime the immune system for an enhanced antiviral response and

cyclic GM-AMP cyclase can bind to extracellular DNA and trigger downstream antiviral/Type 1 IFN responses[139, 140]. Furthermore, antiviral/interferon response gene modules identified in CK-p25 mice were found to be significantly upregulated in microglia isolated from a genetic mouse model of DNA damage and aging; Ercc1$^{\Delta/-}$ mice[194, 261].

Research that utilized human postmortem samples gives us an important glimpse into the microglial responses to bonafide disease states, whereas murine studies give us the power to manipulate the system. Yet, both of these experimental approaches have inherent flaws. Collecting human samples can be technically challenging and the agonal state and long hours spent in postmortem processing are typically unavoidable. Ironically, when tissue is fresh from still living patients it is often labeled as “control” while in reality surgical removal of brain tissue remains an incredibly invasive procedure reserved for those with operable brain tumors or epileptic patients in need of temporal lobe resections[137]. The assumption that these samples are “controls” begs the question: do microglia residing in the margins of tumors or within a brain subjected to extensive hyperexcitability truly represent appropriate “control” samples? Cells isolated from human samples are also often flash frozen for later extraction and sequencing of nuclei, something that allows one to avoid sequencing batch effects but which itself introduces new problems as transcriptomes gleaned from nuclei do not fully capture the full microglial immune response, especially when microglia are activated[262].

With mice these issues are more easily addressed, a Wild Type animal and however many nearly genetically identical replicates are simply ordered or bred, and mice can be perfused with transcription and translation inhibitors and kept on ice, all

measures that can slow transcriptional changes prior to sequencing. And yet, mice are not people, and their genetics cannot fully capture a human response to disease, many genes and proteins lack good homologues across species and this is especially apparent in AD genetics[55].

As an important alternative, researchers may turn to other sources of human cells to study genetics, such as iPSC derived microglia[25, 27]. iPSC modeling allows for high throughput functional and genetic studies and when coupled with CRISPR gene editing can alter a given gene of interest and examine the resulting function changes. Such *in vitro* iPSC-microglial models have an important place in modern neuroimmunological research and yet several caveats remain, for one *in vitro* cells cannot age in the way that *in vivo* cells can, something that adds an additional challenge to studying diseases of the aging brain like Alzheimer's. For example, recent studies have shown that iPSC-derived neurons loose most the age-related epigenetic marks, whereas neurons that are directly reprogrammed from fibroblasts maintain many age-dependent transcriptional and functional changes[263, 264]. In the case of microglia, the culture dish itself presents an important challenge, where microglia isolated from human patients rapid alter their transcriptional profiles in response to culture, and iPSC microglia likewise fail to express key environment dependent microglial genes when grown *in vitro*[19, 36].

To address these challenges, we have developed and fully validated the chimeric microglia models described herein. These novel models utilize the transplantation of human iPSC-derived microglial progenitors (iHPCs) into immunodeficient mice that are humanized for hCSF1 and harboring mutant human transgenes to produce mice that

develop amyloid and/or tau pathologies. We show that transplanted human iHPCs can robustly engraft within the murine forebrain including the cortex, hippocampus, and striatum and further differentiate into mature microglia that transcriptomically resemble those freshly isolated from human tissue samples. These xenotransplanted human microglia (xMG) respond to chronic concussive models, acute laser induced damage, and to systemic LPS challenge, where cells recover the expanded bacterial immune response profiles described in murine studies that are typically lost *in vitro*. This model has also been utilized in collaborations within UCI to study human microglial responses to human brain breast cancer metastases (with Katrina Evans, PhD and Devon Lawson, PhD; in review), and is currently being adopted in labs across the world. In our own group, these chimeric models have been used to further study AD risk genes by transplanting isogenic CRISPR modified lines either knocking out (TREM2 and MS4A6A) or integrating disease relevant mutations (TREM2-R47H; PLCG2-P522R), revealing alterations in microglial motility and response to ADP (TREM2 KO; in review works by Amanda McQuade, PhD), response to beta-amyloid plaques (TREM2 KO and R47H)[36, 192], and antigen presentation (PLCG2-P522R; in review works by Christel Claes, PhD).

However, this chimeric model is not without its own caveats. One outstanding issue is that chimeric mice are by necessity immunodeficient in order to support engraftment of xenotransplanted human cells. Thus, these mice lack T cells, B cells, and NK cells. Our group has previously reported that the adaptive immune system is important in restraining AD pathology as immunodeficient mice experience earlier and expanded amyloid pathology which can be rescued by bone marrow transplantation[148].

As a result, critical aspects of peripheral immune responses to AD pathology are likely lost in our chimeric models, for instance T Cells and NK cells both produce and respond to Type 1 Interferons and also produce Type 2 Interferons[129]. It has also been shown that the *human* version of CSF1 is critical for survival and maturation of *human* microglia and protein homology is known to be low between mice and humans, this begs the question of what other murine signaling molecules are not quite compatible with their complementary human receptors in xMGs[36, 55]. Importantly, t mouse models of AD are also genetically manipulated as mice do not inherently develop either beta-amyloid plaques or neurofibrillary tangles. Here we've chosen to utilize the 5XFAD model which harbors two mutations in human PSEN1 (M146 L/L286 V) combined with three human APP mutations (Swe/Flo/Lon) that increase Aβ production and cleavage, respectively, and cause familial early-onset AD (FAD), which has notably different genetic drivers from that of late-onset AD (LOAD)[52]. Though the PS19 mouse is often used to model AD-related tauopathy for the pathological resemblance to neurofibrillary tangles, this mouse harbor the P301S mutation in MAPT which leads to Frontotemporal Dementia (FTD), but not AD[265]. Despite these caveats, the chimeric mouse models of AD presented here have provided important new insight into the development and progression of AD and the interactions between human microglia and AD pathologies.

As detailed in this thesis, we show that our chimeric microglia model can be used to study uniquely human microglial genetic responses to Alzheimer's pathology. We have recapitulated the previous findings of expanded Type 1 Interferon Responsive, DAM, and IL-1β subclusters in mice and humans, and delve further into the specific characteristics of these microglial subgroups. We further show that tauopathy along is

insufficient to induce a DAM phenotype at 6 months of age, however tau does induce a Type 1 Interferon Response that is dramatically increased when amyloid and tau pathologies are combined. These changes in Type 1 Interferon Responsive microglia are further correlated with a massive increase in little understood Rod-Like microglia phenotype, which we found can be elicited *in vitro* through the treatment of iPS Microglia with IFNα and or β. Other *in vitro* scratch rod-microglia models have been described, but to our knowledge this is the first time they have been shown to occur in response to specific molecular drivers. Our *in vitro* rod-microglia also display increases in fine processes along the main elongated axis of the cell, which are not present in other trace rod-microglia found in other treatment conditions.

Rod-Like microglia have been described several times in different human pathological states, including Alzheimer's and Huntington's[225, 226]. Further reference to these Rod-Like Microglia or "Staebchenzellen" can be dated back to the early 1900's, describing them in paresis, epilepsy, dementia, glioma, and tuberculous meningitis, though whether they were glia or not was often debated by Nissl and Alzheimer[256]. More recent descriptions of Rod-Like microglia are in mouse models of TBI, which depending on the injury can be a transient population, arriving 7 days post injury and lasting for only a week, or much more sudden and long lasting[119, 255]. Here we show that Rod xMGs express P2RY12, something that has been reported only once in TBI, and to our knowledge never before in AD[119]. In AD, microglia have been shown to have small populations of P2RY12+/HLA-DR+ cells, something that is interesting on its own, as P2RY12 is often regarded as a "Homeostatic" marker[247]. Given the precarious location of these fascinating cells within the degenerating hippocampus, more research into

what these Rod-Like microglia are functionally doing is necessary; are they neuroprotective as Type 1 Interferon responses are in viral and prion infection[133, 134]? Do they suppress inflammasome activity that has been associated with worsening amyloidopathy[97, 110]? And are these responses damaging to the system, stripping synapses from the neurons they so closely align to[138]? Synaptic loss has been reported in both TBI and AD numerous time, related to an intriguing satellite phenotype in the former and a Type 1 Interferon Response in the latter[138, 227]. The *in vitro* rod model also points to some potential functionality that would be fascinating to explore, recently tunneling-nanotubes (TNT; thin membranous structures bridging nearby cells, containing f-actin alone or with microtubules) have been described in myeloid cells infected with HIV and have been shown to facilitate transfer of virus as well as large cellular components like mitochondria and lysosomes between cells[266]. These TNTs have also been implicated in the spreading of α-synuclein fibrils, the protein that misfolds and aggregates in Parkinson's Disease[267].

Taken together, the data presented in this dissertation describe the development of three novel chimeric models and their utility in studying uniquely human microglial responses in health and disease. Using these models, we have been able to directly study how Alzheimer's pathologies effect both wild type microglia and human microglia harboring disease relevant mutations. These studies have further uncovered how exposure to amyloid and/or tau pathologies lead to differential activation states, and that the combination of these two hallmark pathologies elicits a fascinating Type 1 Interferon responsive Rod-Microglia phenotype. In summary, these studies have laid the groundwork for further examination of human *in vivo* microglial genetic responses and

may open the door for future cellular and molecular therapeutics in a vast array of developmental, degenerative, auto-immune, infectious, and other brain states where microglial activation has been implicated.

References

1. Alzheimer, A., et al., *An English translation of Alzheimer's 1907 paper, "Uber eine eigenartige Erkankung der Hirnrinde&quot.* Clin Anat, 1995. **8**(6): p. 429-31.

2. Butovsky, O., et al., *Identification of a unique TGF-beta-dependent molecular and functional signature in microglia.* Nat Neurosci, 2014. **17**(1): p. 131-43.

3. Schafer, D.P., et al., *Microglia sculpt postnatal neural circuits in an activity and complement-dependent manner.* Neuron, 2012. **74**(4): p. 691-705.

4. Lehrman, E.K., et al., *CD47 Protects Synapses from Excess Microglia-Mediated Pruning during Development.* Neuron, 2018. **100**(1): p. 120-134 e6.

5. Krasemann, S., et al., *The TREM2-APOE Pathway Drives the Transcriptional Phenotype of Dysfunctional Microglia in Neurodegenerative Diseases.* Immunity, 2017. **47**(3): p. 566-581 e9.

6. Keren-Shaul, H., et al., *A Unique Microglia Type Associated with Restricting Development of Alzheimer's Disease.* Cell, 2017. **169**(7): p. 1276-1290 e17.

7. Mathys, H., et al., *Single-cell transcriptomic analysis of Alzheimer's disease.* Nature, 2019. **570**(7761): p. 332-337.

8. Efthymiou, A.G. and A.M. Goate, *Late onset Alzheimer's disease genetics implicates microglial pathways in disease risk.* Mol Neurodegener, 2017. **12**(1): p. 43.

9. Prinz, M., D. Erny, and N. Hagemeyer, *Ontogeny and homeostasis of CNS myeloid cells.* Nat Immunol, 2017. **18**(4): p. 385-392.

10. Ginhoux, F., et al., *Fate mapping analysis reveals that adult microglia derive from primitive macrophages.* Science, 2010. **330**(6005): p. 841-5.

11. Davalos, D., et al., *ATP mediates rapid microglial response to local brain injury in vivo.* Nat Neurosci, 2005. **8**(6): p. 752-8.

12. Nimmerjahn, A., F. Kirchhoff, and F. Helmchen, *Resting microglial cells are highly dynamic surveillants of brain parenchyma in vivo.* Science, 2005. **308**(5726): p. 1314-8.

13. Gold, E.M., et al., *Repeated Mild Closed Head Injuries Induce Long-Term White Matter Pathology and Neuronal Loss That Are Correlated With Behavioral Deficits.* ASN Neuro, 2018. **10**: p. 1759091418781921.

14. Lively, S. and L.C. Schlichter, *Microglia Responses to Pro-inflammatory Stimuli (LPS, IFNgamma+TNFalpha) and Reprogramming by Resolving Cytokines (IL-4, IL-10).* Front Cell Neurosci, 2018. **12**: p. 215.

15. Elmore, M.R., et al., *Colony-stimulating factor 1 receptor signaling is necessary for microglia viability, unmasking a microglia progenitor cell in the adult brain.* Neuron, 2014. **82**(2): p. 380-97.

16. Rojo, R., et al., *Deletion of a Csf1r enhancer selectively impacts CSF1R expression and development of tissue macrophage populations.* Nat Commun, 2019. **10**(1): p. 3215.

17. McGeer, P.L., et al., *Occurrence of HLA-DR reactive microglia in Alzheimer's disease.* Ann N Y Acad Sci, 1988. **540**: p. 319-23.

18. Karch, C.M. and A.M. Goate, *Alzheimer's disease risk genes and mechanisms of disease pathogenesis.* Biol Psychiatry, 2015. **77**(1): p. 43-51.

19. Gosselin, D., et al., *An environment-dependent transcriptional network specifies human microglia identity.* Science, 2017. **356**(6344).

20. Buttgereit, A., et al., *Sall1 is a transcriptional regulator defining microglia identity and function.* Nat Immunol, 2016. **17**(12): p. 1397-1406.

21. Friedman, B.A., et al., *Diverse Brain Myeloid Expression Profiles Reveal Distinct Microglial Activation States and Aspects of Alzheimer's Disease Not Evident in Mouse Models.* Cell Rep, 2018. **22**(3): p. 832-847.

22. Timmerman, R., S.M. Burm, and J.J. Bajramovic, *An Overview of in vitro Methods to Study Microglia.* Front Cell Neurosci, 2018. **12**: p. 242.

23. Manabe, T., et al., *Pneumonia-associated death in patients with dementia: A systematic review and meta-analysis.* PLoS One, 2019. **14**(3): p. e0213825.

24. Tay, T.L., et al., *Unique microglia recovery population revealed by single-cell RNAseq following neurodegeneration.* Acta Neuropathol Commun, 2018. **6**(1): p. 87.

25. Abud, E.M., et al., *iPSC-Derived Human Microglia-like Cells to Study Neurological Diseases.* Neuron, 2017. **94**(2): p. 278-293 e9.

26. Pocock, J.M. and T.M. Piers, *Modelling microglial function with induced pluripotent stem cells: an update.* Nat Rev Neurosci, 2018. **19**(8): p. 445-452.

27. McQuade, A., et al., *Development and validation of a simplified method to generate human microglia from pluripotent stem cells.* Mol Neurodegener, 2018. **13**(1): p. 67.

28. Bennett, M.L., et al., *New tools for studying microglia in the mouse and human CNS.* Proc Natl Acad Sci U S A, 2016. **113**(12): p. E1738-46.

29. Ueda, Y., D. Gullipalli, and W.C. Song, *Modeling complement-driven diseases in transgenic mice: Values and limitations.* Immunobiology, 2016. **221**(10): p. 1080-90.

30. Durafourt, B.A., et al., *Comparison of polarization properties of human adult microglia and blood-derived macrophages.* Glia, 2012. **60**(5): p. 717-27.

31. Muffat, J., et al., *Efficient derivation of microglia-like cells from human pluripotent stem cells.* Nat Med, 2016. **22**(11): p. 1358-1367.

32. Haenseler, W., et al., *A Highly Efficient Human Pluripotent Stem Cell Microglia Model Displays a Neuronal-Co-culture-Specific Expression Profile and Inflammatory Response.* Stem Cell Reports, 2017. **8**(6): p. 1727-1742.

33. Cong, L., et al., *Multiplex genome engineering using CRISPR/Cas systems.* Science, 2013. **339**(6121): p. 819-23.

34. Lin, Y.T., et al., *APOE4 Causes Widespread Molecular and Cellular Alterations Associated with Alzheimer's Disease Phenotypes in Human iPSC-Derived Brain Cell Types.* Neuron, 2018. **98**(6): p. 1294.

35. Ilic, D., et al., *Human embryonic and induced pluripotent stem cells in clinical trials.* Br Med Bull, 2015. **116**: p. 19-27.

36. Hasselmann, J., et al., *Development of a Chimeric Model to Study and Manipulate Human Microglia In Vivo.* Neuron, 2019. **103**(6): p. 1016-1033 e10.

37. Choi, S.H., et al., *A three-dimensional human neural cell culture model of Alzheimer's disease.* Nature, 2014. **515**(7526): p. 274-8.

38. Ormel, P.R., et al., *Microglia innately develop within cerebral organoids.* Nat Commun, 2018. **9**(1): p. 4167.

39. Song, L., et al., *Functionalization of Brain Region-specific Spheroids with Isogenic Microglia-like Cells.* Sci Rep, 2019. **9**(1): p. 11055.

40. de Leeuw, S. and C. Tackenberg, *Alzheimer's in a dish - induced pluripotent stem cell-based disease modeling.* Transl Neurodegener, 2019. **8**: p. 21.

41. Raja, W.K., et al., *Self-Organizing 3D Human Neural Tissue Derived from Induced Pluripotent Stem Cells Recapitulate Alzheimer's Disease Phenotypes.* PLoS One, 2016. **11**(9): p. e0161969.

42. Blanchard, J.W., et al., *Reconstruction of the human blood-brain barrier in vitro reveals a pathogenic mechanism of APOE4 in pericytes.* Nat Med, 2020. **26**(6): p. 952-963.

43. Sweeney, M.D., A.P. Sagare, and B.V. Zlokovic, *Blood-brain barrier breakdown in Alzheimer disease and other neurodegenerative disorders.* Nat Rev Neurol, 2018. **14**(3): p. 133-150.

44. Weinhard, L., et al., *Microglia remodel synapses by presynaptic trogocytosis and spine head filopodia induction.* Nat Commun, 2018. **9**(1): p. 1228.

45. Sala Frigerio, C., et al., *The Major Risk Factors for Alzheimer's Disease: Age, Sex, and Genes Modulate the Microglia Response to Abeta Plaques.* Cell Rep, 2019. **27**(4): p. 1293-1306 e6.

46. Liddelow, S.A., et al., *Neurotoxic reactive astrocytes are induced by activated microglia.* Nature, 2017. **541**(7638): p. 481-487.

47. Lian, H., et al., *Astrocyte-Microglia Cross Talk through Complement Activation Modulates Amyloid Pathology in Mouse Models of Alzheimer's Disease.* J Neurosci, 2016. **36**(2): p. 577-89.

48. Grommes, C., et al., *Regulation of microglial phagocytosis and inflammatory gene expression by Gas6 acting on the Axl/Mer family of tyrosine kinases.* J Neuroimmune Pharmacol, 2008. **3**(2): p. 130-40.

49. Cho, C.Y., et al., *Negative feedback regulation of AXL by miR-34a modulates apoptosis in lung cancer cells.* RNA, 2016. **22**(2): p. 303-15.

50. Kukurba, K.R. and S.B. Montgomery, *RNA Sequencing and Analysis.* Cold Spring Harb Protoc, 2015. **2015**(11): p. 951-69.

51. Haque, A., et al., *A practical guide to single-cell RNA-sequencing for biomedical research and clinical applications.* Genome Med, 2017. **9**(1): p. 75.

52. Oakley, H., et al., *Intraneuronal beta-amyloid aggregates, neurodegeneration, and neuron loss in transgenic mice with five familial Alzheimer's disease mutations: potential factors in amyloid plaque formation.* J Neurosci, 2006. **26**(40): p. 10129-40.

53. Hammond, T.R., et al., *Single-Cell RNA Sequencing of Microglia throughout the Mouse Lifespan and in the Injured Brain Reveals Complex Cell-State Changes.* Immunity, 2019. **50**(1): p. 253-271 e6.

54. Srinivasan, K., et al., *Untangling the brain's neuroinflammatory and neurodegenerative transcriptional responses.* Nat Commun, 2016. **7**: p. 11295.

55. Hasselmann, J. and M. Blurton-Jones, *Human iPSC-derived microglia: A growing toolset to study the brain's innate immune cells.* Glia, 2020. **68**(4): p. 721-739.

56. Jung, S., et al., *Analysis of fractalkine receptor CX(3)CR1 function by targeted deletion and green fluorescent protein reporter gene insertion.* Mol Cell Biol, 2000. **20**(11): p. 4106-14.

57. Jolivel, V., et al., *Perivascular microglia promote blood vessel disintegration in the ischemic penumbra.* Acta Neuropathol, 2015. **129**(2): p. 279-95.

58. Kim, I., et al., *A postnatal peak in microglial development in the mouse hippocampus is correlated with heightened sensitivity to seizure triggers.* Brain Behav, 2015. **5**(12): p. e00403.

59. Parkhurst, C.N., et al., *Microglia promote learning-dependent synapse formation through brain-derived neurotrophic factor.* Cell, 2013. **155**(7): p. 1596-609.

60. Yona, S., et al., *Fate mapping reveals origins and dynamics of monocytes and tissue macrophages under homeostasis.* Immunity, 2013. **38**(1): p. 79-91.

61. Hwang, H.W., et al., *cTag-PAPERCLIP Reveals Alternative Polyadenylation Promotes Cell-Type Specific Protein Diversity and Shifts Araf Isoforms with Microglia Activation.* Neuron, 2017. **95**(6): p. 1334-1349 e5.

62. Jung, C.K., et al., *Fibrillar amyloid plaque formation precedes microglial activation.* PLoS One, 2015. **10**(3): p. e0119768.

63. Jankowsky, J.L., et al., *Mutant presenilins specifically elevate the levels of the 42 residue beta-amyloid peptide in vivo: evidence for augmentation of a 42-specific gamma secretase.* Hum Mol Genet, 2004. **13**(2): p. 159-70.

64. Klunk, W.E., et al., *Imaging Abeta plaques in living transgenic mice with multiphoton microscopy and methoxy-X04, a systemically administered Congo red derivative.* J Neuropathol Exp Neurol, 2002. **61**(9): p. 797-805.

65. Zhao, Y., et al., *TREM2 Is a Receptor for beta-Amyloid that Mediates Microglial Function.* Neuron, 2018. **97**(5): p. 1023-1031 e7.

66. *Alzheimer's Disease: Facts and Figures*. 2019 11/15/19]; Available from: https://www.alz.org/alzheimers-dementia/facts-figures.

67. Leonenko, G., et al., *Polygenic risk and hazard scores for Alzheimer's disease prediction.* Ann Clin Transl Neurol, 2019. **6**(3): p. 456-465.

68. Hansen, D.V., J.E. Hanson, and M. Sheng, *Microglia in Alzheimer's disease.* J Cell Biol, 2018. **217**(2): p. 459-472.

69. Kleinberger, G., et al., *TREM2 mutations implicated in neurodegeneration impair cell surface transport and phagocytosis.* Sci Transl Med, 2014. **6**(243): p. 243ra86.

70. Takahashi, K., C.D. Rochford, and H. Neumann, *Clearance of apoptotic neurons without inflammation by microglial triggering receptor expressed on myeloid cells-2.* J Exp Med, 2005. **201**(4): p. 647-57.

71. Jin, S.C., et al., *Coding variants in TREM2 increase risk for Alzheimer's disease.* Hum Mol Genet, 2014. **23**(21): p. 5838-46.

72. Paloneva, J., et al., *Mutations in two genes encoding different subunits of a receptor signaling complex result in an identical disease phenotype.* Am J Hum Genet, 2002. **71**(3): p. 656-62.

73. Lue, L.F., C. Schmitz, and D.G. Walker, *What happens to microglial TREM2 in Alzheimer's disease: Immunoregulatory turned into immunopathogenic?* Neuroscience, 2015. **302**: p. 138-50.

74. Frank, S., et al., *TREM2 is upregulated in amyloid plaque-associated microglia in aged APP23 transgenic mice.* Glia, 2008. **56**(13): p. 1438-47.

75. Jay, T.R., et al., *TREM2 deficiency eliminates TREM2+ inflammatory macrophages and ameliorates pathology in Alzheimer's disease mouse models.* J Exp Med, 2015. **212**(3): p. 287-95.

76. Mahley, R.W., *Apolipoprotein E: cholesterol transport protein with expanding role in cell biology.* Science, 1988. **240**(4852): p. 622-30.

77. Corder, E.H., et al., *Gene dose of apolipoprotein E type 4 allele and the risk of Alzheimer's disease in late onset families.* Science, 1993. **261**(5123): p. 921-3.

78. Strittmatter, W.J., et al., *Binding of human apolipoprotein E to synthetic amyloid beta peptide: isoform-specific effects and implications for late-onset Alzheimer disease.* Proc Natl Acad Sci U S A, 1993. **90**(17): p. 8098-102.

79. Kim, J., J.M. Basak, and D.M. Holtzman, *The role of apolipoprotein E in Alzheimer's disease.* Neuron, 2009. **63**(3): p. 287-303.

80. Castellano, J.M., et al., *Human apoE isoforms differentially regulate brain amyloid-beta peptide clearance.* Sci Transl Med, 2011. **3**(89): p. 89ra57.

81. Tokuda, T., et al., *Lipidation of apolipoprotein E influences its isoform-specific interaction with Alzheimer's amyloid beta peptides.* Biochem J, 2000. **348 Pt 2**: p. 359-65.

82. Lee, C.Y., et al., *Apolipoprotein E promotes beta-amyloid trafficking and degradation by modulating microglial cholesterol levels.* J Biol Chem, 2012. **287**(3): p. 2032-44.

83. Karch, C.M., et al., *Expression of novel Alzheimer's disease risk genes in control and Alzheimer's disease brains.* PLoS One, 2012. **7**(11): p. e50976.

84. Cruse, G., et al., *The CD20 homologue MS4A4 directs trafficking of KIT toward clathrin-independent endocytosis pathways and thus regulates receptor signaling and recycling.* Mol Biol Cell, 2015. **26**(9): p. 1711-27.

85. Einfeld, D.A., et al., *Molecular cloning of the human B cell CD20 receptor predicts a hydrophobic protein with multiple transmembrane domains.* EMBO J, 1988. **7**(3): p. 711-7.

86. Magno, L., et al., *Alzheimer's disease phospholipase C-gamma-2 (PLCG2) protective variant is a functional hypermorph.* Alzheimers Res Ther, 2019. **11**(1): p. 16.

87. Xing, J., A.R. Titus, and M.B. Humphrey, *The TREM2-DAP12 signaling pathway in Nasu-Hakola disease: a molecular genetics perspective.* Res Rep Biochem, 2015. **5**: p. 89-100.

88. Harold, D., et al., *Genome-wide association study identifies variants at CLU and PICALM associated with Alzheimer's disease.* Nat Genet, 2009. **41**(10): p. 1088-93.

89. Chapuis, J., et al., *Increased expression of BIN1 mediates Alzheimer genetic risk by modulating tau pathology.* Mol Psychiatry, 2013. **18**(11): p. 1225-34.

90. Crotti, A., et al., *BIN1 favors the spreading of Tau via extracellular vesicles.* Sci Rep, 2019. **9**(1): p. 9477.

91. Musiek, E.S. and D.M. Holtzman, *Three dimensions of the amyloid hypothesis: time, space and 'wingmen'.* Nat Neurosci, 2015. **18**(6): p. 800-6.

92. Zhang, C., et al., *Amyloid-beta production via cleavage of amyloid-beta protein precursor is modulated by cell density.* J Alzheimers Dis, 2010. **22**(2): p. 683-984.

93. Anderson, R.M., et al., *Why do so many clinical trials of therapies for Alzheimer's disease fail?* Lancet, 2017. **390**(10110): p. 2327-2329.

94. Doody, R.S., et al., *A phase 3 trial of semagacestat for treatment of Alzheimer's disease.* N Engl J Med, 2013. **369**(4): p. 341-50.

95. Vandenberghe, R., et al., *Bapineuzumab for mild to moderate Alzheimer's disease in two global, randomized, phase 3 trials.* Alzheimers Res Ther, 2016. **8**(1): p. 18.

96. The Lancet, N., *Solanezumab: too late in mild Alzheimer's disease?* Lancet Neurol, 2017. **16**(2): p. 97.

97. Venegas, C., et al., *Microglia-derived ASC specks cross-seed amyloid-beta in Alzheimer's disease.* Nature, 2017. **552**(7685): p. 355-361.

98. Bolmont, T., et al., *Dynamics of the microglial/amyloid interaction indicate a role in plaque maintenance.* J Neurosci, 2008. **28**(16): p. 4283-92.

99. Yuan, P., et al., *TREM2 Haplodeficiency in Mice and Humans Impairs the Microglia Barrier Function Leading to Decreased Amyloid Compaction and Severe Axonal Dystrophy.* Neuron, 2016. **92**(1): p. 252-264.

100. Weingarten, M.D., et al., *A protein factor essential for microtubule assembly.* Proc Natl Acad Sci U S A, 1975. **72**(5): p. 1858-62.

101. Iqbal, K., et al., *Tau in Alzheimer disease and related tauopathies.* Curr Alzheimer Res, 2010. **7**(8): p. 656-64.

102. Hernandez, F., et al., *Differences in structure and function between human and murine tau.* Biochim Biophys Acta Mol Basis Dis, 2019. **1865**(8): p. 2024-2030.

103. Andorfer, C., et al., *Hyperphosphorylation and aggregation of tau in mice expressing normal human tau isoforms.* J Neurochem, 2003. **86**(3): p. 582-90.

104. Yoshiyama, Y., et al., *Synapse loss and microglial activation precede tangles in a P301S tauopathy mouse model.* Neuron, 2007. **53**(3): p. 337-51.

105. Luo, W., et al., *Microglial internalization and degradation of pathological tau is enhanced by an anti-tau monoclonal antibody.* Sci Rep, 2015. **5**: p. 11161.

106. Hopp, S.C., et al., *The role of microglia in processing and spreading of bioactive tau seeds in Alzheimer's disease.* J Neuroinflammation, 2018. **15**(1): p. 269.

107. Leyns, C.E.G., et al., *TREM2 function impedes tau seeding in neuritic plaques.* Nat Neurosci, 2019. **22**(8): p. 1217-1222.

108. Litvinchuk, A., et al., *Complement C3aR Inactivation Attenuates Tau Pathology and Reverses an Immune Network Deregulated in Tauopathy Models and Alzheimer's Disease.* Neuron, 2018. **100**(6): p. 1337-1353 e5.

109. Matarin, M., et al., *A genome-wide gene-expression analysis and database in transgenic mice during development of amyloid or tau pathology.* Cell Rep, 2015. **10**(4): p. 633-44.

110. Rexach, J.E., et al., *Tau Pathology Drives Dementia Risk-Associated Gene Networks toward Chronic Inflammatory States and Immunosuppression.* Cell Rep, 2020. **33**(7): p. 108398.

111. Cheffer, A., et al., *Purinergic system in psychiatric diseases.* Mol Psychiatry, 2018. **23**(1): p. 94-106.

112. Cserep, C., et al., *Microglia monitor and protect neuronal function through specialized somatic purinergic junctions.* Science, 2020. **367**(6477): p. 528-537.

113. Gomez Morillas, A., V.C. Besson, and D. Lerouet, *Microglia and Neuroinflammation: What Place for P2RY12?* Int J Mol Sci, 2021. **22**(4).

114. Madry, C., et al., *Microglial Ramification, Surveillance, and Interleukin-1beta Release Are Regulated by the Two-Pore Domain K(+) Channel THIK-1.* Neuron, 2018. **97**(2): p. 299-312 e6.

115. Pfeiffer, T. and D. Attwell, *Brain's immune cells put the brakes on neurons.* Nature, 2020. **586**(7829): p. 366-367.

116. Badimon, A., et al., *Negative feedback control of neuronal activity by microglia.* Nature, 2020. **586**(7829): p. 417-423.

117. Sanchez-Mejias, E., et al., *Soluble phospho-tau from Alzheimer's disease hippocampus drives microglial degeneration.* Acta Neuropathol, 2016. **132**(6): p. 897-916.

118. Eyo, U.B., et al., *Neuronal hyperactivity recruits microglial processes via neuronal NMDA receptors and microglial P2Y12 receptors after status epilepticus.* J Neurosci, 2014. **34**(32): p. 10528-40.

119. Witcher, K.G., et al., *Traumatic brain injury-induced neuronal damage in the somatosensory cortex causes formation of rod-shaped microglia that promote astrogliosis and persistent neuroinflammation.* Glia, 2018. **66**(12): p. 2719-2736.

120. Sperlagh, B. and P. Illes, *Purinergic modulation of microglial cell activation.* Purinergic Signal, 2007. **3**(1-2): p. 117-27.

121. He, Y., et al., *The role of microglial P2X7: modulation of cell death and cytokine release.* J Neuroinflammation, 2017. **14**(1): p. 135.

122. Kelley, N., et al., *The NLRP3 Inflammasome: An Overview of Mechanisms of Activation and Regulation.* Int J Mol Sci, 2019. **20**(13).

123. Heneka, M.T., et al., *NLRP3 is activated in Alzheimer's disease and contributes to pathology in APP/PS1 mice.* Nature, 2013. **493**(7434): p. 674-8.

124. Stancu, I.C., et al., *Aggregated Tau activates NLRP3-ASC inflammasome exacerbating exogenously seeded and non-exogenously seeded Tau pathology in vivo.* Acta Neuropathol, 2019. **137**(4): p. 599-617.

125. Lee, S., et al., *CX3CR1 deficiency alters microglial activation and reduces beta-amyloid deposition in two Alzheimer's disease mouse models.* Am J Pathol, 2010. **177**(5): p. 2549-62.

126. Eyo, U.B., et al., *Regulation of Physical Microglia-Neuron Interactions by Fractalkine Signaling after Status Epilepticus.* eNeuro, 2016. **3**(6).

127. Todd, L., et al., *Reactive microglia and IL1beta/IL-1R1-signaling mediate neuroprotection in excitotoxin-damaged mouse retina.* J Neuroinflammation, 2019. **16**(1): p. 118.

128. Lee, A.J. and A.A. Ashkar, *The Dual Nature of Type I and Type II Interferons.* Front Immunol, 2018. **9**: p. 2061.

129. Lee, A.J., et al., *Inflammatory monocytes require type I interferon receptor signaling to activate NK cells via IL-18 during a mucosal viral infection.* J Exp Med, 2017. **214**(4): p. 1153-1167.

130. McNab, F., et al., *Type I interferons in infectious disease.* Nat Rev Immunol, 2015. **15**(2): p. 87-103.

131. Cavanaugh, S.E., A.M. Holmgren, and G.F. Rall, *Homeostatic interferon expression in neurons is sufficient for early control of viral infection.* J Neuroimmunol, 2015. **279**: p. 11-9.

132. Thaney, V.E., et al., *IFNbeta Protects Neurons from Damage in a Murine Model of HIV-1 Associated Brain Injury.* Sci Rep, 2017. **7**: p. 46514.

133. Delhaye, S., et al., *Neurons produce type I interferon during viral encephalitis.* Proc Natl Acad Sci U S A, 2006. **103**(20): p. 7835-40.

134. Ishibashi, D., et al., *Type I interferon protects neurons from prions in in vivo models.* Brain, 2019. **142**(4): p. 1035-1050.

135. Eshleman, E.M., et al., *Down regulation of macrophage IFNGR1 exacerbates systemic L. monocytogenes infection.* PLoS Pathog, 2017. **13**(5): p. e1006388.

136. Aw, E., Y. Zhang, and M. Carroll, *Microglial responses to peripheral type 1 interferon.* J Neuroinflammation, 2020. **17**(1): p. 340.

137. Olah, M., et al., *Single cell RNA sequencing of human microglia uncovers a subset associated with Alzheimer's disease.* Nat Commun, 2020. **11**(1): p. 6129.

138. Roy, E.R., et al., *Type I interferon response drives neuroinflammation and synapse loss in Alzheimer disease.* J Clin Invest, 2020. **130**(4): p. 1912-1930.

139. Sun, L., et al., *Cyclic GMP-AMP synthase is a cytosolic DNA sensor that activates the type I interferon pathway.* Science, 2013. **339**(6121): p. 786-91.

140. Hartlova, A., et al., *DNA damage primes the type I interferon system via the cytosolic DNA sensor STING to promote anti-microbial innate immunity.* Immunity, 2015. **42**(2): p. 332-343.

141. Deczkowska, A., et al., *Mef2C restrains microglial inflammatory response and is lost in brain ageing in an IFN-I-dependent manner.* Nat Commun, 2017. **8**(1): p. 717.

142. Dorman, L.C., et al., *A type I interferon response defines a conserved microglial state required for effective phagocytosis.* bioRxiv, 2021: p. 2021.04.29.441889.

143. Kobayashi, K.S. and P.J. van den Elsen, *NLRC5: a key regulator of MHC class I-dependent immune responses.* Nat Rev Immunol, 2012. **12**(12): p. 813-20.

144. Hsu, D.C., *JANEWAY'S IMMUNOBIOLOGY, 7TH EDITION.* Shock, 2008. **29**(6): p. 770.

145. McGeer, P.L., et al., *Reactive microglia in patients with senile dementia of the Alzheimer type are positive for the histocompatibility glycoprotein HLA-DR.* Neurosci Lett, 1987. **79**(1-2): p. 195-200.

146. Lu, R.C., et al., *Association of HLA-DRB1 polymorphism with Alzheimer's disease: a replication and meta-analysis.* Oncotarget, 2017. **8**(54): p. 93219-93226.

147. Patel, D., et al., *Cell-type-specific expression quantitative trait loci associated with Alzheimer disease in blood and brain tissue.* Transl Psychiatry, 2021. **11**(1): p. 250.

148. Marsh, S.E., et al., *The adaptive immune system restrains Alzheimer's disease pathogenesis by modulating microglial function.* Proc Natl Acad Sci U S A, 2016. **113**(9): p. E1316-25.

149. Kipnis, J., et al., *Neuronal survival after CNS insult is determined by a genetically encoded autoimmune response.* J Neurosci, 2001. **21**(13): p. 4564-71.

150. Kipnis, J., et al., *Myelin specific Th1 cells are necessary for post-traumatic protective autoimmunity.* J Neuroimmunol, 2002. **130**(1-2): p. 78-85.

151. Murphy, A.C., et al., *Infiltration of Th1 and Th17 cells and activation of microglia in the CNS during the course of experimental autoimmune encephalomyelitis.* Brain Behav Immun, 2010. **24**(4): p. 641-51.

152. Ren, X., et al., *Programmed death-1 pathway limits central nervous system inflammation and neurologic deficits in murine experimental stroke.* Stroke, 2011. **42**(9): p. 2578-83.

153. Shinohara, M.L., et al., *Engagement of the type I interferon receptor on dendritic cells inhibits T helper 17 cell development: role of intracellular osteopontin.* Immunity, 2008. **29**(1): p. 68-78.

154. Chai, Y.L., et al., *Plasma osteopontin as a biomarker of Alzheimer's disease and vascular cognitive impairment.* Sci Rep, 2021. **11**(1): p. 4010.

155. Salter, M.W. and B. Stevens, *Microglia emerge as central players in brain disease.* Nat Med, 2017. **23**(9): p. 1018-1027.

156. Stevens, B., et al., *The classical complement cascade mediates CNS synapse elimination.* Cell, 2007. **131**(6): p. 1164-78.

157. Wu, Y., et al., *Microglia: Dynamic Mediators of Synapse Development and Plasticity.* Trends Immunol, 2015. **36**(10): p. 605-613.

158. Perry, V.H. and C. Holmes, *Microglial priming in neurodegenerative disease.* Nat Rev Neurol, 2014. **10**(4): p. 217-24.

159. Karch, C.M., C. Cruchaga, and A.M. Goate, *Alzheimer's disease genetics: from the bench to the clinic.* Neuron, 2014. **83**(1): p. 11-26.

160. Dawson, T.M., T.E. Golde, and C. Lagier-Tourenne, *Animal models of neurodegenerative diseases.* Nat Neurosci, 2018. **21**(10): p. 1370-1379.

161. Bennett, F.C., et al., *A Combination of Ontogeny and CNS Environment Establishes Microglial Identity.* Neuron, 2018. **98**(6): p. 1170-1183 e8.

162. Capotondo, A., et al., *Intracerebroventricular delivery of hematopoietic progenitors results in rapid and robust engraftment of microglia-like cells.* Sci Adv, 2017. **3**(12): p. e1701211.

163. Rongvaux, A., et al., *Development and function of human innate immune cells in a humanized mouse model.* Nat Biotechnol, 2014. **32**(4): p. 364-72.

164. Rathinam, C., et al., *Efficient differentiation and function of human macrophages in humanized CSF-1 mice.* Blood, 2011. **118**(11): p. 3119-28.

165. Sieff, C.A., *Hematopoietic growth factors.* J Clin Invest, 1987. **79**(6): p. 1549-57.

166. De Lucia, C., et al., *Microglia regulate hippocampal neurogenesis during chronic neurodegeneration.* Brain Behav Immun, 2016. **55**: p. 179-190.

167. Shapiro, L.A., et al., *Morphological and ultrastructural features of Iba1-immunolabeled microglial cells in the hippocampal dentate gyrus.* Brain Res, 2009. **1266**: p. 29-36.

168. Savchenko, V.L., et al., *Microglia and astrocytes in the adult rat brain: comparative immunocytochemical analysis demonstrates the efficacy of lipocortin 1 immunoreactivity.* Neuroscience, 2000. **96**(1): p. 195-203.

169. Goldmann, T., et al., *Origin, fate and dynamics of macrophages at central nervous system interfaces.* Nat Immunol, 2016. **17**(7): p. 797-805.

170. Allen, M., et al., *Late-onset Alzheimer disease risk variants mark brain regulatory loci.* Neurol Genet, 2015. **1**(2): p. e15.

171. Shitaka, Y., et al., *Repetitive closed-skull traumatic brain injury in mice causes persistent multifocal axonal injury and microglial reactivity.* J Neuropathol Exp Neurol, 2011. **70**(7): p. 551-67.

172. Varley, A.W., Coulthard, M.G., Meidell, R.S., Gerard, R.D., and Munford, R.S., *Inflammation-induced recombinant protein expression in vivo using promoters from acute-phase protein genes.* Proc. Natl. Acad. Sci., 1995. **USA 92**: p. 5346–5350.

173. Subramanian, A., et al., *Gene set enrichment analysis: a knowledge-based approach for interpreting genome-wide expression profiles.* Proc Natl Acad Sci U S A, 2005. **102**(43): p. 15545-50.

174. Pulido-Salgado, M., et al., *RNA-Seq transcriptomic profiling of primary murine microglia treated with LPS or LPS + IFNgamma.* Sci Rep, 2018. **8**(1): p. 16096.

175. Hickman, S., et al., *Microglia in neurodegeneration.* Nat Neurosci, 2018. **21**(10): p. 1359-1369.

176. Kauppinen, T.M., et al., *Zinc triggers microglial activation.* J Neurosci, 2008. **28**(22): p. 5827-35.

177. Jay, T.R., et al., *Disease Progression-Dependent Effects of TREM2 Deficiency in a Mouse Model of Alzheimer's Disease.* J Neurosci, 2017. **37**(3): p. 637-647.

178. Ulrich, J.D., et al., *Altered microglial response to Abeta plaques in APPPS1-21 mice heterozygous for TREM2.* Mol Neurodegener, 2014. **9**: p. 20.

179. Wang, Y., et al., *TREM2-mediated early microglial response limits diffusion and toxicity of amyloid plaques.* J Exp Med, 2016. **213**(5): p. 667-75.

180. Wang, Y., et al., *TREM2 lipid sensing sustains the microglial response in an Alzheimer's disease model.* Cell, 2015. **160**(6): p. 1061-71.

181. Song, W.M., et al., *Humanized TREM2 mice reveal microglia-intrinsic and -extrinsic effects of R47H polymorphism.* J Exp Med, 2018. **215**(3): p. 745-760.

182. Kamphuis, W., et al., *Transcriptional profiling of CD11c-positive microglia accumulating around amyloid plaques in a mouse model for Alzheimer's disease.* Biochim Biophys Acta, 2016. **1862**(10): p. 1847-60.

183. Yin, Z., et al., *Immune hyperreactivity of Abeta plaque-associated microglia in Alzheimer's disease.* Neurobiol Aging, 2017. **55**: p. 115-122.

184. Boza-Serrano, A., et al., *Galectin-3, a novel endogenous TREM2 ligand, detrimentally regulates inflammatory response in Alzheimer's disease.* Acta Neuropathol, 2019. **138**(2): p. 251-273.

185. Svoboda, D.S., et al., *Human iPSC-derived microglia assume a primary microglia-like state after transplantation into the neonatal mouse brain.* Proc Natl Acad Sci U S A, 2019.

186. Mancuso, R., et al., *Stem-cell-derived human microglia transplanted in mouse brain to study human disease.* Nat Neurosci, 2019. **22**(12): p. 2111-2116.

187. Bertram, L. and R.E. Tanzi, *Genomic mechanisms in Alzheimer's disease.* Brain Pathol, 2020. **30**(5): p. 966-977.

188. Tanzi, R.E., *A brief history of Alzheimer's disease gene discovery.* J Alzheimers Dis, 2013. **33 Suppl 1**: p. S5-13.

189. Griciuc, A. and R.E. Tanzi, *The role of innate immune genes in Alzheimer's disease.* Curr Opin Neurol, 2021. **34**(2): p. 228-236.

190. Podlesny-Drabiniok, A., E. Marcora, and A.M. Goate, *Microglial Phagocytosis: A Disease-Associated Process Emerging from Alzheimer's Disease Genetics.* Trends Neurosci, 2020. **43**(12): p. 965-979.

191. Chaudhury, S., et al., *Polygenic risk score in postmortem diagnosed sporadic early-onset Alzheimer's disease.* Neurobiol Aging, 2018. **62**: p. 244 e1-244 e8.

192. McQuade, A., et al., *Gene expression and functional deficits underlie TREM2-knockout microglia responses in human models of Alzheimer's disease.* Nat Commun, 2020. **11**(1): p. 5370.

193. Claes, C., et al., *Plaque-associated human microglia accumulate lipid droplets in a chimeric model of Alzheimer's disease.* Mol Neurodegener, 2021. **16**(1): p. 50.

194. Mathys, H., et al., *Temporal Tracking of Microglia Activation in Neurodegeneration at Single-Cell Resolution.* Cell Rep, 2017. **21**(2): p. 366-380.

195. Gerrits, E., et al., *Distinct amyloid-beta and tau-associated microglia profiles in Alzheimer's disease.* Acta Neuropathol, 2021. **141**(5): p. 681-696.

196. Lee, S.H., et al., *Trem2 restrains the enhancement of tau accumulation and neurodegeneration by beta-amyloid pathology.* Neuron, 2021. **109**(8): p. 1283-1301 e6.

197. Santiago, J.A. and J.A. Potashkin, *The Impact of Disease Comorbidities in Alzheimer's Disease.* Front Aging Neurosci, 2021. **13**: p. 631770.

198. Jacquemet, G., H. Hamidi, and J. Ivaska, *Filopodia Quantification Using FiloQuant.* Methods Mol Biol, 2019. **2040**: p. 359-373.

199. Hui, C.W., et al., *Nonfunctional mutant Wrn protein leads to neurological deficits, neuronal stress, microglial alteration, and immune imbalance in a mouse model of Werner syndrome.* Brain Behav Immun, 2018. **73**: p. 450-469.

200. St-Pierre, M.K., M. Bordeleau, and M.E. Tremblay, *Visualizing Dark Microglia.* Methods Mol Biol, 2019. **2034**: p. 97-110.

201. Nahirney, P.C. and M.E. Tremblay, *Brain Ultrastructure: Putting the Pieces Together.* Front Cell Dev Biol, 2021. **9**: p. 629503.

202. Yates, A.D., et al., *Ensembl 2020.* Nucleic Acids Res, 2020. **48**(D1): p. D682-D688.

203. Butler, A., et al., *Integrating single-cell transcriptomic data across different conditions, technologies, and species.* Nat Biotechnol, 2018. **36**(5): p. 411-420.

204. Fabbrini, F., et al., *Probing the Mechanisms of Repetition Suppression in Inferior Temporal Cortex with Optogenetics.* Curr Biol, 2019. **29**(12): p. 1988-1998 e4.

205. Cao, Y., et al., *scDC: single cell differential composition analysis.* BMC Bioinformatics, 2019. **20**(Suppl 19): p. 721.

206. Hao, Y., et al., *Integrated analysis of multimodal single-cell data.* Cell, 2021. **184**(13): p. 3573-3587 e29.

207. Stuart, T., et al., *Comprehensive Integration of Single-Cell Data.* Cell, 2019. **177**(7): p. 1888-1902 e21.

208. van Buuren, S. and K. Groothuis-Oudshoorn, *mice: Multivariate Imputation by Chained Equations in R.* Journal of Statistical Software, 2011. **45**(3): p. 1 - 67.

209. Hothorn, T., F. Bretz, and P. Westfall, *Simultaneous inference in general parametric models.* Biom J, 2008. **50**(3): p. 346-63.

210. Trapnell, C., et al., *The dynamics and regulators of cell fate decisions are revealed by pseudotemporal ordering of single cells.* Nat Biotechnol, 2014. **32**(4): p. 381-386.

211. Mi, H., A. Muruganujan, and P.D. Thomas, *PANTHER in 2013: modeling the evolution of gene function, and other gene attributes, in the context of phylogenetic trees.* Nucleic Acids Res, 2013. **41**(Database issue): p. D377-86.

212. Merico, D., et al., *Enrichment map: a network-based method for gene-set enrichment visualization and interpretation.* PLoS One, 2010. **5**(11): p. e13984.

213. Shannon, P., et al., *Cytoscape: a software environment for integrated models of biomolecular interaction networks.* Genome Res, 2003. **13**(11): p. 2498-504.

214. Khan, A., et al., *JASPAR 2018: update of the open-access database of transcription factor binding profiles and its web framework.* Nucleic Acids Res, 2018. **46**(D1): p. D260-D266.

215. Gratuze, M., et al., *Impact of TREM2R47H variant on tau pathology-induced gliosis and neurodegeneration.* J Clin Invest, 2020. **130**(9): p. 4954-4968.

216. Iba, M., et al., *Tau pathology spread in PS19 tau transgenic mice following locus coeruleus (LC) injections of synthetic tau fibrils is determined by the LC's afferent and efferent connections.* Acta Neuropathol, 2015. **130**(3): p. 349-62.

217. Sayed, F.A., et al., *Differential effects of partial and complete loss of TREM2 on microglial injury response and tauopathy.* Proc Natl Acad Sci U S A, 2018. **115**(40): p. 10172-10177.

218. Pascoal, T.A., et al., *Microglial activation and tau propagate jointly across Braak stages.* Nat Med, 2021. **27**(9): p. 1592-1599.

219. Chen, W., et al., *Increased tauopathy drives microglia-mediated clearance of beta-amyloid.* Acta Neuropathol Commun, 2016. **4**(1): p. 63.

220. Oddo, S., et al., *Amyloid deposition precedes tangle formation in a triple transgenic model of Alzheimer's disease.* Neurobiol Aging, 2003. **24**(8): p. 1063-70.

221. Pooler, A.M., et al., *Amyloid accelerates tau propagation and toxicity in a model of early Alzheimer's disease.* Acta Neuropathol Commun, 2015. **3**: p. 14.

222. Ribe, E.M., et al., *Accelerated amyloid deposition, neurofibrillary degeneration and neuronal loss in double mutant APP/tau transgenic mice.* Neurobiol Dis, 2005. **20**(3): p. 814-22.

223. Heraud, C., et al., *Increased misfolding and truncation of tau in APP/PS1/tau transgenic mice compared to mutant tau mice.* Neurobiol Dis, 2014. **62**: p. 100-12.

224. Stancu, I.C., et al., *Tauopathy contributes to synaptic and cognitive deficits in a murine model for Alzheimer's disease.* FASEB J, 2014. **28**(6): p. 2620-31.

225. Bachstetter, A.D., et al., *Disease-related microglia heterogeneity in the hippocampus of Alzheimer's disease, dementia with Lewy bodies, and hippocampal sclerosis of aging.* Acta Neuropathol Commun, 2015. **3**: p. 32.

226. Sapp, E., et al., *Early and progressive accumulation of reactive microglia in the Huntington disease brain.* J Neuropathol Exp Neurol, 2001. **60**(2): p. 161-72.

227. Krukowski, K., et al., *Novel microglia-mediated mechanisms underlying synaptic loss and cognitive impairment after traumatic brain injury.* Brain Behav Immun, 2021. **98**: p. 122-135.

228. Marschallinger, J., et al., *Lipid-droplet-accumulating microglia represent a dysfunctional and proinflammatory state in the aging brain.* Nat Neurosci, 2020. **23**(2): p. 194-208.

229. Andreone, B.J., et al., *Alzheimer's-associated PLCgamma2 is a signaling node required for both TREM2 function and the inflammatory response in human microglia.* Nat Neurosci, 2020. **23**(8): p. 927-938.

230. Konnecke, H. and I. Bechmann, *The role of microglia and matrix metalloproteinases involvement in neuroinflammation and gliomas.* Clin Dev Immunol, 2013. **2013**: p. 914104.

231. Jansen, I.E., et al., *Genome-wide meta-analysis identifies new loci and functional pathways influencing Alzheimer's disease risk.* Nat Genet, 2019. **51**(3): p. 404-413.

232. Kunkle, B.W., et al., *Genetic meta-analysis of diagnosed Alzheimer's disease identifies new risk loci and implicates Abeta, tau, immunity and lipid processing.* Nat Genet, 2019. **51**(3): p. 414-430.

233. Sims, R., et al., *Rare coding variants in PLCG2, ABI3, and TREM2 implicate microglial-mediated innate immunity in Alzheimer's disease.* Nat Genet, 2017. **49**(9): p. 1373-1384.

234. Lambert, J.C., et al., *Meta-analysis of 74,046 individuals identifies 11 new susceptibility loci for Alzheimer's disease.* Nat Genet, 2013. **45**(12): p. 1452-8.

235. Novikova, G., et al., *Integration of Alzheimer's disease genetics and myeloid genomics identifies disease risk regulatory elements and genes.* Nat Commun, 2021. **12**(1): p. 1610.

236. Choi, U.Y., et al., *Oligoadenylate synthase-like (OASL) proteins: dual functions and associations with diseases.* Exp Mol Med, 2015. **47**: p. e144.

237. Salih, D.A., et al., *Genetic variability in response to amyloid beta deposition influences Alzheimer's disease risk.* Brain Commun, 2019. **1**(1): p. fcz022.

238. Magusali, N., et al., *A genetic link between risk for Alzheimer's disease and severe COVID-19 outcomes via the OAS1 gene.* Brain, 2021.

239. Jiang, L., et al., *Interaction of tau with HNRNPA2B1 and N(6)-methyladenosine RNA mediates the progression of tauopathy.* Mol Cell, 2021. **81**(20): p. 4209-4227 e12.

240. Huang, H., et al., *Altered Expression of the m6A Methyltransferase METTL3 in Alzheimer's Disease.* eNeuro, 2020. **7**(5).

241. Apicco, D.J., et al., *Reducing the RNA binding protein TIA1 protects against tau-mediated neurodegeneration in vivo.* Nat Neurosci, 2018. **21**(1): p. 72-80.

242. Eftekharzadeh, B., et al., *Tau Protein Disrupts Nucleocytoplasmic Transport in Alzheimer's Disease.* Neuron, 2018. **99**(5): p. 925-940 e7.

243. Chen, E.Y., et al., *Enrichr: interactive and collaborative HTML5 gene list enrichment analysis tool.* BMC Bioinformatics, 2013. **14**: p. 128.

244. Kuleshov, M.V., et al., *Enrichr: a comprehensive gene set enrichment analysis web server 2016 update.* Nucleic Acids Res, 2016. **44**(W1): p. W90-7.

245. Xie, Z., et al., *Gene Set Knowledge Discovery with Enrichr.* Curr Protoc, 2021. **1**(3): p. e90.

246. Yamada, T., et al., *Immunohistochemistry using antibodies to alpha-interferon and its induced protein, MxA, in Alzheimer's and Parkinson's disease brain tissues.* Neurosci Lett, 1994. **181**(1-2): p. 61-4.

247. Walker, D.G., et al., *Patterns of Expression of Purinergic Receptor P2RY12, a Putative Marker for Non-Activated Microglia, in Aged and Alzheimer's Disease Brains.* Int J Mol Sci, 2020. **21**(2).

248. Griffiths, C.E., J.J. Voorhees, and B.J. Nickoloff, *Gamma interferon induces different keratinocyte cellular patterns of expression of HLA-DR and DQ and intercellular adhesion molecule-I (ICAM-I) antigens.* Br J Dermatol, 1989. **120**(1): p. 1-8.

249. Park, J., et al., *Microglial MERTK eliminates phosphatidylserine-displaying inhibitory post-synapses.* EMBO J, 2021. **40**(15): p. e107121.

250. Ising, C., et al., *NLRP3 inflammasome activation drives tau pathology.* Nature, 2019. **575**(7784): p. 669-673.

251. Au, N.P.B. and C.H.E. Ma, *Recent Advances in the Study of Bipolar/Rod-Shaped Microglia and their Roles in Neurodegeneration.* Front Aging Neurosci, 2017. **9**: p. 128.

252. Tam, W.Y. and C.H. Ma, *Bipolar/rod-shaped microglia are proliferating microglia with distinct M1/M2 phenotypes.* Sci Rep, 2014. **4**: p. 7279.

253. Plantinga, T.S., L.A. Joosten, and M.G. Netea, *Assessment of inflammasome activation in primary human immune cells.* Methods Mol Biol, 2013. **1040**: p. 29-39.

254. Juliana, C., et al., *Non-transcriptional priming and deubiquitination regulate NLRP3 inflammasome activation.* J Biol Chem, 2012. **287**(43): p. 36617-22.

255. Taylor, S.E., et al., *Rod microglia: a morphological definition.* PLoS One, 2014. **9**(5): p. e97096.

256. Noda, U., *A STUDY OF NISSL'S STAEBCHENZELLEN IN THE CEREBRAL CORTEX OF GENERAL PARESIS, SENILE DEMENTIA, EPILEPSY, GLIOMA, TUBERCULOUS MENINGITIS AND DELIRIUM TREMENS.* The Journal of Nervous and Mental Disease, 1921. **53**(3): p. 161-170.

257. Giordano, K.R., et al., *An update on the rod microglia variant in experimental and clinical brain injury and disease.* Brain Commun, 2021. **3**(1): p. fcaa227.

258. Kitazawa, M., et al., *Blocking IL-1 signaling rescues cognition, attenuates tau pathology, and restores neuronal beta-catenin pathway function in an Alzheimer's disease model.* J Immunol, 2011. **187**(12): p. 6539-49.

259. Kitazawa, M., et al., *Lipopolysaccharide-induced inflammation exacerbates tau pathology by a cyclin-dependent kinase 5-mediated pathway in a transgenic model of Alzheimer's disease.* J Neurosci, 2005. **25**(39): p. 8843-53.

260. Alzheimer, A.Ü.e.e.E.d.H. and the task of validating novel late-onset AD rinde. Allg Zeitschr Psychiatr Psychiatr-Gerichtl Med. 109, *Über eine eigenartige Erkrankung der Hirnrinde.* Allg Zeitschr Psychiatr Psychiatr-Gerichtl Med., 1907. **109**: p. 146-148.

261. Holtman, I.R., et al., *Induction of a common microglia gene expression signature by aging and neurodegenerative conditions: a co-expression meta-analysis.* Acta Neuropathol Commun, 2015. **3**: p. 31.

262. Thrupp, N., et al., *Single-Nucleus RNA-Seq Is Not Suitable for Detection of Microglial Activation Genes in Humans.* Cell Rep, 2020. **32**(13): p. 108189.

263. Lee, J., et al., *Induced pluripotency and spontaneous reversal of cellular aging in supercentenarian donor cells.* Biochem Biophys Res Commun, 2020. **525**(3): p. 563-569.

264. Mertens, J., et al., *Age-dependent instability of mature neuronal fate in induced neurons from Alzheimer's patients.* Cell Stem Cell, 2021. **28**(9): p. 1533-1548 e6.

265. Jankowsky, J.L. and H. Zheng, *Practical considerations for choosing a mouse model of Alzheimer's disease.* Mol Neurodegener, 2017. **12**(1): p. 89.

266. Dupont, M., et al., *Tunneling Nanotubes: Intimate Communication between Myeloid Cells.* Front Immunol, 2018. **9**: p. 43.

267. Abounit, S., et al., *Tunneling nanotubes spread fibrillar alpha-synuclein by intercellular trafficking of lysosomes.* EMBO J, 2016. **35**(19): p. 2120-2138.